

Copyright

by

Stephan Patrick Willias

2015

**The Dissertation Committee for Stephan Patrick Willias**

**Certifies that this is the approved version of the following dissertation:**

**Carbon Catabolite Regulation of *Yersinia pestis* Pathogenesis**

**Committee:**

---

Vladimir L. Motin, PhD  
Mentor

---

Donald Bouyer, PhD

---

Ashok Chopra, PhD, CSc

---

Sanjeev Sahni, PhD

---

Joshua Adkins, PhD

---

---

Dean, Graduate School

**Carbon Catabolite Regulation of *Yersinia pestis* Pathogenesis**

**by**

**Stephan Patrick Willias, B.S.**

**Dissertation**

Presented to the Faculty of the Graduate School of

The University of Texas Medical Branch

in Partial Fulfillment

of the Requirements

for the Degree of

**Experimental Pathology**

**The University of Texas Medical Branch**

**May, 2015**

## **Dedication**

I would like dedicate this body of research to my love, Zina N. Zander.

## **Acknowledgements**

Foremost, I would like to acknowledge my principal investigator, Dr. Vladimir L. Motin, for his mentorship, guidance, and support throughout my research pursuits. I greatly appreciate his dedication to education as conveyed by his willingness to share his vast knowledge and expertise. His encouragement to pursue unique and challenging research opportunities was instrumental in fostering the development of my dissertation project. Moreover, his ceaseless support was fundamental in surpassing obstacles and provided a productive research environment. I would also like to thank members of Dr. Motin's laboratory, notably Drs. Sadhana Chauhan and Maxim V. Telepnev, for their patient training, generous research contributions, and supportive atmosphere.

I would also like to express my gratitude to Dr. Robert Perry for kindly providing the pCD1Ap plasmid. Moreover, I greatly appreciate the substantial efforts made by Dr. Patrick S.G. Chain's research group, especially Chien-Chi Lo, for performing and analyzing whole-genome sequence data.

I also thank my dearest friends, Matthew B. Huante and Juan Conde, for their ceaseless support, inspiration, and counsel throughout my research pursuits. I extend my deepest appreciation to Dr. Gregory W. Buck who provided fundamental inspiration to pursue graduate studies.

# Functional Characterization of *Yersinia pestis* Aerobic Glycerol Metabolism

Publication No. \_\_\_\_\_ 1 \_\_\_\_\_

Stephan Patrick Willias, PhD

The University of Texas Medical Branch, 2014

Supervisor: Vladimir L. Motin, PhD

*Yersinia pestis* biovar Orientalis isolates have lost the capacity to ferment glycerol. Herein we provide experimental validation that a 93 bp in-frame deletion within the *glpD* gene encoding the glycerol-3-phosphate dehydrogenase present in all biovar Orientalis strains is sufficient to disrupt aerobic glycerol fermentation. Furthermore, the inability to ferment glycerol is often insured by a variety of additional mutations within the *glpFKX* operon which prevents glycerol internalization and conversion to glycerol-3-phosphate. The physiological impact of functional *glpFKX* in the presence of dysfunctional *glpD* was assessed. Results demonstrate no change in growth kinetics at 26°C and 37°C. Mutants deficient in *glpD* displayed decreased intracellular accumulation of glycerol-3-phosphate, a characterized inhibitor of cAMP receptor protein (CRP) activation. Since CRP is rigorously involved in global regulation *Y. pestis* virulence, we tested a possible influence of a single *glpD* mutation on virulence. Nonetheless, subcutaneous and intranasal murine challenge was not impacted by glycerol metabolism. As quantified by crystal violet assay, biofilm formation of the *glpD*-deficient KIM6+ mutant was mildly repressed; whereas, chromosomal restoration of *glpD* in CO92 resulted in a significant increase in biofilm formation.

Permission licensed to reproduce content of this manuscript.

# TABLE OF CONTENTS

List of Tables .....	x
List of Figures .....	xii
List of Abbreviations .....	xv
Chapter 1. General Introduction/Literature Review .....	1
Historical Incidence and Modern Epidemiology .....	1
Weaponization .....	2
<i>Yersinia pestis</i> Morphology, Biochemical Characteristics, and Phylogeny .....	2
<i>Yersinia pestis</i> Genomics and Evolution .....	4
Natural Transmission of Plague.....	5
Molecular Mechanism of Biofilm Production and Regulation.....	7
Adaptive Responses.....	8
37°C Low-Calcium Response and Glucose Toxicity .....	8
Clinical Manifestations .....	9
Therapeutic and Preventative Countermeasures.....	11
Chapter 2. Carbon Catabolite Regulation of <i>Yersinia pestis</i> Biofilm Production is Facilitated by the cAMP Receptor Protein, CRP.....	12
Introduction.....	12
Materials and Methods.....	15
Bacterial Strains, Plasmids, and Oligonucleotides .....	15
Scarless Deletion of <i>crp</i> , Allelic Exchange of <i>glpD</i> , and Plasmid Complementation.....	18
Growth Kinetics .....	20
Crystal Violet Assay Biofilm Quantification.....	21
Rate of <i>pgm</i> Locus Excision .....	21
Semi-Quantitative Reverse Transcriptase PCR (RT-PCR).....	22
Phenotypic Assessment of Glycerol Fermentation .....	22
Phylogenetic Analyses .....	23
Intracellular Glycerol-3-Phosphate Quantification.....	23
Results.....	24

Growth Kinetics of the <i>crp</i> Deficient Mutants .....	24
Alternate Carbon Source Metabolism Promotes <i>Y. pestis</i> Biofilm Production.....	27
CRP Facilitates Carbon Catabolite Regulation of <i>Y. pestis</i> Biofilm Formation.....	30
CRP does not Regulate Transcription of Characterized Biofilm-Related Genes .....	34
Molecular Basis of Glycerol Deficiency of biovar Orientalis Isolates. ...	35
Sole Deficiency of <i>glpD</i> does not Enhance G3P Accumulation.....	38
Growth Kinetics and Biofilm formation of the <i>glpD</i> mutants. ....	40
Discussion.....	44
Chapter 3. The Carbon Storage Regulator Protein, CsrA, is Essential for Robust <i>Yersinia pestis</i> Biofilm Formation.....	48
Introduction.....	48
Materials and Methods.....	49
Bacterial Strains, Plasmids, and Oligonucleotides .....	49
Scarless Deletion and Chromosomal Restoration.....	51
Growth Kinetics and Crystal Violet Biofilm Quantification Assay .....	51
Congo Red Binding Assay.....	52
Whole Genome Sequencing.....	52
Results.....	53
CsrA is Essential for Robust <i>Y. pestis</i> Biofilm Production.....	53
CsrA Stimulates <i>Y. pestis</i> Biofilm Production Independent of Glycogen Regulation.....	57
Deletion of <i>hmsP</i> Restores Biofilm Production of the <i>csrA</i> -deficient Mutant.....	59
Spontaneous Pigmentation Reversions of <i>csrA</i> -deficient Mutants.....	61
Discussion.....	66
Chapter 4. Elucidating the Involvement of sRNA upon <i>Y. pestis</i> Carbon Catabolite Regulation of Biofilm Formation .....	72
Introduction.....	72
Materials and Methods.....	75
Bacterial Strains, Plasmids, and Oligonucleotides .....	75

Scarless Deletion and Chromosomal Restoration.....	77
Growth Kinetics and Crystal Violet Biofilm Quantification Assay .....	77
Results.....	77
Pestoides F is not Subject to Carbon Catabolite Regulation of Biofilm Production.....	77
<i>Y. pestis</i> pPCP1, Encoding sR084 sRNA, is Dispensable for Biofilm Formation.....	79
<i>Y. pestis</i> Ysr172 does not Contribute to Biofilm Carbon Catabolite Regulation.....	80
pCD1 does not contribute to <i>Y. pestis</i> Biofilm Production.....	81
Hfq, Dependent upon Available Carbon Sources, Differentially Modulates <i>Y. pestis</i> CO92 Biofilm Production.....	82
Discussion.....	84
Chapter 5. Carbon Catabolite Regulation of <i>Y. pestis</i> Pathogenesis.....	88
Introduction.....	88
Materials and Methods.....	89
Bacterial Strains, Plasmids, and Oligonucleotides .....	89
Deletion of the <i>glpABC</i> operon.....	91
37°C Growth Kinetics.....	92
Semi-quantitative RT-PCR.....	92
Murine-like Macrophage Challenge .....	93
<i>Y. pestis</i> Glycerol Mutant Murine Challenge.....	94
Results.....	95
Disruption of Aerobic Glycerol Metabolism does not affect 37°C Growth .....	95
Temperature Shift from 26°C to 37°C Prompts a Rapid Transient Up- Regulation of Aerobic Glycerol Metabolism.....	96
Glycerol Metabolism does not influence <i>Y. pestis</i> survival in macrophages .....	98
Glycerol Metabolism does not alter <i>Y. pestis</i> virulence during <i>in vivo</i> infection .....	99
37°C Toxicity of the <i>csrA</i> -deficient <i>Y. pestis</i> Mutants .....	102
CsrA Promotes <i>Y. pestis</i> survival in Macrophages .....	109
Discussion.....	109

Chapter 6. Concluding Remarks and Future Directions .....	112
Appendix A. Chapter 2 .....	117
Appendix A Table 1: List of Oligonucleotides. ....	117
Appendix A Figure 1. CRP Promotes KIM6+ Biofilm Production. ....	121
Appendix A Figure 2. Biofilm qRT-PCR Agarose Gels.....	122
Appendix A Figure 3. Phenotypic <i>Y. pestis</i> Glycerol Fermentation .....	124
Appendix A Figure 4. <i>glpD</i> Allelic Exchange Glycerol Fermentation. ....	124
Appendix B. Chapter 3 .....	124
Appendix B Table 1: List Of Oligonucleotides. ....	124
Appendix C. Chapter 4 .....	128
Appendix C Table 1: List Of Oligonucleotides. ....	128
Appendix D. Chapter 5 .....	131
Appendix D Table 1: List Of Oligonucleotides. ....	131
Appendix D Figure 1. Glycerol Metabolism qRT-PCR Agarose Gels. ....	132
Appendix D Figure 2. qRT-PCR Temperature Sensitive Control .....	133
Bibliography/References.....	134
Vita	144

## List of Tables

Table 1:	<i>Yersinia pestis</i> biovar Phenotypic Characteristics .....	3
Table 2:	Bacterial Strains and Plasmids.....	16
Table 3:	Characterization of <i>Y. pestis</i> Glycerol Fermentation .....	36
Table 4:	Bacterial Strains and Plasmids.....	49
Table 5:	Frequency of <i>csrA</i> -deficient Congo Red Pigmentation Revertants .....	62
Table 6:	Whole Genome Sequencing Coverage of <i>csrA</i> -deficient Congo Red Pigmentation Impaired and Pigmentation Positive Revertants .....	64
Table 7:	Whole Genome Sequencing Contig Mapping of <i>csrA</i> -deficient Congo Red Pigmentation Impaired and Pigmentation Positive Revertants .....	64
Table 8:	Unique Genetic Variants Amongst the <i>csrA</i> -deficient Congo Red Pigmentation Impaired and Pigmentation Positive Revertants .....	65
Table 9:	<i>Y. pestis</i> Thermo-regulated sRNA Species .....	74
Table 10:	Bacterial Strains and Plasmids.....	76
Table 11:	Pestoides F Biofilm Synthesis/Regulation Missense Mutations .....	86
Table 12:	Bacterial Strains and Plasmids.....	90
Table 13:	<i>Y. pestis</i> Glycerol Mutant Log <sub>10</sub> CFU/mL Intracellular Viability upon RAW 264.7 Murine Macrophage-like Cell Challenge .....	98

Table 14: Log<sub>10</sub> CFU/mL Intracellular Viability of *Y. pestis* CsrA Mutants after  
RAW Murine Macrophage-like Cell Challenge .....109

## List of Figures

Figure 1:	CRP-mediated Carbon Catabolite Repression. ....	13
Figure 2:	<i>Y. pestis</i> Aerobic Glycerol Metabolism and Putative CRP Interplay. ...	15
Figure 3:	Scarless Deletion and Allelic Exchange Procedure. ....	19
Figure 4:	Impaired Alternate Carbon Source Metabolism of the <i>Y. pestis crp</i> - deficient Mutants. ....	25
Figure 5:	Impaired 26°C Growth of the <i>Y. pestis crp</i> -deficient Mutants in HIB. ...	26
Figure 6:	BCS Carbon Catabolite Regulation of <i>Y. pestis</i> Biofilm Production. ...	27
Figure 7:	HIB Carbon Catabolite Regulation of <i>Y. pestis</i> Biofilm Production. ...	29
Figure 8:	CRP Enables Robust <i>Y. pestis</i> Biofilm Production. ....	31
Figure 9:	Exogenous cAMP Enhances <i>Y. pestis</i> Biofilm Formation. ....	32
Figure 10:	CRP Promotes <i>Y. pestis</i> Biofilm Production in HIB. ....	34
Figure 11:	Semi-quantitative RT-PCR of the <i>Y. pestis</i> Hms System. ....	35
Figure 12:	Biovar Orientalis Glycerol Metabolism Maximum Parsimony Tree. ....	38
Figure 13:	Intracellular G3P Detection of the <i>glpD</i> Allelic Exchange Mutants. ...	39
Figure 14:	Growth Kinetics of <i>glpD</i> -dysfunctional KIM6+ .....	40
Figure 15:	Loss of <i>glpD</i> impairs KIM6+ Biofilm Production. ....	41

Figure 16:	Functional <i>glpD</i> Stimulates CO92 Biofilm Production.....	43
Figure 17:	26°C Growth Kinetics of the CO92 <i>csrA</i> -deficient Mutant.....	54
Figure 18:	CsrA is a Positive Regulator of <i>Y. pestis</i> Biofilm Formation. ....	55
Figure 19:	Impaired Congo red Assimilation of <i>Y. pestis csrA</i> -deficient Mutants	56
Figure 20:	CsrA Enhances <i>Y. pestis</i> Biofilm Production Independent of Glycogen Regulation.....	57
Figure 21:	Congo Red Binding of <i>Y. pestis csrA</i> -deficient Mutant is not Restored by Loss of the <i>glgCAP</i> Operon. ....	58
Figure 22:	Deletion of <i>hmsP</i> in a CO92 $\Delta$ <i>csrA</i> Mutant Enables Excessive Biofilm Production.....	60
Figure 23:	Loss of <i>hmsP</i> Restores Congo Red Pigmentation of the CO92 <i>csrA</i> - deficient Mutant. ....	61
Figure 24:	<i>csrA</i> -deficient Congo Red Pigmentation Positive Revertant Clones. ....	63
Figure 25:	<i>E. coli</i> and <i>Y. pestis</i> PNAG biosynthesis operon 5' UTR Comparison. .....	67
Figure 26:	Proposed Mechanism of <i>Y. pestis</i> CsrA Biofilm Regulation.....	68
Figure 27:	<i>E. coli</i> and <i>Y. pestis glgCAP</i> biosynthesis operon 5' UTR Comparison. .....	69
Figure 28:	<i>Y. pestis hmsP</i> 5' UTR Predicted CsrA-binding Sites. ....	70

Figure 29:	Pestoides F Lacks Biofilm Carbon Catabolite Regulation .....	78
Figure 30:	pPCP, encoding sR084, does not alter CO92 Biofilm Production .....	79
Figure 31:	Ysr172 has not Impact upon CO92 Biofilm Production.....	80
Figure 32:	pCD1 has no influence upon <i>Y. pestis</i> Biofilm Production .....	81
Figure 33:	Impaired Growth of the CO92 $\Delta$ <i>hfq</i> mutant .....	83
Figure 34:	Hfq Differentially Modulates <i>Y. pestis</i> Biofilm Production Dependent upon Available Carbon Sources. ....	84
Figure 35:	37°C Growth Kinetics of the <i>glpD</i> -impaired KIM6+.....	95
Figure 36:	Semi-quantitative RT-PCR of the Aerobic Glycerol Metabolic Pathway during Incubation at either 26°C or 37°C.....	97
Figure 37:	<i>Y. pestis</i> Intranasal Virulence is not altered by Glycerol Metabolism..	100
Figure 38:	<i>Y. pestis</i> Subcutaneous Virulence is Unaffected by Glycerol Metabolism .....	101
Figure 39:	CsrA Promotes <i>Y. pestis</i> CO92 Proliferation at 37°C.....	103
Figure 40:	Cessation of CO92 $\Delta$ <i>csrA</i> Growth at 37°C .....	105
Figure 41:	37°C Toxicity of the KIM6+ <i>csrA</i> -deficient Mutant. ....	107
Figure 42:	37°C Growth of $\Delta$ <i>csrA</i> is not Restored by loss of <i>glgCAP</i> or <i>nhaR</i> .....	108
Figure 43:	Proposed <i>Y. pestis</i> Biofilm Regulation Network .....	115

## List of Abbreviations

Alternate	non-PTS carbon source
BCS	Best case scenario chemically defined medium
BHI	Brain heart infusion medium
c-di-GMP	bis-(3',5')-cyclic dimeric GMP/cyclic diguanylate
Cb	Carbenicillin
CR	Congo red
CRP	cAMP receptor protein
CsrA	Carbon storage regulator protein
CV	Crystal violet
cAMP	3'-5'-cyclic AMP
DHAP	Dihydroxyacetone phosphate
DPBS	Dulbecco's phosphate-buffered saline
<i>E.</i>	<i>Escherichia</i>
EPS	Extracellular polymeric substance
FBS	Fetal bovine serum
FAD	Flavin adenine dinucleotide
G3P	Glycerol-3-phosphate
HIA	Heart infusion agar
HIB	Heart infusion broth
i.n.	Intranasal
IS element	Insertion element

Km	Kanamycin
LPS	Lipopolysaccharide
<i>O.</i>	<i>Oropsylla</i>
PEP : PTS	Phosphoenolpyruvate : carbohydrate phosphotransferase system
PNAG	Polymeric- $\beta$ -1,6- <i>N</i> -acetyl-D-glucosamine
Primary	PTS carbon source
s.c.	Subcutaneous
sRNA	small, non-coding RNA
Suc	Sucrose
TMH	Straley and Bowmer chemically defined medium
Tm	Trimethoprim
<i>Y.</i>	<i>Yersinia</i>
<i>X.</i>	<i>Xenopsylla</i>

# Chapter 1. General Introduction/Literature Review

## HISTORICAL INCIDENCE AND MODERN EPIDEMIOLOGY

*Yersinia pestis*, the etiological agent of plague, is historically accountable for an estimated 200 million deaths through three pandemics and a plethora of epidemics [1]. These pandemics include the Justinian plague (6<sup>th</sup> century), the Medieval plague including the Black Death epidemic (14<sup>th</sup> century), and the Modern Indo-China plague (19<sup>th</sup> century) [2,3,4]. The Justinian plague originated in Egypt and subsequently spread throughout the Middle East and the Mediterranean basin [5]. The second plague pandemic, which devastated Medieval Europe, was likely imported from Central Asia through the Silk Road trade routes [6,7]. The third plague pandemic was initiated in the Yunnan province of China and disseminated worldwide through marine shipping [4]. In 1894, amid the Hong Kong epidemic of the third plague pandemic, Alexandre Yersin isolated the plague bacillus, thereby identifying the causative agent of plague [8].

With a current global distribution of endemic foci, *Y. pestis* remains a public health concern. Considered to be a re-emerging pathogen, *Y. pestis* is responsible for approximately 1,000-5,000 worldwide annual cases of plague [9]. The modern incidence of plague is primarily localized to Africa, which accounts for greater than 95% of worldwide annual plague cases and deaths. In particular, the Democratic Republic of the Congo and Madagascar are the countries currently most strongly affected by plague. In late 2014, a localized plague outbreak in Madagascar resulted in 119 confirmed cases of plague, resulting in 40 deaths [10]. Within the United States, cases of plague are sequestered to the southwestern states, most notably the Four Corners region, in accordance with the natural host and vector range [11]. However, as potentially facilitated by climate change, the natural incidence of plague may be amplified through geographical host expansion [12].

## **WEAPONIZATION**

*Y. pestis* has an extensive history of biological warfare exploitations. During one of the earliest incidences of recorded biological warfare (1346-1347), invading Mongol forces catapulted plague-infected cadavers into the besieged Crimean city of Caffa (alternately denoted as Kaffa), thereby transmitting the disease to the inhabitants [13]. During World War II, the Imperial Japanese Army research Unit 731 bombarded the Chinese with clay bombs containing fleas infected with *Y. pestis*. Amid the Cold War era, both American and Soviet scientists devised means to effectively aerosolize *Y. pestis* [14]. It has been predicted that aerosolized dissemination of 50 kg of *Y. pestis* over a city of 5 million inhabitants may yield 150,000 cases of pneumonic plague, resulting in an estimated 36,000 fatalities [15]. In modern times, multiple countries are suspected to pursue the development of offensive biological warfare capabilities [16]. Due to prior application as a bioweapon and current bioterrorism concerns, *Y. pestis* is categorized as a Tier I select agent [17].

## **YERSINIA PESTIS MORPHOLOGY, BIOCHEMICAL CHARACTERISTICS, AND PHYLOGENY**

*Y. pestis* is a pleomorphic Gram-negative coccobacillus in the family Enterobacteriaceae. Within the *Yersinia* genus, there are three human pathogens: *Yersinia enterocolitica*, *Yersinia pseudotuberculosis*, and *Y. pestis*. Contrary to *Y. enterocolitica* and *Y. pseudotuberculosis*, *Y. pestis* is non-motile as result of a frameshift mutation in the *flhD* gene encoding a flagellar transcriptional activator [18,19]. *Y. pestis* is further distinguished from *Y. enterocolitica* and *Y. pseudotuberculosis* through production of a truncated lipopolysaccharide (LPS). *Y. enterocolitica* and *Y. pseudotuberculosis* both produce a smooth phenotype LPS comprised of lipid A, core oligosaccharide, and O antigen [20]. As a consequence of frameshift mutations within the O-antigen gene cluster,

*Y. pestis* produces a rough phenotype LPS consisting of lipid A and core oligosaccharides [21].

Strains of *Y. pestis* are subdivided into four major biovars (Microtus, Antiqua, Medievalis, and Orientalis) distinguished by phenotypic biochemical traits (**Table 1**) [22,23]. Epidemiological evidence as supported by molecular techniques suggest the three plague pandemics have been attributed to unique *Y. pestis* biovars: the Justinian plague has been accredited to species of biovar Antiqua, biovar Medievalis type species have been implicated to cause the second pandemic, and biovar Orientalis strains were responsible for the third plague pandemic [22,24]. Phylogenetic analyses indicate that *Y. pestis* has evolved as a monomorphic clone from a *Y. pseudotuberculosis* serotype O1b ancestor less than 20,000 years ago [24]. However, *Y. pestis* biovar designations are only partially compatible with molecular analyses, indicating phenotypic classifications are not entirely monophyletic [7,25].

**Table 1: *Yersinia pestis* biovar Phenotypic Characteristics**

<b>Biochemical Traits</b>	<b><i>Y. pestis</i> Biovar [22,23]</b>			
	Estimated Divergence (Years Ago) [7]			
	<b>Microtus</b> 2.6K-28K	<b>Antiqua</b> 500-8K	<b>Medievalis</b> 200-2.5K	<b>Orientalis</b> 100-2.3K
Glycerol Fermentation	+	+	+	-
Arabinose Fermentation	+/-	+	+	+
Rhamnose Fermentation	+	-	-	-
Nitrate Reduction	+/-	+	-	+

## ***YERSINIA PESTIS* GENOMICS AND EVOLUTION**

*Y. pestis* has a single circular chromosome of approximately 4.6 Mb encoding for ~4,000 open reading frames. *Y. pestis* typically contains three plasmids: pMT1 (~110 Kb), pPCD1 (~70 Kb), and pPCP1 (~9.5 Kb). The pPCD1 plasmid is present in all pathogenic *Yersinia* species and encodes a type 3 secretion system (T3SS) and effector molecules [26]. The pMT1 and pPCP1 plasmids are unique to *Y. pestis*, and notably encode the F1 anti-phagocytic capsular antigen and the Pla plasminogen-activating protease virulence factors, respectively [27,28].

Despite the acquisition of horizontally transferable genetic elements and integration of 32 novel chromosomal genes, the microevolution of *Y. pestis* is principally characterized by reductionist gene loss or inactivation [19]. Approximately ~13% of ancestral *Y. pseudotuberculosis* genes have been inactivated in *Y. pestis*. Sequencing has revealed the evolution of *Y. pestis* is associated with a substantial expansion of insertion (IS) elements. In stark contrast to *Y. pseudotuberculosis* strain IP32953 which contains 20 identified chromosomal IS elements, *Y. pestis* IS elements are notably augmented by >5-fold. Furthermore, the microevolution of *Y. pestis* demonstrates continued IS element amplification and transposition. It is unclear whether *Y. pestis* IS element excision and transposition is a spontaneous periodic occurrence or induced in response to specific stimuli.

The inactivation of ancestral genes has been demonstrated to promote the establishment of the *Y. pestis* infectious cycle. Elimination of urease activity through inactivation of UreD in *Y. pestis* has been shown to significantly decrease toxicity to the flea vector, thereby improving transmissibility [29]. Both the *flhD* and *rcsA* genes, encoding negative regulators of biofilm production, have been inactivated in *Y. pestis* [18,30]. Furthermore, FlhD represses the *yop* regulon in *Y. enterocolitica* thereby disrupting T3SS toxin secretion, implicating a potential mechanism of augmented *Y.*

*pestis* virulence [31]. The *rtn* gene, which confers c-di-GMP phosphodiesterase activity in *Salmonella*, is not functional in *Y. pestis* as result of an N-terminal truncation [32,33].

## NATURAL TRANSMISSION OF PLAGUE

*Y. pestis* naturally circulates amongst rodent reservoir hosts and flea vectors [1]. A wide range of mammalian species are capable of being infected with *Y. pestis*; however, many species fail to develop sufficient bacteremia to transmit the pathogen [34,35]. Moreover, despite the apparent diversity of potential flea vector species, few species readily associate with ecologically-relevant mammalian hosts and efficiently transmit plague [36,37]. Even the most proficient *Y. pestis* vector flea species, the rat flea *Xenopsylla cheopis*, has been demonstrated to exhibit poor vector competence [38]. There are two accepted modes of flea-borne transmission of *Y. pestis*: 1) biofilm-mediated proventricular blockage and 2) early-phase transmission. The precise contributions of these distinct transmission schemes toward zoonotic maintenance and/or epidemic spread of plague are not fully understood.

The zoonotic maintenance of plague is suggested to be facilitated by biofilm-mediated proventricular blockage. Upon consumption of a highly bacteremic mammalian blood meal by a naïve flea, *Y. pestis* auto-aggregates and forms an extracellular polymeric substance (EPS) biofilm in association with the flea proventriculus, which is a valve-like structure separating the esophagus and the midgut [39]. The biofilm physically obstructs the passage of blood during subsequent feeding attempts and enhances regurgitation of *Y. pestis* into the mammalian dermis, thereby promoting the transmission of plague [40]. Through acquisition of the pMT1 plasmid, encoding the *Yersinia* murine toxin phospholipase D, *Y. pestis* survives within the flea digestive tract [41,42]. Similar to *Y. pestis*, *Y. pseudotuberculosis* is capable of producing cohesive biofilms, *in vitro*. However, only *Y. pestis* is capable of producing biofilms during infection of the flea [43].

These findings suggest a *Y. pestis* progenitor, through modification of adaptive responses controlling existing biofilm formation networks, has evolved the ability to synthesize biofilms in response to the flea midgut milieu. The transmission by blocked fleas requires an extensive extrinsic incubation period followed by a brief infectious state prior to starvation-induced death of the vector [38,44]. Thus, biofilm-mediated proventricular blockage may be insufficient to explain the rapid spread of plague during epidemics and epizootics. However, complete biofilm-mediated blockage is not essential for efficient transmission; rather, partially blocked fleas may be more effective in transmitting *Y. pestis* [45].

Early-phase transmission of plague, through an undetermined mechanical and/or biological process, enables rapid biofilm-independent dissemination of plague [37]. Following contamination of flea mouthparts, *Y. pestis* is viable for only a few hours, discounting simple mechanical transmission [46]. Early-phase transmission efficacy notably wanes following 3 days post-infection of the flea vector. Thus, *Y. pestis* does not readily multiply and persist on the flea mouthparts, potentially refuting a biological transmission scheme [47]. Regardless of the precise mode of action, a *Y. pestis* KIM6 $\Delta$ *hmsR* mutant, incapable of biofilm production, has been demonstrated to be transmitted from *X. cheopis*, providing experimental support for the early-phase transmission model [48]. Many characterized *Y. pestis* vector flea species such as *Oropsylla montana* (*O. montana*), the primary vector of *Y. pestis* in the United States, do not readily form proventricular biofilm blockages, further stressing the importance of biofilm-independent modes of transmission [49]. Due to the swift capacity to disseminate plague, some investigators advocate that early-phase transmission may promote the epidemic spread of *Y. pestis* [47].

## MOLECULAR MECHANISM OF BIOFILM PRODUCTION AND REGULATION

The *Y. pestis* biofilm is comprised of polymeric- $\beta$ -1,6-*N*-acetyl-D-glucosamine (PNAG) synthesized and exported by protein products of the *hmsHFRS* operon [50]. The *hmsHFRS* operon lies within an unstable 102-kb region flanked by IS100 elements which has been characterized to spontaneously excise *en bloc* at a frequency of  $10^{-5}$  [50,51,52]. Retention of the 102-kb region, designated as the pigmentation (*pgm*) locus, can be readily determined via phenotypic association of chromogens to the biofilm polysaccharide [53].

The secondary structure and predicted domains of the HmsHFRS proteins are highly conserved to the *E. coli* PgaABCD and *Staphylococcus* spp. IcaABCD homologs [54,55]. The inner membrane-associating HmsR contains a putative glycosyl transferase domain which, when in complex with HmsS, has been implicated to enable synthesis of intracellular  $\beta$ -1,6-linked *N*-acetylglucosamine residues [56]. HmsH, in association with the putative HmsF polysaccharide deacetylase, is an outer membrane-spanning protein which is predicted to enable the extracellular export of the biofilm polysaccharides [57]. The stability of the HmsHFRS protein interactions are subject to temperature regulation. At 37°C, the HmsHFRS protein interactions are unstable; therefore, *Y. pestis* does not synthesize biofilms during mammalian infection. Rather, *Y. pestis* biofilm production is restricted to temperatures <34°C in accordance to physiological conditions of the flea vector [58].

The catalytic activity of the HmsHFRS system is subject to post-translational regulation in response to the bis-(3',5')-cyclic dimeric GMP (cyclic diguanylate/c-di-GMP) second messenger [59]. Cyclic diguanylate, synthesized by HmsT and HmsD diguanylate cyclases, stimulates HmsR activity [33,60]. Conversely, c-di-GMP is degraded by the HmsP phosphodiesterase [61,62,63]. However, not much is understood regarding the regulatory response networks which control *Y. pestis* biofilm production.

## **ADAPTIVE RESPONSES**

In order to survive in unique host milieus, *Y. pestis* evokes regulatory adaptive responses which differentially modulate gene expression. The *Y. pestis* genome encodes for approximately 250 putative transcriptional regulators including 29 two-component phosphor-transfer systems (of which 25 are complete, and 4 are pseudogenes), 6 sigma/anti-sigma factors ( $\sigma$ D,  $\sigma$ N,  $\sigma$ S,  $\sigma$ H,  $\sigma$ F, and  $\sigma$ E), histone-like factors, and other DNA-binding global regulatory elements; however, a significant minority of the putative transcriptional factors have been experimentally characterized [64]. In addition to DNA-associating regulatory factors, a wide range of putative small, non-coding RNA (sRNA) species have been identified in *Y. pestis* [65,66,67]. As often facilitated by chaperone molecules, sRNA species interact with complementary mRNA to differentially modulate gene expression through multiple modes of action [68,69]. However, little is known regarding the DNA-binding transcriptional regulators which control the expression of the sRNA species. Furthermore, the physiological significance of the vast majority of sRNA species has not been ascertained.

## **37°C LOW-CALCIUM RESPONSE AND GLUCOSE TOXICITY**

There are two potentially inter-related 37°C-induced *in vitro* phenomena described for *Y. pestis*: 1) the low-calcium response (Lcr) and 2) glucose toxicity. When cultured at 37°C in the absence of calcium, virulent *Y. pestis* containing the pCD1 plasmid enter into a viable, but non-replicative Lcr state [70,71]. During induction of Lcr bacteriostasis, expression of the T3SS is induced, resulting in excessive secretion of substrate molecules [72,73]. Upon temperature transition to 26°C or media supplementation with concentrations of Ca<sup>2+</sup> in accordance with physiological levels in mammalian blood, proliferation is restored. Avirulent *Y. pestis* strains lacking the entire pCD1 plasmid or with sole loss of the pCD1-encoded V antigen do not demonstrate the

Lcr phenotype [74]. The precise molecular mechanism defining the Lcr has not been ascertained; however, the underlying physiological basis for the bacteriostasis has been implicated to inadequate adenylate energy charge [74,75]. Media supplementation with the alternate carbon source, D-gluconate, was shown to mitigate the Lcr 37°C growth restriction [76]. However, the utilization of glucose as the primary carbon source at 37°C has been shown to be selectively toxic to Lcr+ but not Lcr- strains of *Y. pestis* [77].

When cultured in chemically defined medium utilizing 0.25% glucose as the sole carbon source at 37°C, virulent *Y. pestis* strains demonstrate an approximate 1-2 log reduction in magnitude associated with considerable cell lysis culminating 6-12 hours post-inoculation [77,78]. Following the decrease in magnitude, affected strains recover and logarithmic growth resumes. Glucose toxicity is associated with low respiratory quotients, indicative of metabolic dysfunction. The catabolism of glucose is extremely rapid, and is notably depleted from the culture medium within 30 minutes post-inoculation. However, despite glucose depletion, oxygen uptake persists indicating the oxidation of an alternate compound or intermediate. Glucose toxicity was found to be associated with secretion of alpha-ketoglutarate and lactic acid into the culture media; however, the toxic effect was demonstrated to be independent of pH change.

## **CLINICAL MANIFESTATIONS**

There are three major forms of plague: bubonic, septicemic, and pneumonic [14]. Bubonic plague, the most common form, typically arises from the natural acquisition of plague resulting from the bite of an infected flea vector. Upon entry in the host dermis, *Y. pestis* migrates through the cutaneous lymphatics to a region lymph node. Either during lymphatic migration or upon lymph node entry, *Y. pestis* is phagocytosed yet resists destruction [79]. *Y. pestis* escapes from the phagocyte and rapidly proliferates, causing

destruction of local lymph node architecture, resulting in the pathognomonic bubo formation [80].

Patients infected with *Y. pestis* may also develop a septicemic form of plague without a discernable bubo. Consistent with other Gram-negative bacterial sepsis, septicemic plague may culminate with patient multi-organ failure. Moreover, septicemic plague is often associated with disseminated intravascular coagulation consumptive coagulopathy, resulting in the necrosis of small vessels and purpuric skin lesions. Widespread clotting of the microvasculature during the advanced progression of plague septicemia may result in gangrene of acral regions, which is believed to be responsible for the term “Black Death” during the second plague pandemic [81].

Pneumonic plague, acquired by the inhalation of aerosolized *Y. pestis*, is the most acute and threatening form of plague with an incubation period of approximately 1-3 days. Symptoms of severe pneumonia associated with intra-alveolar hemorrhage and edema are followed by cardiovascular dysfunction, cardiopulmonary failure and coma [82,83]. If antibiotic regimens are not initiated within 24 hours following presentation of pneumonic plague symptoms, the mortality rate approaches 100% [84]. Contrary to bubonic and septicemic forms of plague which are not directly communicable, pneumonic plague is transmissible from person-to-person through respiratory droplets [85].

As a general caveat, *Y. pestis* infections often do not exclusively present as a single form of plague, yet may develop multiple secondary forms. Thus, primary bubonic plague may result in secondary pneumonic plague which may further exacerbate patient morbidity, mortality, and the spread of plague. *Y. pestis* infections may also present in a variety of atypical forms, including meningitis and pharyngitis [86,87].

## THERAPEUTIC AND PREVENTATIVE COUNTERMEASURES

There is currently no licensed vaccine approved for use in the United States to prevent plague [88]. A killed whole-cell *Y. pestis* vaccine previously approved for use in the United States has been discontinued for, amongst other reasons, an inability to elicit protection against pneumonic plague [89]. Countries of the former Soviet Union utilize a *Y. pestis* live-attenuated EV76-lineage vaccine strain. EV76 is primarily attenuated due to *pgm* locus deficiency [90,91,92]. Immunization with EV76, although providing protection against plague, has been characterized to elicit adverse effects [93].

Current recombinant subunit vaccine candidates comprised of LcrV and F1 antigens demonstrate efficacy against bubonic/septicemic forms of plague; however, provide questionable efficacy against pneumonic plague, the primary risk of *Y. pestis* weaponization [94]. Live vaccination, which evokes both humoral and cellular immune aspects, may provide superior protection in respect to recombinant vaccine strategies [95,96]. However, the inherent risks of live vaccination pose serious safety concerns.

Therefore, current therapeutic strategies in the United States are restricted to post-exposure antibiotic regimens, including aminoglycosides (streptomycin and gentamicin), doxycycline, and fluoroquinolones (ciprofloxacin and levofloxacin) [14,97]. However, the threat of naturally acquired or genetically modified antibiotic resistant strains negates current treatment strategies. Natural isolates of *Y. pestis* have been documented to have developed streptomycin resistance [98,99]. In an experimental setting, *Y. pestis* strains resistant to nalidixic acid demonstrate decreased susceptibility to fluoroquinolones [100]. Allegedly, the bioweapons program of the former Soviet Union succeeded in constructing multi-drug resistant pathogens, including *Y. pestis* [14].

## Chapter 2. Carbon Catabolite Regulation of *Yersinia pestis* Biofilm

### Production is Facilitated by the cAMP Receptor Protein, CRP

#### INTRODUCTION

Transcriptomics of *Y. pestis* during infection of the flea vector indicate components of the *Y. pestis* phosphoenolpyruvate (PEP) : carbohydrate phosphotransferase system (PTS) (primary) carbon source metabolic pathways are notably down-regulated; whereas, the expression of non-PTS (alternate) carbon source metabolic pathways and peptide utilization pathways are induced [101]. Despite the presence of substantial lipids in blood, *Y. pestis* fatty acid uptake and catabolism genes were not induced during survival in the flea. Taken together these observations suggest *Y. pestis* biofilm production may be dependent upon the metabolism of alternate carbon sources; however, the underlying adaptive response regulatory networks have not been characterized.

In a process widely described in *E. coli* known as carbon catabolite repression, the presence of primary carbon sources inhibits alternate carbon source metabolism. The cAMP receptor protein (CRP), a central mediator of carbon catabolite repression, facilitates the metabolism of alternate carbon sources when available primary carbon sources are scarce (**Fig. 1**) [102]. Moreover, CRP is a global DNA-binding transcriptional regulator which differentially modulates >6% of the *Y. pestis* total protein encoding capacity [103]. In other pathogens, CRP regulation has been shown to enhance biofilm production [104]. Taken together, I postulate the metabolism of alternate carbon sources, as facilitated by CRP, promotes *Y. pestis* biofilm production. Furthermore, I hypothesize that the expansive global regulatory network of CRP does not exclusively enable the uptake and catabolism of alternate carbon sources, but confers a regulatory impact upon

the *Y. pestis* biofilm formation factors, thereby promoting the natural transmission of plague.

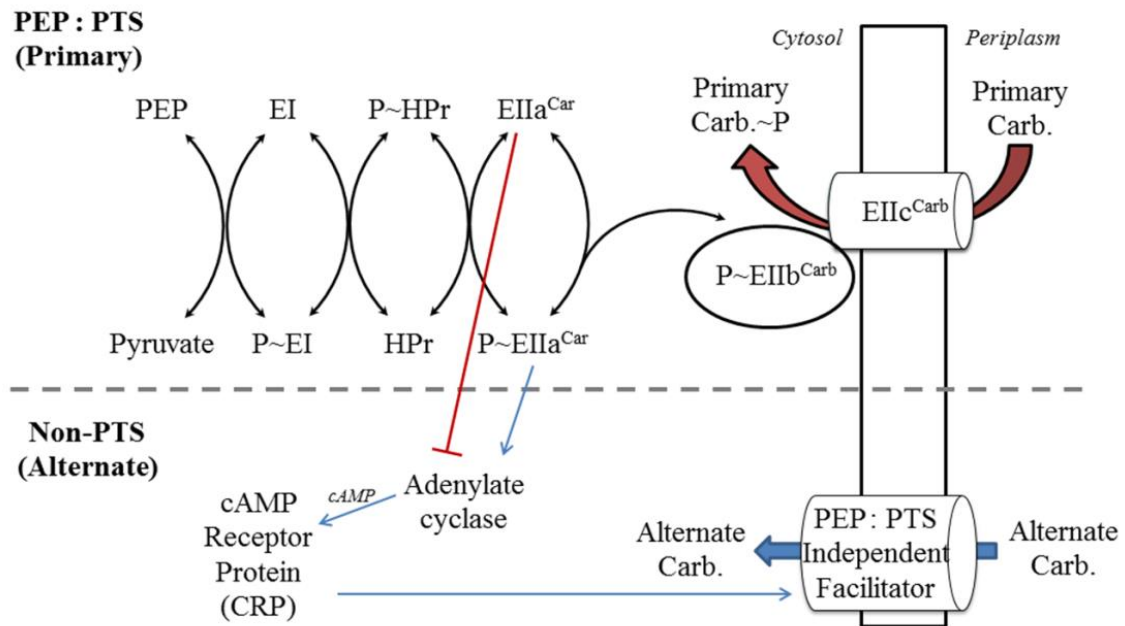


**Figure 1: CRP-mediated Carbon Catabolite Repression.**

The internalization of primary carbon sources (denoted as “Primary Carb.”) is dependent upon a highly conserved phosphorelay cascade initiated by phosphoenolpyruvate. In the presence of available primary carbon sources, carbohydrate-specific EIIa is predominately in a dephosphorylated state, thereby inhibiting the synthesis of 3'-5'-cyclic adenosine monophosphate (cAMP) by adenylate cyclase. CRP is allosterically activated by cAMP and stimulates the expression of alternate carbon source (designated as “Alternate Carb.”) metabolic networks. Ultimately, the metabolism of primary carbon sources, through indirect inhibition of CRP activation, prevents the uptake and catabolism of alternate carbon sources.

Studies in *E. coli* have demonstrated that glycerol-3-phosphate (G3P) prevents stimulation of adenylate cyclase, thereby obstructing cAMP synthesis and indirectly disrupting CRP activation [105]. Isolates of *Y. pestis* biovar Orientalis, the most recent evolutionary divergent responsible for the 3rd plague pandemic, have lost the capacity to

ferment glycerol [24]. *Y. pestis* anaerobic metabolism of glycerol is facilitated by the *glpABC* operon; whereas, *glpD* and the *glpFKX* operon enable aerobic glycerol fermentation. Under aerobic conditions, glycerol is internalized by the GlpF facilitator. The GlpK aerobic glycerol kinase converts glycerol into glycerol-3-phosphate (G3P). Bioinformatics analyses suggest the presence of an additional glycerol kinase in *Y. pestis* chromosome (KIM10, y0876); however, it is uncertain whether this putative protein is functional [106]. Glycerol-3-phosphate can be converted into dihydroxyacetone phosphate (DHAP) by the *sn*-glycerol-3-phosphate dehydrogenase, GlpD. Both G3P and DHAP may serve as precursors for phospholipid biosynthesis [107,108]. Alternately, the TpiA triose phosphate isomerase can convert DHAP into glyceraldehyde-3-phosphate, thereby enabling the glycolytic catabolism of glycerol [109].

The inability for biovar Orientalis isolates to ferment glycerol is presumed to result from a hallmark 93 bp in-frame deletion within the *glpD* gene [110]. However, genomic comparison of biovar Orientalis isolates indicate a wide variety of disruptions within the *glpK* gene, potentially preventing the formation and accumulation of the G3P in the absence of functional *glpD*. Therefore, the acquired defect in *Y. pestis* glycerol metabolism may reflect a negative selection event which minimizes CRP inhibition (**Fig. 2**). I postulate the inactivation of the *glpD* and/or *glpK* in biovar Orientalis isolates adjusts intracellular accumulation of G3P, thereby potentially modifying CRP regulation of *Y. pestis* biofilm formation [111].

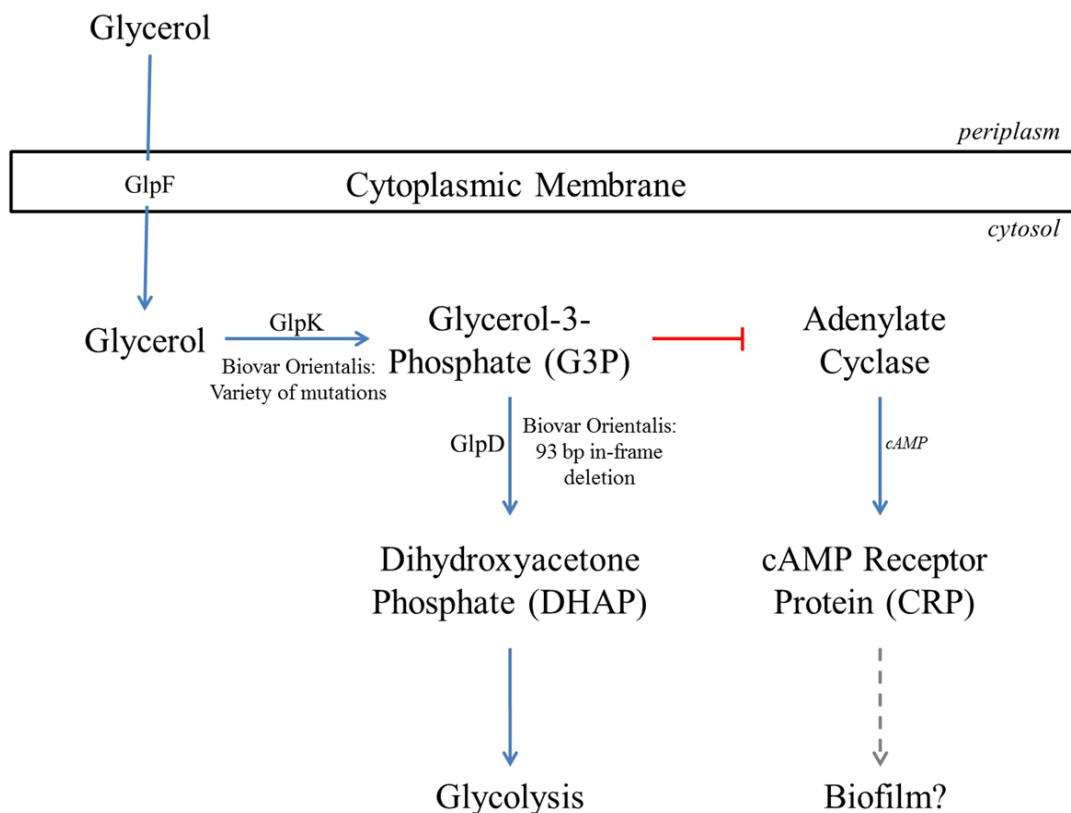


**Figure 2: *Y. pestis* Aerobic Glycerol Metabolism and Putative CRP Interplay.**

*Y. pestis* aerobic glycerol metabolism is afforded by protein products of the *glpFKX* operon and the *glpD* gene. Isolates of *Y. pestis* biovar Orientalis have acquired a hallmark 93 bp in-frame deletion which is suggested to disrupt the glycolytic metabolism of glycerol. Studies in *E. coli* have shown that glycerol-3-phosphate, the enzymatic product of GlpK, indirectly impairs activation of the CRP global regulator by inhibiting the synthesis of cAMP. As consequence of a wide variety of mutations evident in the *glpK* gene, it is uncertain whether GlpK is functional in biovar Orientalis strains.

## MATERIALS AND METHODS

### Bacterial Strains, Plasmids, and Oligonucleotides

Bacterial strains and plasmids used in this chapter are described in **Table 2**. Oligonucleotides are detailed in **Appendix A Table 1**.

**Table 2: Bacterial Strains and Plasmids**

<i>Y. pestis</i> strain	Characteristics*	Reference
CO92	Pgm <sup>+</sup> pCD <sup>+</sup> pPCP <sup>+</sup> Gly <sup>-</sup>	[112]
CO92L	Pgm <sup>+</sup> pCD <sup>-</sup> pPCP <sup>+</sup> Gly <sup>-</sup> (cured of virulence plasmid pCD1)	Motin collection [111]
CO92L <i>glpD</i> <sup>+</sup>	Pgm <sup>+</sup> pCD <sup>-</sup> pPCP <sup>+</sup> Gly <sup>-</sup> (defective <i>glpD</i> ' allele replaced with functional <i>glpD</i> gene in the chromosome)	Motin collection [111]
CO92Δ <i>crp</i>	Scarless Deletion of the <i>crp</i> gene	Motin collection Unpublished
KIM 5 (D27)	Pgm <sup>-</sup> pCD <sup>+</sup> pPCP <sup>+</sup> Gly <sup>+</sup>	Brubaker collection
KIM 6+	Pgm <sup>+</sup> pCD <sup>-</sup> pPCP <sup>+</sup> Gly <sup>+</sup>	Brubaker collection
KIM 6+ <i>glpD</i> '	Pgm <sup>+</sup> pCD <sup>-</sup> pPCP <sup>+</sup> Gly <sup>-</sup> (functional <i>glpD</i> gene replaced with defective <i>glpD</i> ' allele in the chromosome)	Motin collection [111]
KIM 6+Δ <i>crp</i>	Scarless deletion of the <i>crp</i> gene	Motin collection Unpublished
195-P2	Pgm <sup>-</sup> pCD <sup>+</sup> pPCP <sup>+</sup> Gly <sup>-</sup>	Hinnebusch collection
TS	Pgm <sup>+</sup> pCD <sup>-</sup> pPCP <sup>+</sup> Gly <sup>-</sup>	Brubaker collection
Salazar	Pgm <sup>-</sup> pCD <sup>-</sup> pPCP <sup>+</sup> Gly <sup>-</sup>	Brubaker collection
EV76H	Pgm <sup>+</sup> pCD <sup>-</sup> pPCP <sup>+</sup> Gly <sup>-</sup> (derivative of the live plague vaccine strain EV76)	Brubaker collection

M23	Pgm <sup>-</sup> pCD <sup>+</sup> pPCP <sup>+</sup> Gly <sup>-</sup>	Brubaker collection
Kimberley	Pgm <sup>+</sup> pCD <sup>-</sup> pPCP <sup>+</sup> Gly <sup>-</sup>	Perry collection
PEXU-2	Pgm <sup>+</sup> pCD <sup>+</sup> pPCP <sup>+</sup> Gly <sup>-</sup>	CDC collection
<b><i>E. coli</i> strains</b>	<b>Characteristics</b>	<b>Reference</b>
DH5 $\alpha$	F- $\phi$ 80lacZ $\Delta$ M15 $\Delta$ (lacZYA-argF) U169 recA1 endA1 hsdR17 (rk <sup>-</sup> , mk <sup>+</sup> ) gal <sup>-</sup> phoA supE44 $\lambda$ -thi-1 gyrA96 relA1	Invitrogen (Carlsbad, CA)
BW25141	F <sup>-</sup> , $\Delta$ ( <i>araD-araB</i> )567, $\Delta$ <i>lacZ</i> 4787(::rrnB-3), $\Delta$ ( <i>phoB-phoR</i> )580, $\lambda$ <sup>-</sup> , <i>galU</i> 95, $\Delta$ <i>uidA</i> 3:: <i>pir</i> <sup>+</sup> , <i>recA</i> 1, <i>endA</i> 9(del-ins)::FRT, <i>rph</i> -1, $\Delta$ ( <i>rhaD-rhaB</i> )568, <i>hsdR</i> 514	[113]
<b>Plasmids</b>	<b>Characteristics</b>	<b>Reference</b>
pBluescript SK <sup>+</sup>	Cloning vector, Ap <sup>R</sup>	Stratagene (La Jolla, CA)
pBBR1Tp	Cloning vector, Tp <sup>R</sup>	ATCC (Manassas, VA)
pKD46	Mutagenesis helper plasmid, source of Lambda Red Recombinase, Ap <sup>R</sup>	[113]
pKD4	Mutagenesis helper plasmid, source of <i>kan</i> cassette, Km <sup>R</sup> Ap <sup>R</sup>	[113]
pCVD442	Source of <i>sacB</i> gene, Ap <sup>R</sup>	[114]
pKD4_Km-sacB	Cloned <i>sacB</i> from pCVD442 in NgoMIV site of pKD4, source of <i>kan-sacB</i> cassette, Km <sup>R</sup> Ap <sup>R</sup> , Suc <sup>S</sup>	Motin collection [111]
pBGLPD5	Cloned <i>glpD</i> from KIM 6 <sup>+</sup> in Hind III and BamHI sites of pBluescript SK <sup>+</sup>	Motin collection [111]

pTpGLPFKX6	Cloned <i>glpFKX</i> from KIM 6+ in XbaI and XhoI sites of pBBR1Tp	Motin collection [111]
pB/crp	Cloned <i>crp</i> from KIM6+ in pBluescript SK+	Motin collection Unpublished
pCD1Ap	Virulence plasmid pCD1 of <i>Y. pestis</i> KIM labeled with Ap <sup>R</sup> marker	Provided by R. Perry

\* All *Y. pestis* strains contained plasmids pMT and pPCP. Pgm: pigmentation locus. pCD: virulence plasmid encoding T3SS. Gly: aerobic glycerol fermentation. *glpD*<sup>+</sup>: functional *glpD* gene of KIM6+. *glpD*<sup>'</sup>: defective *glpD* gene of CO92. Km<sup>R</sup>, Ap<sup>R</sup>, Tp<sup>R</sup>, and Suc<sup>S</sup> are markers of resistance to kanamycin, ampicillin, trimethoprim, and sensitivity to sucrose, respectively. The *kan* and *sacB* genes correspondingly enable kanamycin resistance and sucrose sensitivity.

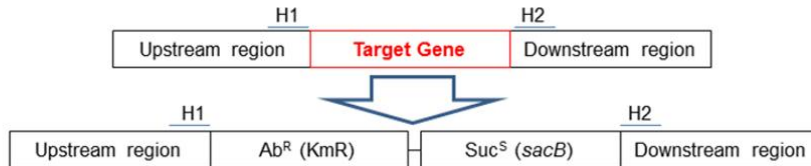
### Scarless Deletion of *crp*, Allelic Exchange of *glpD*, and Plasmid Complementation

The *crp* gene was excised from *Y. pestis* KIM6+ and CO92 strains in a scarless fashion [30,113] (**Fig. 3**). To do so, the counter-selective *sacB* gene was incorporated alongside the kanamycin resistance *kan* gene in pKD4 to obtain pKD4\_Km-*sacB* plasmid [111]. The target gene was replaced with a kanamycin-resistant/sucrose sensitive cassette (Km<sup>R</sup>/Suc<sup>S</sup>) deletion construct via Lambda Red Recombinase mediated crossover recombination in electrocompetent *Y. pestis* expressing the pKD46 helper plasmid. A secondary recombination event was employed to expel the deletion construct with a customized commercial gBlock (IDT, San Jose, CA) comprised of the upstream/downstream sequences directly flanking the gene of interest. Verification of gene deletion was afforded by sequencing. Retention of the *pgm* locus was confirmed via PCR of the *hmsHFRS* operon. Plasmid complementation was afforded by incorporation of *crp* in the pBluescript II SK(+) expression vector.

**Step 1.** Independently amplify antibiotic resistance ( $Ab^R$ )/sucrose sensitivity ( $Suc^S$ ) cassette with primers containing overhangs homologous to target gene flanking regions; gBlock consisting of target gene flanking sequence; and the target gene of interest



**Step 2.** Transformation and  $\lambda$  Red-mediated recombination to replace target gene with the selection cassette



**Step 3.** Secondary transformation and recombination to replace the selection cassette with the gene of interest (via gBlock) or to restore wild-type gene (via target gene amplicon)

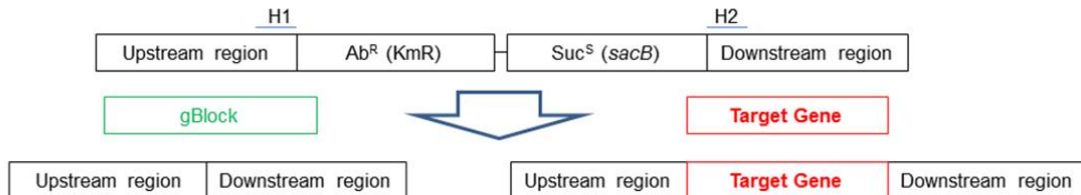


**Figure 3: Scarless Deletion and Allelic Exchange Procedure.**

**Step 1.** A dual selection kanamycin-resistance ( $Km^R$ ) and sucrose-sensitivity ( $Suc^S$ ) cassette incorporated in pKD4 was amplified with primers containing overhangs homologous to the target gene upstream/downstream flanking sequences. The gene of interest (allelic exchange) or gBlock gene fragment comprised of target gene flanking regions (scarless deletion) was amplified in an analogous fashion.

**Step 2.** Via  $\lambda$ -Red recombination afforded by pKD46 induction, the target gene was replaced with the  $Km^R$ -  $Suc^S$  deletion cassette.

**Step 3.** A secondary recombination event was utilized to either replace the deletion cassette with the previously amplified gene of interest, thereby exchanging the target gene with the gene of interest (allelic exchange). Alternately, the deletion cassette was exchanged with a gBlock fragment, thus excising the target gene (scarless deletion). Moreover, through subsequent recombination events, excised genes can be chromosomally restored, circumventing the need for plasmid complementation.

The functional *glpD* gene of *Y. pestis* strain KIM6+ (biovar Medievalis) was chromosomally exchanged with the disrupted *glpD'* allele of *Y. pestis* strain CO92 (biovar Orientalis), yielding strain KIM6+ *glpD'* [111]. Furthermore, a reciprocal exchange repaired the defective *glpD'* of CO92L with the functional *glpD* of KIM6+, yielding strain CO92L *glpD*+. To do so, crossover homologous recombination was utilized to replace the native *glpD* gene in both CO92L and KIM6+ with a Km<sup>R</sup>/Suc<sup>S</sup> cassette amplified from the pKD4\_Km-sacB plasmid via Lambda Red recombination afforded by the pKD46 helper plasmid. A secondary recombination event scarlessly replaced the deletion cassette with the desired *glpD* sequence attained through 10% sucrose counter-selection as verified by sequencing. The *glpD* gene and the *glpFKX* operon derived from KIM6+ were cloned into pBluescript II SK(+) and pBBR1Tp expression vectors, respectively.

### **Growth Kinetics**

Bacteria derived from glycerol stocks were cultured on Heart Infusion Agar (HIA) plates for 18-24 hours at 26°C. Bacteria were sub-cultured in Heart Infusion Broth (HIB) at 26°C for 12-18 hours whilst shaking at 250 rpm. Fresh HIB was inoculated with OD<sub>600</sub> = 0.2 and grown for 3 hours at 26°C whilst shaking at 250 rpm to obtain actively growing bacteria. Cultures were centrifuged at 4.5K rpm for 15 min at 26°C. Residual media was aspirated and the bacteria were washed in K-phosphate buffer (pH = 7.2). Bacteria were re-suspended to an OD<sub>600</sub> = 1.0 in K-phosphate buffer. Twenty-five milliliters of either HIB or BCS [76] chemically defined media supplemented with 0.2% of designated carbon sources were inoculated to an OD<sub>600</sub> = 0.1 and incubated at 26°C whilst shaking at 250 rpm. One milliliter aliquots were extracted at 0, 2, 6, 12, 24, 48, and 72 hours post-inoculation for optical density determination.

### **Crystal Violet Assay Biofilm Quantification**

Biofilm formation was quantified via crystal violet assay [30,111]. Bacterial strains were cultured and suspended to an  $OD_{600} = 1.0$  in K-phosphate buffer as previously described for the growth kinetic experiments. 24-well polystyrene plates were inoculated with 4-6 replicates of 0.75 ml of HIB or BCS supplemented with 0.2% of designated carbon sources containing  $OD_{600} = 0.1$  bacteria. Plates were incubated at 26°C for 24 or 72 hours whilst shaking at 250 rpm. Media was aspirated, wells were washed with dH<sub>2</sub>O, and bacteria retained in the biofilms were stained with 0.01% crystal violet for 20 min. Crystal violet dye was aspirated and wells were washed three times with dH<sub>2</sub>O. Bound crystal violet was solubilized with 1.5 ml of 33% acetic acid while shaking at 150 rpm for 15 min. Absorbance was measured utilizing a BioTek Synergy HT (BioTek, Winooski, VT) at 570 nm. In order to augment CRP activity, either BCS medium utilizing 0.2% glucose as the sole carbon sources or HIB medium were supplemented with 3 mM cAMP. In all cases, error bars reflect standard deviation from the mean of two independent experiments, each consisting of 4-6 technical replicates. Moreover, statistical significance (p-value <0.05) was determined by two-tailed Student's T test.

### **Rate of *pgm* Locus Excision**

CO92 and CO92 $\Delta$ *crp* were cultured and suspended to an  $OD_{600} = 1.0$  in K-phosphate buffer as previously described for the growth kinetic experiments. Fifty milliliters of fresh HIB media was inoculated with  $OD_{600} = 0.1$  of either strain in 500 ml flasks incubated at 26°C while shaking at 250 rpm. Alternately, CO92 was cultured in BCS media supplemented with either 0.2% K-gluconate or 0.2% glucose. After 3 hours post-inoculation to ensure entry to the logarithmic growth phase, dilution series were plated on Congo red media supplemented with 0.2% galactose [53]. Following incubation

at 26°C for 24-48 hours, the frequency of pigmentation negative clones were phenotypically determined.

### **Semi-Quantitative Reverse Transcriptase PCR (RT-PCR)**

The Access RT-PCR System (Promega, Madison, WI) was utilized to compare the expression of previously characterized biofilm-related genes amongst CO92 and CO92 $\Delta$ *crp* during growth in HIB medium as well as between CO92 cultured in chemically defined BCS media supplemented with either 0.2% glucose or 0.2% K-gluconate. Cultures were pre-grown as previously described. 300 ml of the appropriate media was inoculated with OD<sub>600</sub> = 0.075 of bacteria in 1 L flask. The culture was incubated at 26°C while shaking at 250 rpm for 6 hours. At this time, approximately 4.0x10<sup>9</sup> cells per sample as determined by optical density were added to an equal volume of 4°C RNAlater Stabilization Solution (Ambion, Austin, TX). Total RNA was isolated using the RNeasy mini column kit (Qiagen, Hilden, Germany) and processed by the TURBO DNA-free kit (Ambion) for DNase treatment. RNA concentration and purity was determined through Synergy HT Take3 Multi-Volume Plate (BioTek). RT-PCR reactions were performed in accordance with manufacturer guidelines using 25 ng of total RNA for 25 PCR cycles. Three microliter aliquots of the RT-PCR reactions were visualized on 2% agarose gels infused with ethidium bromide. Semi-quantitative analyses were performed by ImageJ v1.47 (<http://rsb.info.nih.gov/ij/>) with normalization to the *gyrB* gene [111,115,116,117].

### **Phenotypic Assessment of Glycerol Fermentation**

To determine the capacity for the various mutants to ferment glycerol, strains were cultured on MacConkey Agar Base indicator plates (Difco 281810) supplemented

with 0.2% glycerol and incubated for 18-24 hours at both 26°C and 37°C. Results were verified via growth on acid-fuchsin plates utilizing 0.2% glycerol as the sole carbon source [111,118].

### **Phylogenetic Analyses**

Full-length genomic sequences of *glpD*, *glpK*, and *glpX* of 41 biovar Orientalis isolates obtained from GenBank were evaluated with SeaView version 4.5.0 [119]. Sequence read archive (SRA) reads were pre-aligned using NCBI BLAST. A maximum parsimony tree was generated with 200 bootstrap replicates. The tree was rooted to biovar Orientalis predicted ancestral strain, E1979001 [7]. The *glpFKX* operon of strain Salazar was sequenced and submitted to GenBank as accession number KJ719254 [111].

### **Intracellular Glycerol-3-Phosphate Quantification**

*Y. pestis* strains KIM6+ : pCD1Ap and KIM6+ *glpD*' : pCD1Ap were cultured on HIA plates containing 50 µg/mL carbenicillin (Cb50) and incubated at 26°C for 18-24 hours. Bacteria were re-streaked on fresh HIA/Cb50 plates and incubated for an additional 12-18 hours at 26°C. 50 ml of HIB/Cb50 were inoculated with OD<sub>600</sub> = 0.1 and incubated for 12 hours at 26°C whilst shaking at 250 rpm. Bacteria were sub-cultured to an OD<sub>600</sub> = 0.1 in seventy-five milliliters of fresh HIB/Cb50 supplemented with 0.2% glycerol and incubated at either 26°C or 37°C whilst shaking at 250 rpm. At 3 hours post-inoculation, approximately 2x10<sup>9</sup> cells of either strain as determined by optical density readings were harvested. Following centrifugation at 4.5K rpm for 10 min at 4°C, growth media was aspirated.

One set of samples was processed by methanol/chloroform extraction [120]. Briefly, the bacterial pellets were washed with 1 ml of 150 mM ammonium bicarbonate

and re-suspended in 0.75 ml cold methanol (-20°C). The mixture was homogenized with approximately 300 µl of cold zirconia beads (-20°C) utilizing a microtube homogenizer (Benchmark, South Plainfield, NJ) for 3 series at 4.5K rpm for 30 sec followed by a resting stage on ice for 60 sec. 0.4 ml of molecular grade water and 0.25 ml of chloroform were added each sample. Approximately 0.75 ml of the aqueous phase was extracted following phase separation by centrifugation (5 min, 13K rpm).

Alternately, direct cell lysates of duplicate samples were prepared by suspending the bacterial pellets in 400 µl of G3P detection assay buffer (Biovision, Milpitas, CA). Samples were homogenized with 300 µl of cold zirconia beads (-20°C) utilizing a microtube homogenizer (Benchmark) for 3 series at 4.5K rpm for 30 sec followed by a resting stage on ice for 60 sec. Samples were centrifuged at 12K rpm for 10 min at 4°C and approximately 350 µl of the supernatant was extracted.

Two-fold dilution series of 50 µl, 25 µl, and 12.5 µl of sample extracts were assessed by G3P detection via colorimetric assay (Biovision) performed in accordance with manufacturer guidelines. In addition, direct lysates of CO92L and CO92L *glpD*<sup>+</sup> grown at 37°C were analyzed as previously described. Statistical significance amongst relative sample G3P concentrations was determined by Student's T test [111].

## RESULTS

### Growth Kinetics of the *crp* Deficient Mutants

Growth kinetics during incubation at 26°C in BCS medium of the *Y. pestis* CO92Δ*crp* (**Fig. 4A**) and KIM6+Δ*crp* (**Fig. 4B**) scarless deletion mutants were assessed.

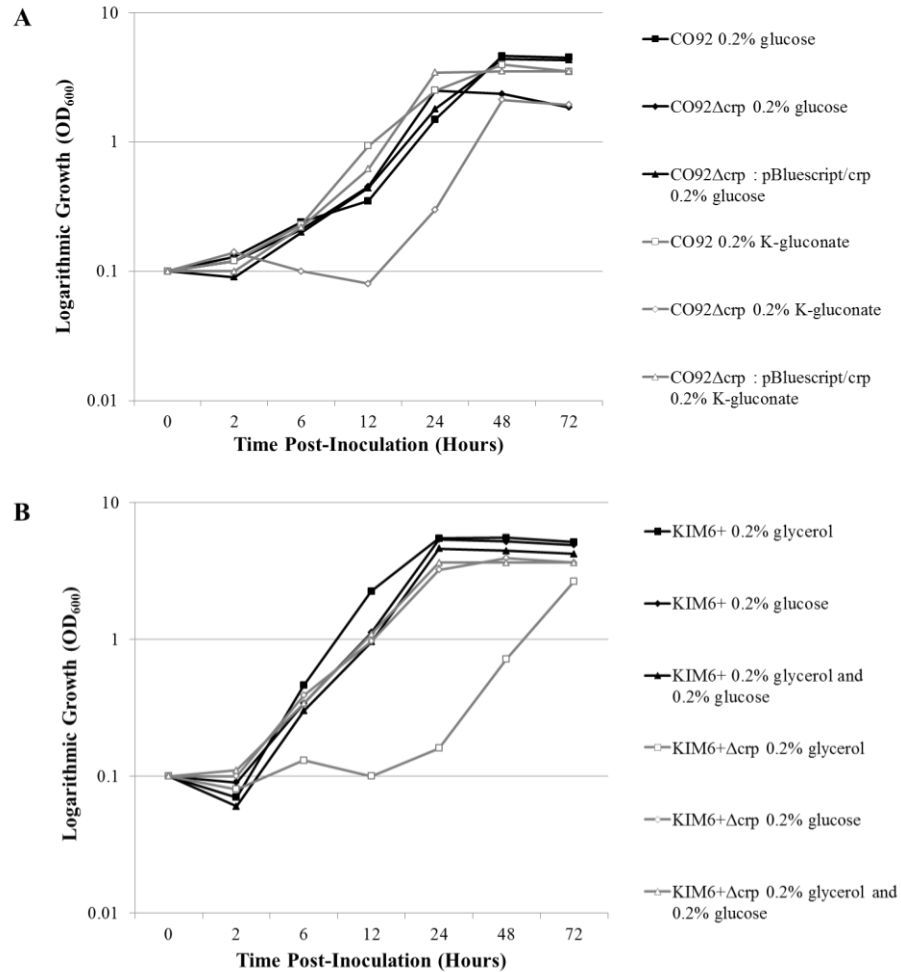


**Figure 4: Impaired Alternate Carbon Source Metabolism of the *Y. pestis crp*-deficient Mutants.**

- A.** Growth curves of CO92, CO92 $\Delta$ crp, and plasmid complemented CO92 $\Delta$ crp : pB/crp when grown in BCS medium supplemented with 0.2% glucose or 0.2% K-gluconate.
- B.** Growth curves of KIM6+ and KIM6+ $\Delta$ crp when cultured in BCS medium supplemented with either 0.2% glucose, 0.2% glycerol, or both 0.2% glucose and 0.2% glycerol.

Growth of the *crp*-deficient mutants were consistent with the respective isogenic controls during growth at 26°C in chemically defined BCS medium supplemented with glucose. However, the  $\Delta$ crp mutants demonstrated a stark delay in growth when inoculated in chemically defined medium solely supplemented with alternate carbon sources, demonstrating stringent CRP-mediated carbon catabolite repression in *Y. pestis*.

Exponential growth of the *crp*-deficient mutants resumed approximately 24 hours post-inoculation in chemically defined media solely supplemented with alternate carbon sources. After 72 hours post-inoculation, the bacterial density of the KIM6+ $\Delta$ *crp* and CO92 $\Delta$ *crp* mutants cultured in chemically defined media when solely utilizing alternate carbon sources were approximately 1.9-fold and 1.8-fold less than the respective isogenic controls.

Growth kinetics of the *crp*-deficient mutants demonstrated an approximate 2-fold reduction in bacterial density following 24 hours of growth at 26°C in peptide-rich HIB (Fig. 5).

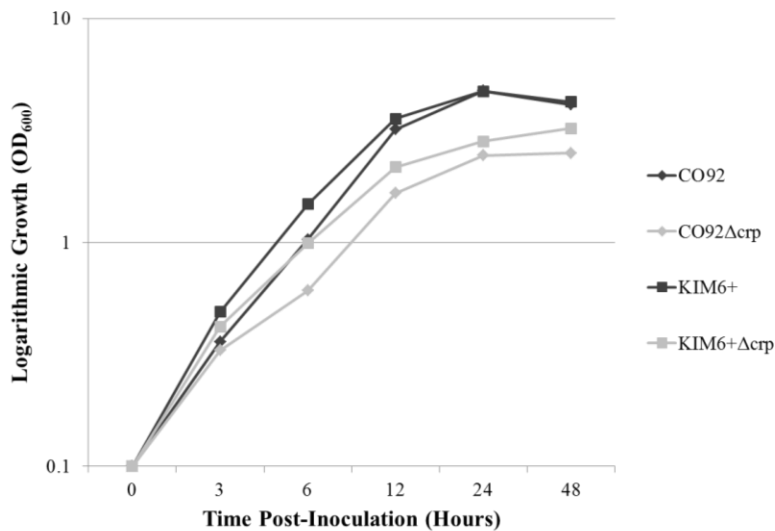


**Figure 5: Impaired 26°C Growth of the *Y. pestis crp*-deficient Mutants in HIB.**

Growth kinetics of the CO92 and KIM6+ *crp*-deficient mutants and respective isogenic controls when grown in HIB medium at 26°C.

Therefore, loss of *crp* in *Y. pestis* confers a significant growth defect during alternate carbon source metabolism as well as peptide catabolism. When cultured in medium solely supplemented with glucose, corresponding with a CRP-inactive environment, deletion of *crp* had not impact upon growth rate.

## Alternate Carbon Source Metabolism Promotes *Y. pestis* Biofilm Production

KIM6+ and CO92 biofilm production was quantified by crystal violet assay during growth in BCS chemically defined media supplemented with 0.2% glucose and/or 0.2% alternate carbon sources (**Fig. 6**).

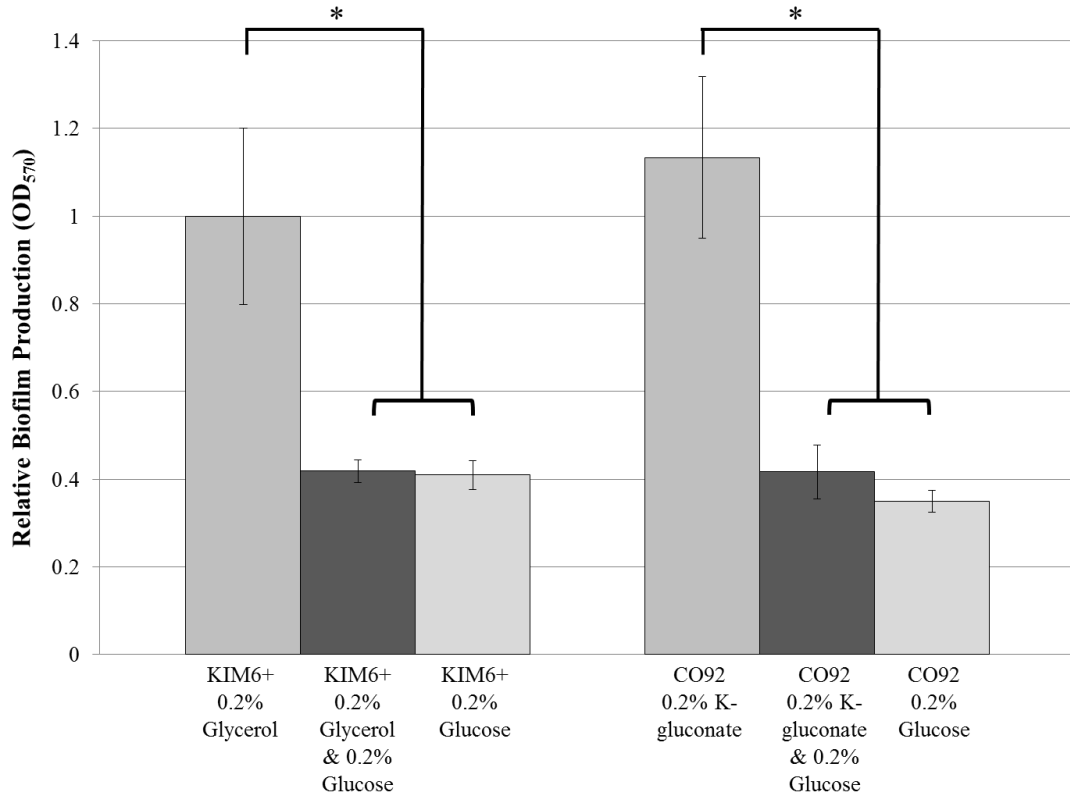


**Figure 6: BCS Carbon Catabolite Regulation of *Y. pestis* Biofilm Production.**

Crystal violet biofilm quantification assay of KIM6+ and CO92 when cultured in BCS media supplemented with primary (glucose) and/or alternate (glycerol or K-gluconate) carbon sources. Identical source inoculums per strain were utilized for each media type. Error bars reflect standard deviation from the mean derived from two independent experiments, each consisting of 6 technical replicates. \* P-value <0.05 determined by two-tailed Student's T test.

After 24 hours post-inoculation, the biofilm production of both KIM6+ and CO92 *Y. pestis* strains was robust when cultured in BCS medium solely supplemented with alternate carbon sources; whereas, the relative biofilm production was significantly impaired when grown in medium supplemented with glucose. Growth of *Y. pestis* in BCS solely supplementation with alternate carbon sources yielded >2-fold enhanced biofilm production in respect to the biofilm production in media containing glucose. It is important to note that the biofilm production during growth in BCS medium containing a combination of both primary and alternate carbon sources was significantly impaired in relative to the biofilm formation when grown in media solely supplemented with alternate carbon sources, indicative of a carbon catabolite repression effect. No change in growth rate was observed for either *Y. pestis* strain during culture in BCS medium supplemented with alternate or primary carbon sources when incubated at 26°C. Thus, the alterations in biofilm formation are independent of carbon source dependent growth discrepancies.

Comparable trends were observed during growth of *Y. pestis* in peptide-rich HIB medium during incubation at 26°C. Supplementation of HIB with alternate carbon sources enhanced biofilm production; however, the addition of glucose to HIB did not significantly alter biofilm formation (**Fig. 7a**). Supplementation of HIB with 2.5% alternate carbon sources produced a greater than 2-fold enhancement of biofilm production in respect to unaltered HIB or HIB supplemented with 2.5% glucose. Therefore, these results demonstrate that *Y. pestis* biofilm production is strongly induced during the metabolism of alternate carbon sources, but repressed during the metabolism of primary carbon sources. Moreover, relative to BCS medium supplemented with alternate carbon sources, growth in non-supplemented HIB medium yielded poor biofilm production, indicating peptide catabolism does not promote robust *Y. pestis* biofilm formation (**Fig. 7b**).

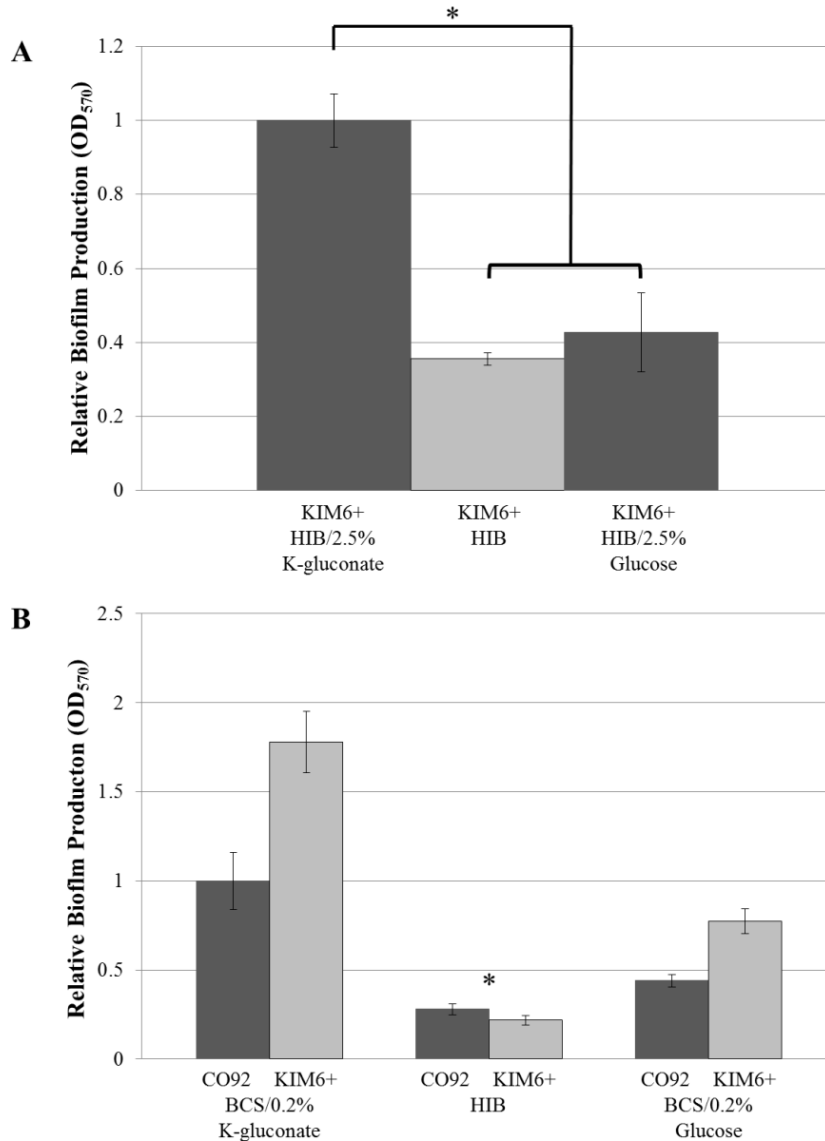


**Figure 7: HIB Carbon Catabolite Regulation of *Y. pestis* Biofilm Production.**

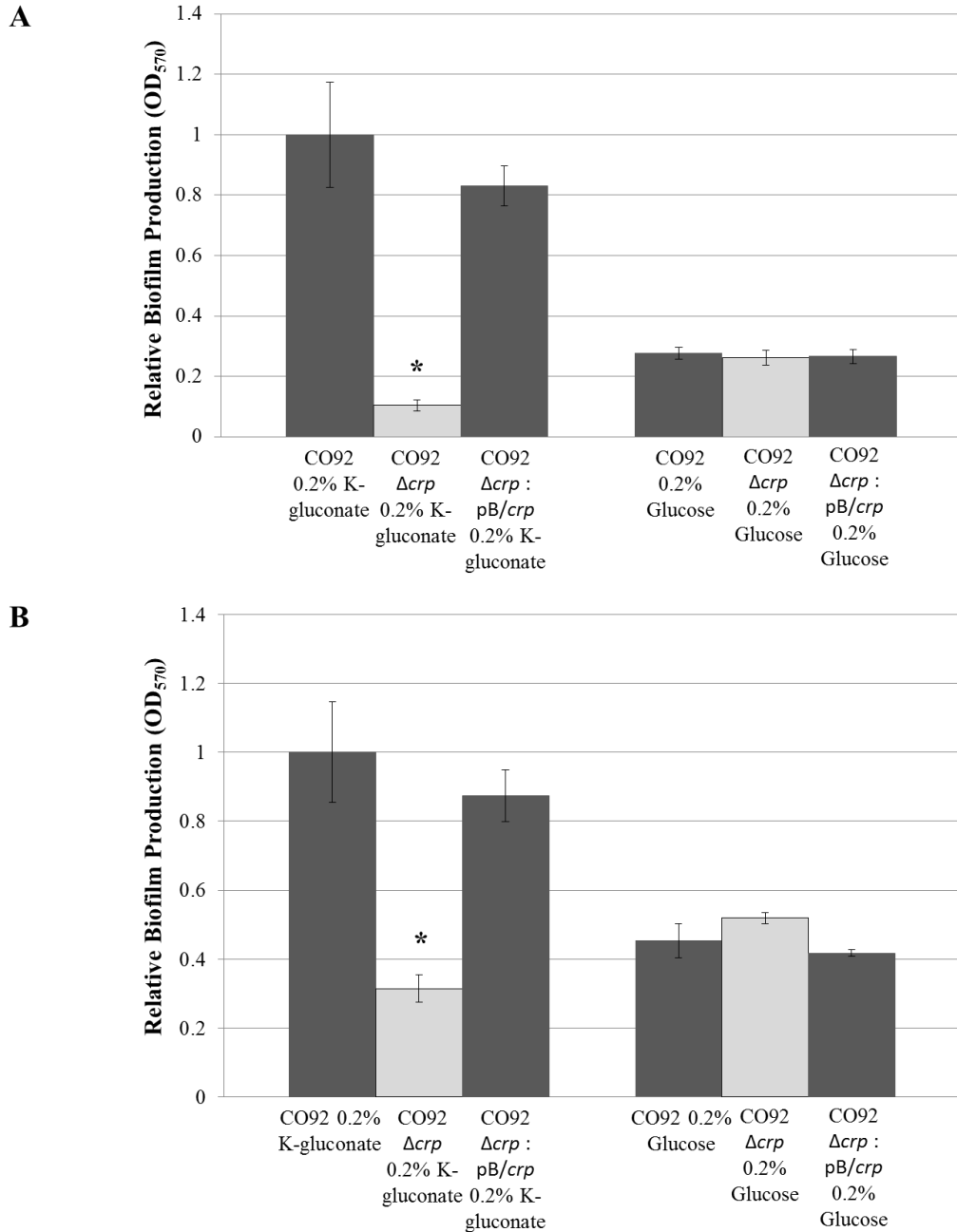
**A.** Relative biofilm production of KIM6+ following 24 hours post-inoculation of standard HIB medium, HIB supplemented with 2.5% K-gluconate, or HIB supplemented with 2.5% glucose.

**B.** Relative biofilm production of both CO92 and KIM6+ after 24 hours post-inoculation of BCS supplemented with 0.2% K-gluconate, HIB, or BCS supplemented with 0.2% glucose.

Identical source inoculums per strain were utilized for each media type. Error bars reflect standard deviation from the mean derived from two independent experiments, each consisting of 6 technical replicates. \* P-value <0.05 determined by two-tailed Student's T test.

## CRP Facilitates Carbon Catabolite Regulation of *Y. pestis* Biofilm Formation

When grown in the presence of glucose, no change in biofilm production was observed amongst the scarless *crp* deletion mutants constructed in both CO92 (**Fig. 8**) and KIM6+ (**Appendix A Fig. 1**) strains of *Y. pestis*.



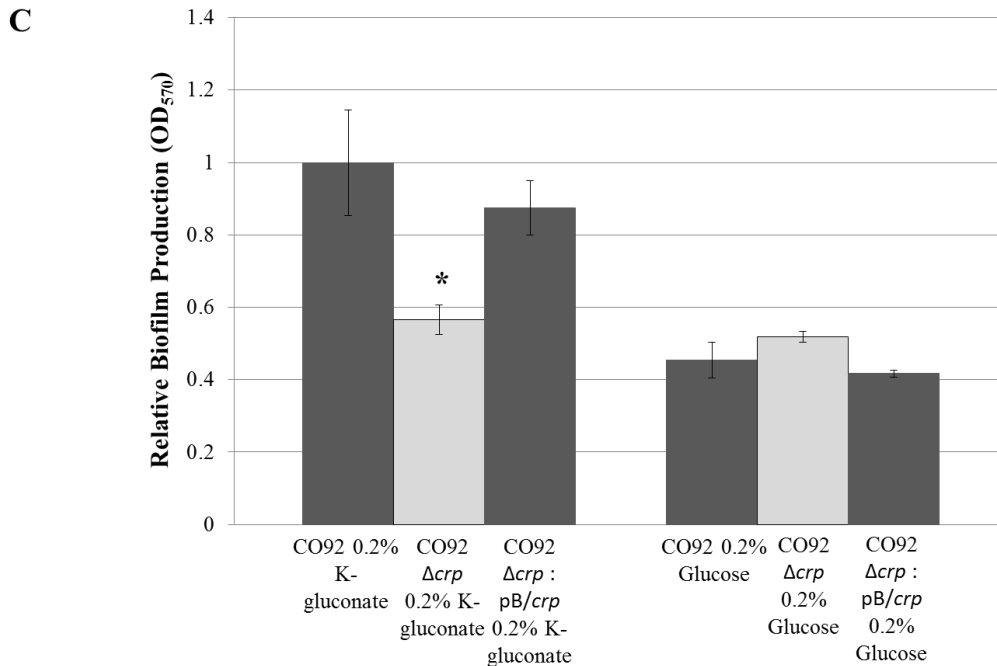


**Figure 8: CRP Enables Robust *Y. pestis* Biofilm Production.**

- A.** Relative biofilm production of CO92, CO92 $\Delta crp$ , and plasmid complemented CO92 $\Delta crp$  : pB/crp following 24 hours post-inoculation of BCS medium supplemented with either 0.2% K-gluconate or 0.2% glucose.
- B.** Relative biofilm production after 72 hours post-inoculation.
- C.** Normalization of the 72 hours post-inoculation relative biofilm production to culture optical density.

Error bars reflect standard deviation from the mean derived from two independent experiments, each consisting of 6 technical replicates. \* P-value <0.05 determined by two-tailed Student's T test.

Deletion of *crp* from either genetic background severely impaired biofilm production after 24 hours post-inoculation in BCS chemically defined medium solely supplemented with alternate carbon sources (**Fig. 8A**). In order to account for the previously described growth deficiency of the *crp*-deficient mutants, biofilm production was determined at 72 hours post-inoculation (**Fig. 8B**) and subsequently normalized to culture optical densities (**Fig. 8C**). Despite normalization, the biofilm formation *crp*-deficient mutant was significantly reduced during growth in BCS chemically defined media supplemented with alternate carbon sources.

*Y. pestis* biofilm production during growth in media supplemented with cAMP, a small molecule activator of CRP, was quantified (**Fig 9**).

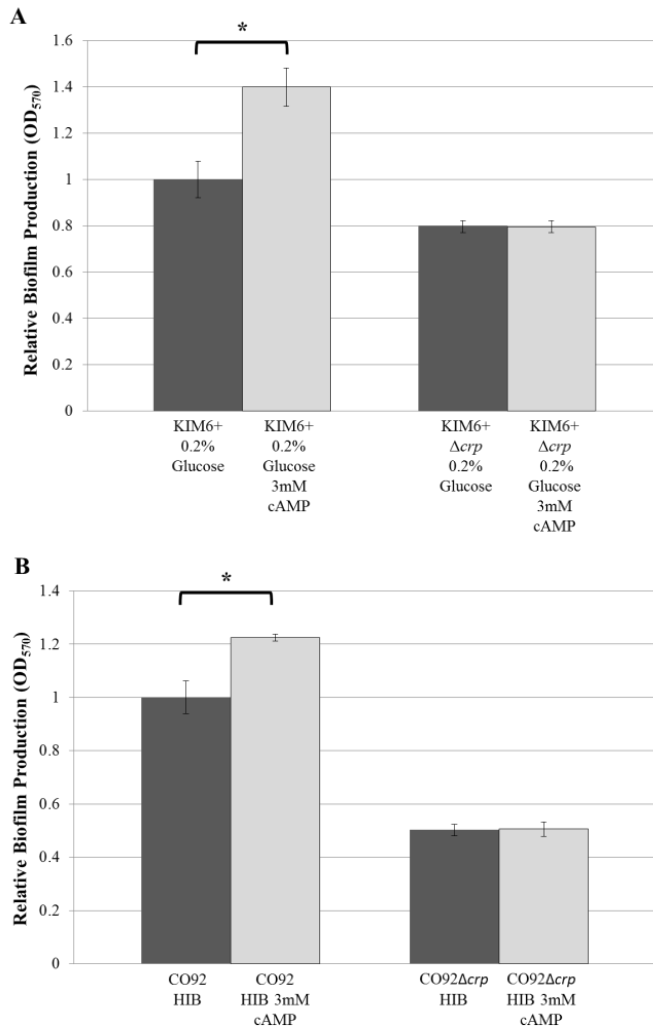


**Figure 9: Exogenous cAMP Enhances *Y. pestis* Biofilm Formation.**

**A.** Relative biofilm production of KIM6+ and KIM6+ $\Delta crp$  when grown in BCS medium supplemented with 0.2% glucose containing either 3 mM cAMP prepared in K-phosphate buffer or K-phosphate.

**B.** Relative biofilm production of CO92 and CO92 $\Delta crp$  when grown in HIB medium in the presence of 3 mM cAMP or K-phosphate buffer.

Identical source inoculum per strain was utilized for each media type. Error bars reflect standard deviation from the mean derived from two independent experiments, each consisting of 6 technical replicates. \* P-value <0.05 determined by two-tailed Student's T test.

Biofilm production of KIM6+ when grown in BCS media supplemented with 0.2% glucose was significantly enhanced upon addition of 3 mM cAMP (**Fig. 9A**). Furthermore, growth of CO92 in peptide-rich HIB containing 3 mM cAMP was similarly enhanced (**Fig. 9B**). However, exogenous cAMP had no effect upon the biofilm formation of either the KIM6+ or CO92 *crp*-deficient mutants regardless of media composition. These observations demonstrate that CRP confers a positive regulatory effect upon *Y. pestis* biofilm production. The cAMP-induced enhancement of *Y. pestis* biofilm production, although statistically significant, is relatively mild. Thus, CRP primarily facilitates the metabolism of alternate carbon sources, thereby indirectly stimulating *Y. pestis* biofilm production.

Biofilm production of the CO92 and KIM6+ *crp*-deficient mutants were also determined to be significantly impaired after 24 hours post-inoculation of HIB medium (**Fig. 10**).

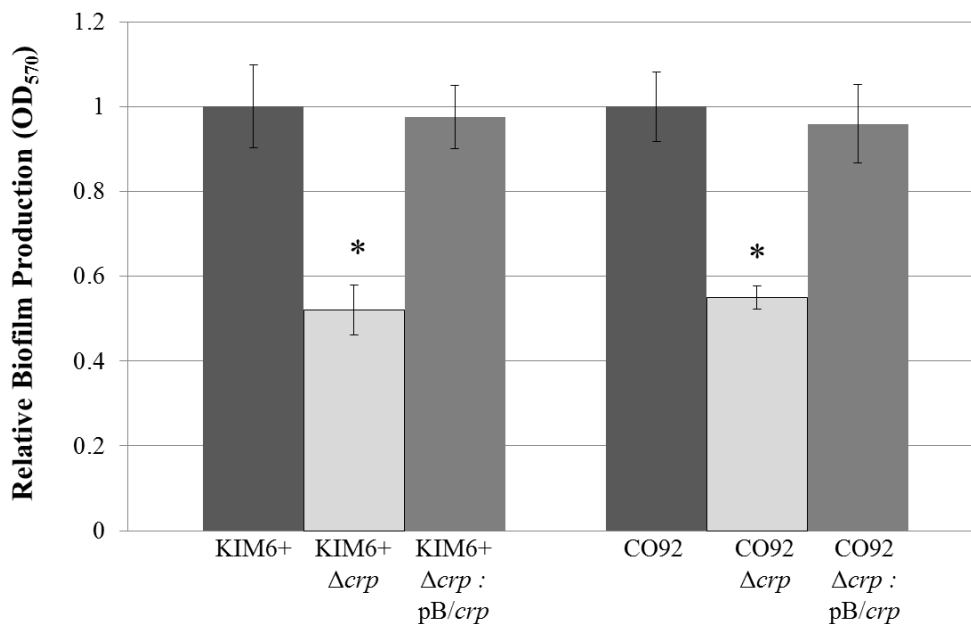


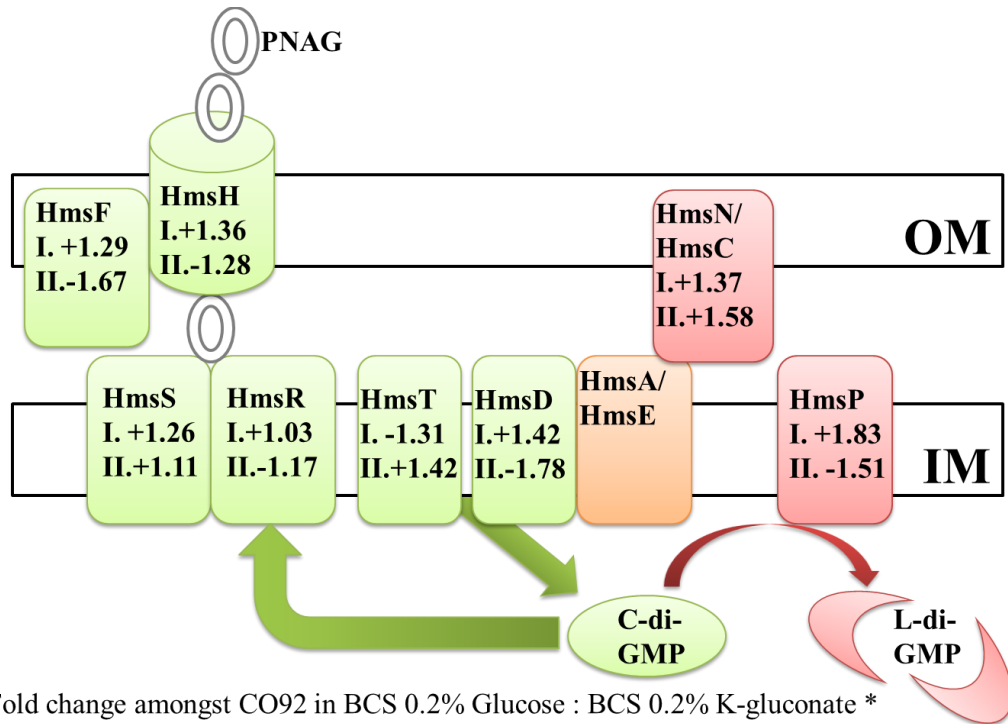
**Figure 10: CRP Promotes *Y. pestis* Biofilm Production in HIB.**

Relative biofilm production of KIM6+ and CO92 *crp*-deficient mutants relative to the respective isogenic controls and plasmid complemented mutants after 24 hours post-inoculation in HIB medium. Error bars reflect standard deviation from the mean derived from two independent experiments, each consisting of 4 technical replicates. \* P-value <0.05 determined by two-tailed Student's T test.

Loss of *crp* resulted in an approximate 2-fold reduction in biofilm production, relative to the isogenic and plasmid complemented controls. However, upon accounting for the aforementioned ~2-fold growth defect of the *crp*-deficient mutants when cultured in HIB medium, no significant alteration in biofilm production was discerned. In accordance with the cAMP supplementation findings, CRP likely promotes *Y. pestis* biofilm production when cultured in HIB by stimulating growth as opposed to direct regulatory modulation.

**CRP does not Regulate Transcription of Characterized Biofilm-Related Genes**

CRP, a global DNA-binding transcriptional regulator, may control the expression of previously characterized *hms* biofilm-related genes. Gene expression amongst CO92 and the CO92 $\Delta$ *crp* mutant during growth in HIB was compared. Moreover, the transcription of biofilm-related genes was analyzed amongst growth of CO92 cultured in chemically defined media utilizing either glucose or K-gluconate as the sole carbon source. Following normalization to the *gyrB* gene, semi-quantitative analyses via ImageJ software did not reveal any changes in the gene expression of biofilm-related genes (**Fig. 11; Appendix A Fig. 2**). Therefore, CRP-mediated carbon catabolite modulation of biofilm formation does not occur through transcriptional regulation of *hms* biofilm-related genes.



I. Fold change amongst CO92 in BCS 0.2% Glucose : BCS 0.2% K-gluconate \*  
 II. Fold change amongst CO92 : CO92Δcrp \*

\* Following *gyrB* normalization

**Figure 11: Semi-quantitative RT-PCR of the *Y. pestis* Hms System.**

Depiction of semi-quantitative RT-PCR fold changes in expression of the *Y. pestis* Hms biofilm formation/regulation system following normalization to the *gyrB* gene. Factors colored in green stimulate biofilm production; whereas, proteins that are colored in red repress biofilm formation.

- I. Fold changes in expression amongst CO92 grown in BCS medium supplemented with either 0.2% glucose or 0.2% K-gluconate.
- II. Fold changes in expression amongst CO92 and CO92Δcrp when grown in HIB medium.

### **Molecular Basis of Glycerol Deficiency of biovar Orientalis Isolates.**

In order to elucidate the potential interplay amongst *Y. pestis* glycerol metabolism and CRP regulation of biofilm formation, the molecular mechanism defining biovar Orientalis glycerol fermentation deficiency had to be discerned. Phenotypic determination of glycerol fermentation afforded by growth on MacConkey and fuchsin-infused indicator plates supplemented with 0.2% glycerol demonstrated the 93 bp in-

frame deletion present in all biovar Orientalis isolates is sufficient to impair glycerol fermentation in KIM6+ strain. Moreover, plasmid complementation of *glpD* from KIM6+ restored glycerol fermentation in the KIM6+ chromosomal allelic exchange mutant.

Conversely, sole chromosomal exchange of the defective CO92L *glpD* with the functional *glpD* gene of KIM6+ was insufficient to restore glycerol fermentation. Furthermore, independent plasmid expression of either the *glpD* gene or the *glpFKX* operon derived from KIM6+ did not facilitate glycerol fermentation in CO92L. However, CO92L glycerol fermentation was enabled by dual expression of KIM6+ derived *glpD* and *glpFKX* genes. The ability to ferment glycerol in seven other biovar Orientalis isolates of *Y. pestis* isolated from distinct geospatial origins were similarly afforded upon complementation of both *glpD* and *glpFKX* genes (**Table 3; Appendix A Figs. 3 & 4**). Therefore, the 93 bp in-frame deletion in the *glpD* gene evident in biovar Orientalis isolates is sufficient to cause the deficiency in glycerol fermentation; however, the inability to ferment glycerol is often ensured by additional impairments of the *glpFKX* operon (all of which notably disrupt the *glpK* gene).

**Table 3: Characterization of *Y. pestis* Glycerol Fermentation**

<i>Y. pestis</i> strain : plasmid	Glycerol fermentation
KIM 6+	Positive
KIM 6+ <i>glpD</i> '	Negative
KIM 6+ <i>glpD</i> ' : pBGLPD5	Positive
CO92L*	Negative
CO92L : pBGLPD5*	Negative
CO92L : pTpGLPFKX6*	Negative
CO92L : pBGLPD5, pTpGLPFKX6*	Positive
CO92L <i>glpD</i> +	Negative
CO92L <i>glpD</i> + : pBGLPD5	Negative
CO92L <i>glpD</i> + : pTpGLPFKX6	Positive

\* Results consistent with 7 other biovar Orientalis strains used in this study.

Reproduced with permission [111].

Analysis of *Y. pestis* genome sequences deposited to date in the GenBank database revealed that all biovar Orientalis isolates, with the exception of strains YN1065 and YN1683, contained identical 93 bp in-frame deletion in *glpD* gene. In addition to the deletion in *glpD*, all biovar Orientalis strains aside from Chinese isolates F1984001, CMCC87001, and YN663 displayed a variety of disruptions in the *glpFKX* operon. Strain CO92L possessed an extensive 941 bp deletion that disrupted both *glpK* and *glpX* genes. Mutations in other isolates consisted of non-synonymous substitutions, single and multiple nucleotide insertions or deletions, as well as point mutation, resulting in amino acid change. In all cases, the various mutations affected *glpK* (**Fig. 12**).

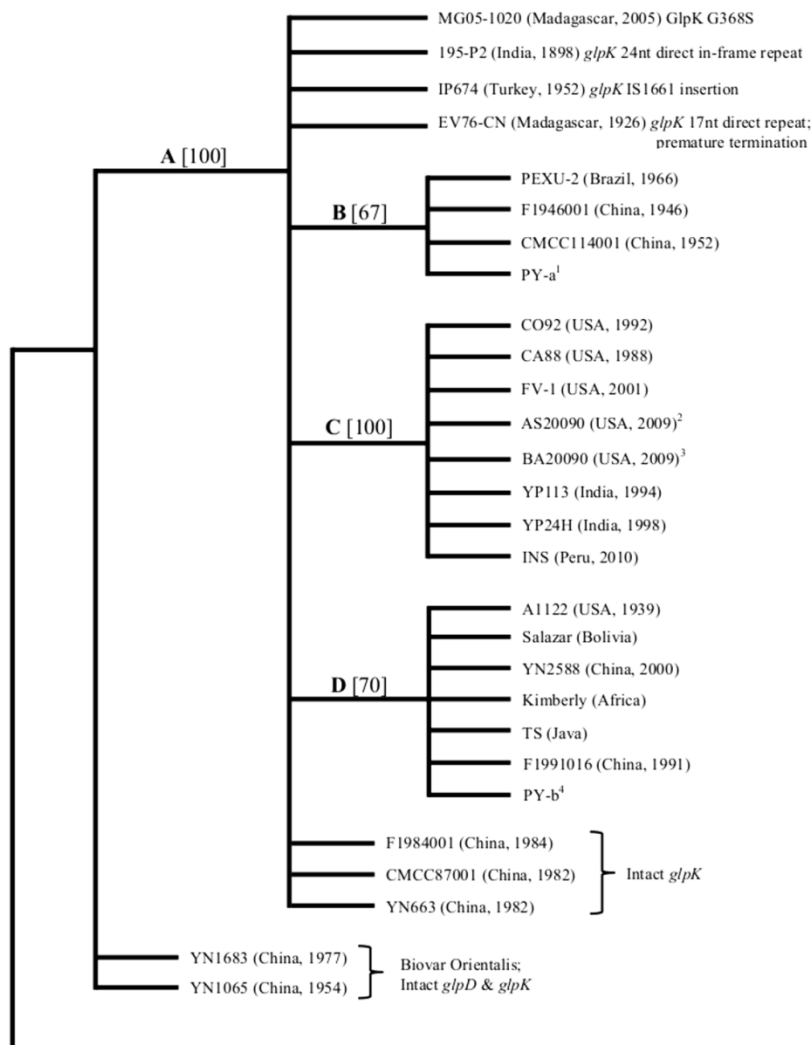


### Figure 12: Biovar Orientalis Glycerol Metabolism Maximum Parsimony Tree.

Maximum parsimony tree comparing *glpD*, *glpK*, and *glpX* amongst biovar Orientalis isolates rooted to biovar Antiqua strain E1979001 [7]. Branch bootstrap values calculated from 200 replicates.

A. Acquisition of the 93 bp in-frame *glpD* deletion and GlpD missense mutation (A125V).

B. *glpK* poly(A) region insertion.

C. *glpKX* pseudogene.

D. *glpK* poly(A) region deletion.

<sup>1</sup> PY strains 01-05; <sup>2</sup> AS20090 strains 1156, 1434, 1509, 1539, 2147; <sup>3</sup> BA20090 strains 1703, 1799, 1990, 2009; <sup>4</sup> PY strains 19, 71, 72, 76.

Reproduced with permission [111].

### Sole Deficiency of *glpD* does not Enhance G3P Accumulation

G3P, the product of GlpK, is capable of repressing CRP activation in *E. coli*, and therefore regulates catabolite repression. Thus, the degree of G3P accumulation in *Y. pestis glpD* allelic exchange mutants was quantified via colorimetric assay. The relative concentrations of G3P were found to be reduced in the *glpD* deficient KIM6+ mutant relative to the isogenic control when cultured to exponential phase following methanol/chloroform extraction. The parent KIM6+ strain demonstrated approximately 2.2-fold and 1.9-fold enhanced concentrations of G3P KIM6+ *glpD*' at either 26°C or 37°C, respectively (**Fig. 13A**). Moreover, KIM6+ direct cell lysates indicated an approximate 3.3-fold increase in G3P comparative to the *glpD*-deficient mutant. (**Fig. 13B**). No change in relative levels of G3P was detected amongst the CO92L and CO92L *glpD*+ mutant (**Fig. 13B**). Taken together, sole dysfunction of *glpD* impairs G3P accumulation. However, either upon combined impairment of both *glpD* and *glpK* or sole restoration of *glpD*, intracellular G3P is normalized. These findings indicate a potential regulatory feedback mechanism which represses G3P formation upon sole dysfunction of *glpD*.

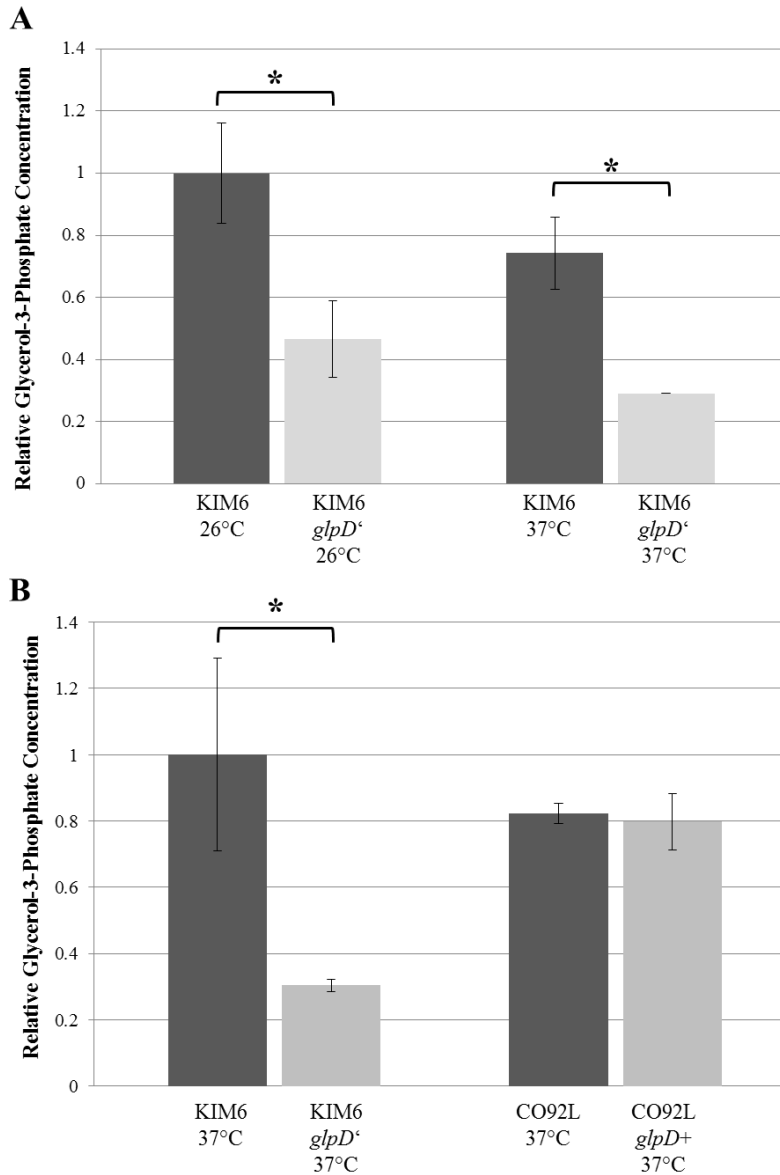


**Figure 13: Intracellular G3P Detection of the *glpD* Allelic Exchange Mutants.**

Relative intracellular G3P concentrations of the *Y. pestis glpD* allelic exchange mutants as determined by colorimetric assay.

**A.** Relative G3P concentrations comparing KIM6+ and KIM6+ *glpD'* when grown in HIB medium supplemented with 0.2% glycerol at both 26°C and 37°C following methanol/chloroform extraction.

**B.** Direct lysate relative G3P concentrations comparing KIM6+, KIM6+ *glpD'*, CO92L, and CO92L *glpD+* were grown to logarithmic phase in HIB medium supplemented with 0.2% glycerol at 37°C.

Error bars reflect standard deviation from the mean. \* P-value < 0.05 as determined by Student's T test. Reproduced with permission [111].

## Growth Kinetics and Biofilm formation of the *glpD* mutants.

Growth kinetics of the KIM6+ *glpD*' allelic exchange mutant were compared to the isogenic controls during growth in BCS medium supplemented with either 0.2% glucose, 0.2% glycerol, or a combination of both 0.2% glucose and 0.2% glycerol. (Fig. 14).

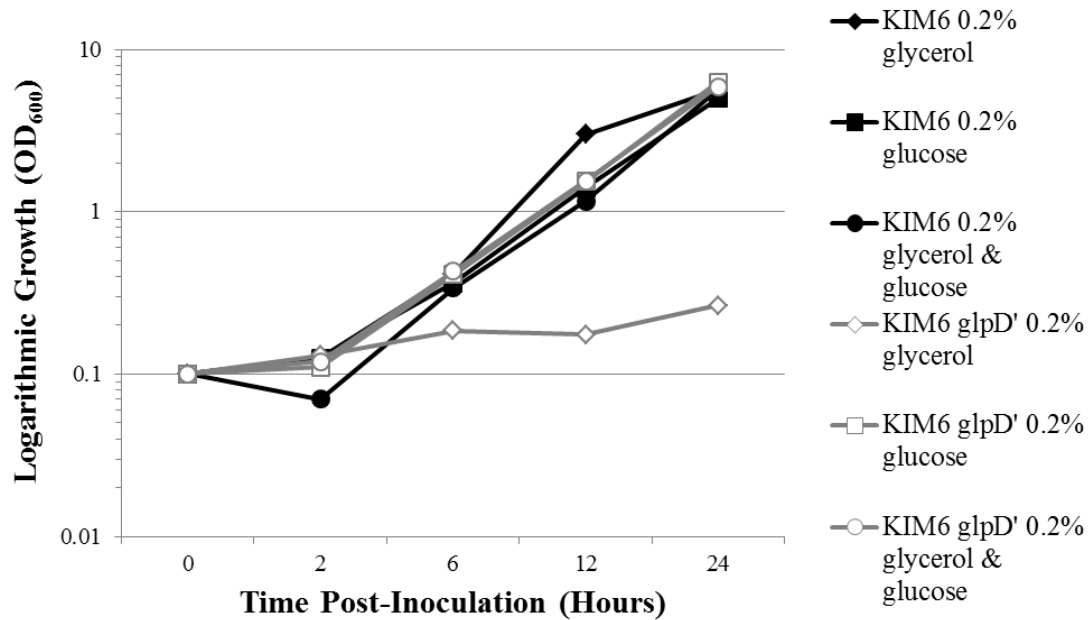


**Figure 14: Growth Kinetics of *glpD*-dysfunctional KIM6+**

26°C growth curve of *Y. pestis* strain KIM6+ *glpD*' mutant and the isogenic KIM6+ control in chemically defined BCS media supplemented with either 0.2% glycerol, 0.2% glucose, or both 0.2% glycerol and 0.2% glucose. Identical inoculum per strain were utilized for each media type. Reproduced with permission [111].

As an expected consequence of *glpD* dysfunction, no growth was observed in BCS medium solely supplemented with 0.2% glycerol. No alteration in growth rate was noted when the *glpD*-dysfunctional mutant was grown in BCS medium solely supplemented with 0.2% glucose or with a combination of both 0.2% glycerol and 0.2% glucose.

Relative biofilm formation comparing KIM6+, the *glpD*-dysfunctional mutant, and the plasmid complemented *glpD* mutant were quantified (**Fig 15**).

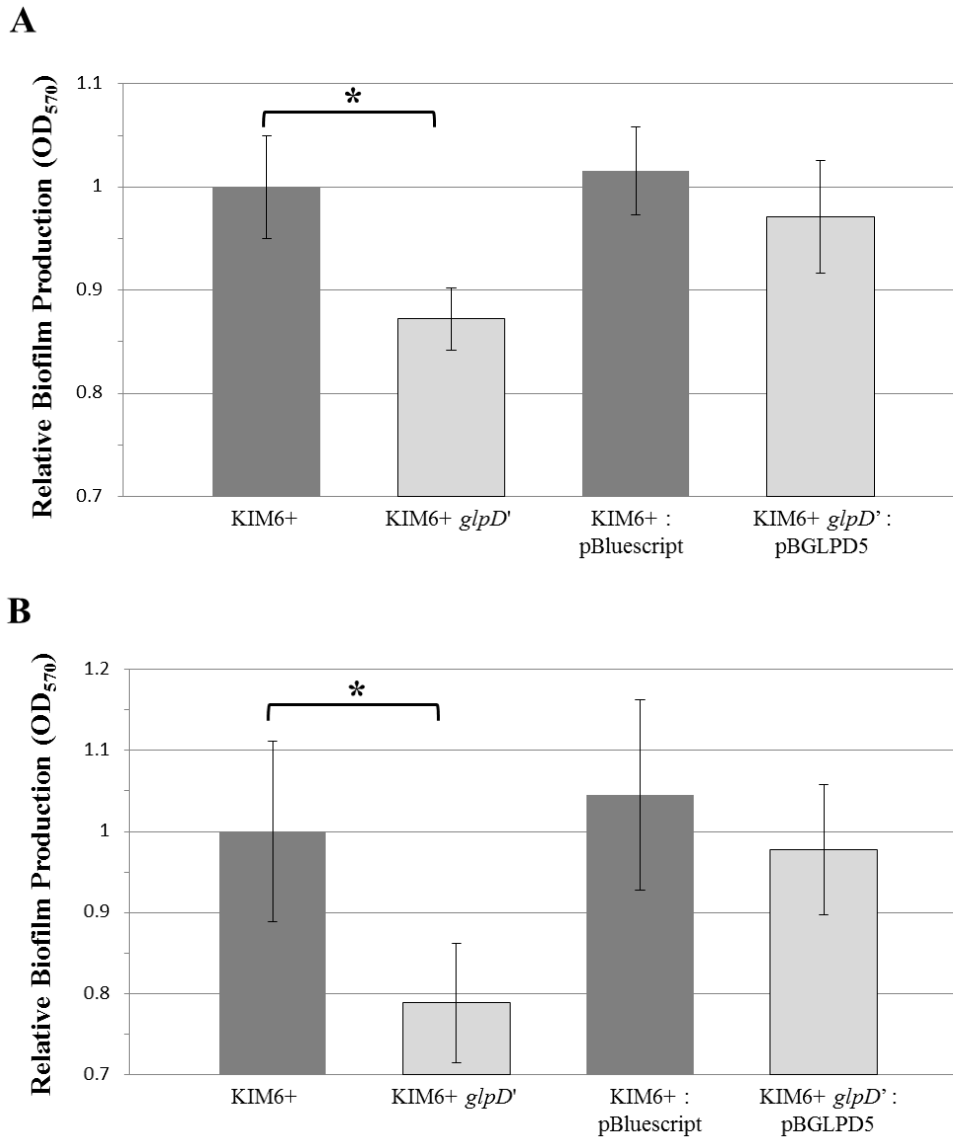
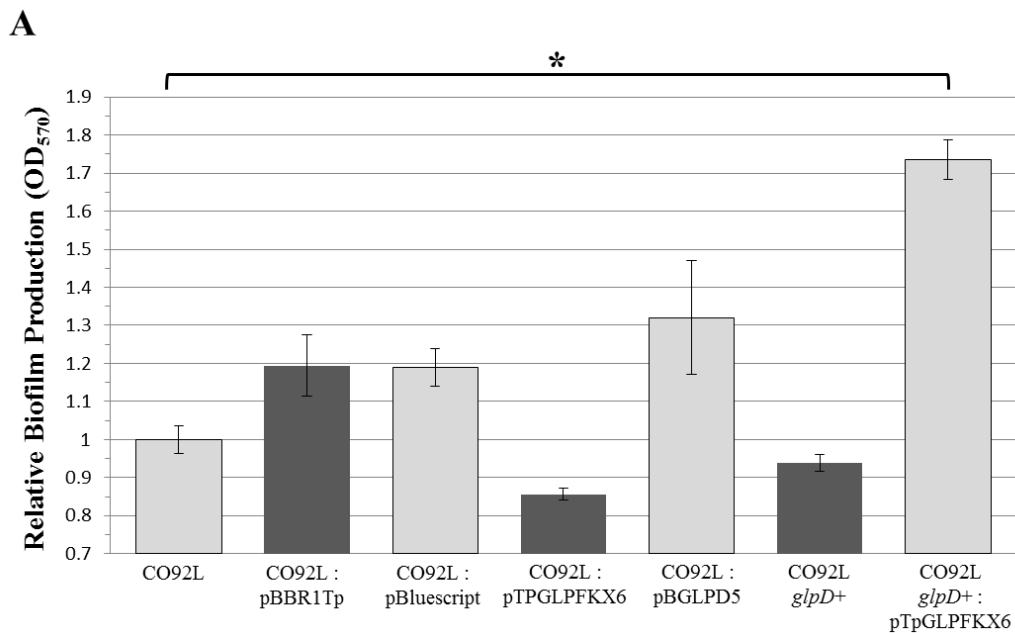


**Figure 15: Loss of *glpD* impairs KIM6+ Biofilm Production.**

Chromosomal replacement of the functional KIM6+ *glpD* gene with the dysfunctional biovar *Orientalis glpD* gene from CO92 significantly impaired biofilm production after 24 hours post-inoculation in either HIB medium (A) or BCS medium supplemented with 0.2% K-gluconate (B). Error bars reflect standard deviation from the mean of two independent experiments, each consisting of 6 technical replicates. \* P-value <0.05 determined by two-tailed Student's T test. Reproduced with permission [111].

Despite displaying a comparable growth rate to the isotype control, the KIM6+ *glpD*-deficient mutant demonstrated a slight, yet significant, defect in biofilm formation as determined by crystal violet assay during growth in both HIB (**Fig. 15A**) as well as BCS chemically defined media utilizing 0.2% K-gluconate as the sole carbon source (**Fig. 15B**). Plasmid-based complementation of functional *glpD* restored wild-type biofilm formation in the KIM6+ *glpD*-deficient mutant. Regardless of media composition, loss of *glpD* has a negative impact upon KIM6+ biofilm formation.

The impact of glycerol metabolism restoration in a biovar *Orientalis* genetic background upon biofilm formation was determined through comparing the relative biofilm production of CO92L, the *glpD* allelic exchange mutant, and the plasmid-expressing *glpD* and/or *glpFKX* mutants (**Fig 16**).



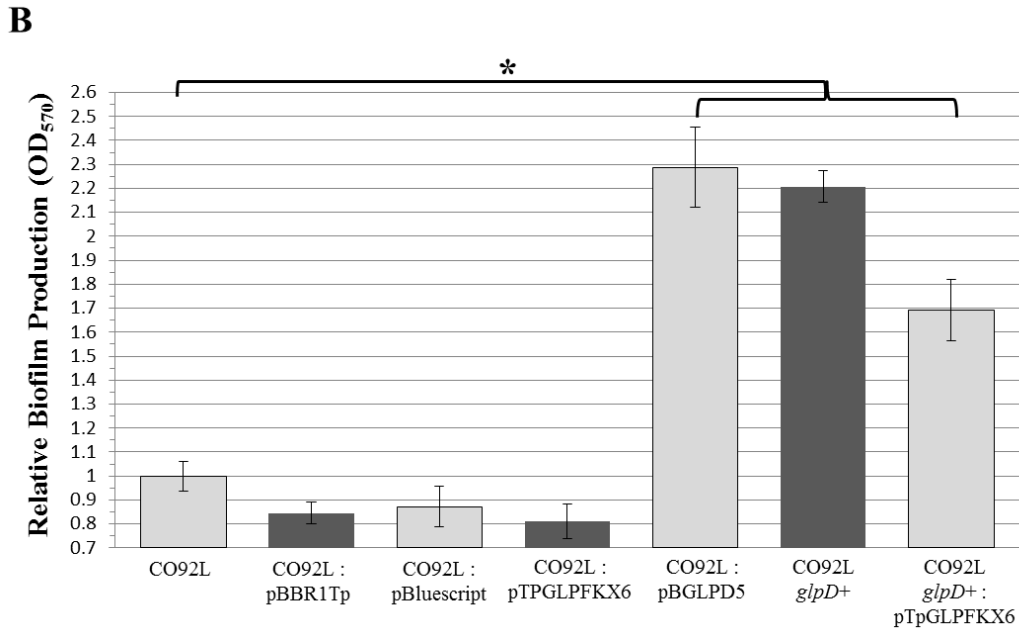


**Figure 16: Functional *glpD* Stimulates CO92 Biofilm Production.**

Biofilm quantification of CO92L, the empty vector controls, mutants solely plasmid complemented with either functional *glpD* or *glpFKX*, the *glpD* restored allelic exchange mutant, and the combined *glpD* allelic exchange mutant plasmid complemented with functional *glpFKX* after 24 hours post-inoculation in either HIB medium (A) or BCS medium supplemented with 0.2% K-gluconate (B). Error bars represent standard deviation from the mean. \* P-value < 0.05 as calculated by 2-tailed Student's T test. Reproduced with permission [111].

Combined restoration of functional *glpD* and *glpFKX* derived from KIM6+ significantly enhanced biofilm formation during growth in HIB (Fig. 16A). Sole restoration of *glpD*, as demonstrated by both plasmid complementation and allelic exchange, significantly increased biofilm formation when grown in BCS medium supplemented with 0.2% K-gluconate as the sole carbon source (Fig. 16B). Furthermore, the simultaneous supplementation of plasmid encoded *glpD* and *glpFKX* enhanced biofilm production. However, sole restoration of *glpFKX* had no appreciable impact upon *Y. pestis* biofilm production when cultured in BCS medium supplemented with 0.2% K-gluconate. Taken together, these findings demonstrate that expression of functional *glpD*, through a process independent of G3P regulation, promotes *Y. pestis* biofilm production.

## DISCUSSION

My findings demonstrate that *Y. pestis* biofilm formation is subject to carbon catabolite regulation. The metabolism of alternate carbon sources promotes robust biofilm formation; whereas, the presence of glucose significantly impairs *Y. pestis* biofilm production. This observation corresponds with *Y. pestis* infection of the flea vector, considering available glucose is not readily abundant in the flea midgut. Furthermore, other investigators have noted that the expression of peptide catabolism and alternate carbon source metabolic pathways are stimulated during *Y. pestis* infection of the flea [101]. I also show that *Y. pestis* biofilm production is not strongly induced during growth in HIB peptide-rich medium. Rather, intense biofilm production is stimulated during the metabolism of alternate carbon sources.

The metabolism of alternate carbon sources in *E. coli* is facilitated by the global transcriptional regulator, CRP. Deletion of *crp* in both KIM6+ as well as CO92 *Y. pestis* strains had no impact upon growth rate when cultured in BCS medium supplemented with glucose. However, growth of the *crp*-deficient mutants was significantly impaired during when cultured in BCS medium solely supplemented with alternate carbon sources, reflective of stringent *crp*-mediated carbon catabolite repression in *Y. pestis*. In accordance with the growth defect, *Y. pestis crp*-deficient mutants demonstrated a significant reduction in biofilm formation when cultured in BCS chemically defined medium solely supplemented with alternate carbon sources. Upon normalization of relative biofilm production to culture optical density, the biofilm formation defect of the  $\Delta crp$  mutants were shown to be independent of stunted growth kinetics. Furthermore, addition of exogenous cAMP, and allosteric activator of CRP, did not alter biofilm formation of the *crp*-deficient mutants yet enhanced biofilm production of the isogenic controls. Ultimately, these findings demonstrate that CRP not only promotes *Y. pestis*

biofilm production by enabling the metabolism of alternate carbon sources, but also confers a positive regulatory impact.

Since CRP is a global transcriptional regulator, I sought to determine whether CRP modulates the expression of previously characterized *Y. pestis* biofilm synthesis and regulatory factors. Gene transcription was assessed amongst the CO92 *crp*-deficient mutant and the isogenic control. Moreover, mRNA abundance was compared amongst wild-type CO92 *Y. pestis* cultured in BCS chemically defined media supplemented with either K-gluconate or glucose, reflective of respective CRP active or inactive states. In both cases, no alterations in transcription of previously-characterized biofilm factors were observed. Thus, CRP-mediated carbon catabolite regulation of *Y. pestis* biofilm formation does not transpire through direct transcriptional modulation of the *hms* genes.

In *E. coli*, G3P has been shown to mediate catabolite repression through inhibition of adenylate cyclase, thus decreasing cAMP and preventing activation of CRP [105]. Components of the glycerol metabolic pathway have been shown to be induced during infection of the flea vector in addition to flowcell biofilm formation [101]. Interestingly, the capacity to ferment glycerol has been lost in *Y. pestis* biovar Orientalis isolates; however, it is uncertain whether GlpK, which catalyzes G3P synthesis, is functional in biovar Orientalis strains. Thus, to discern the regulatory interplay amongst G3P and *Y. pestis* biofilm production, the molecular mechanism defining *Y. pestis* glycerol metabolism was characterized.

This study provides formal proof that the hallmark 93 bp in-frame deletion within the *glpD* gene of *Y. pestis* biovar Orientalis isolates is sufficient to impair glycerol metabolism. Through reduction of flavin adenine dinucleotide (FAD), GlpD concurrently oxidizes G3P to DHAP. The deletion in the biovar Orientalis *glpD* gene (amino acids 7 to 37) corresponds with a characterized *E. coli* GlpD flavin-binding domain (amino acids 5 to 34) [121]. Interestingly, sole restoration of *glpD* was insufficient to restore glycerol metabolism in biovar Orientalis isolates. Rather, glycerol fermentation was afforded upon

co-expression of KIM6+ derived *glpFKX* and *glpD*. These findings demonstrate the inability to ferment glycerol by biovar Orientalis strains is often insured by a variety of impairments within the *glpFKX* operon, all of which notably disrupt *glpK*. It is important to note that the expression of functional *glpD* in biovar Orientalis strains solely dysfunctional in *glpK* (PEXU-2, 195-P2, TS, and Kimberly) was insufficient to restore glycerol fermentation. Therefore, the putative glycerol kinase, y0876, does not support glycerol fermentation [106]; whereas, *glpK* is essential for *Y. pestis* aerobic glycerol fermentation.

Phylogenetic analyses indicate the diverse range of *glpFKX* disruptions in biovar Orientalis isolates were acquired subsequent to the shared deletion in *glpD*. However, 3 biovar Orientalis strains isolated in China (F1984001, CMCC87001, and YN663) containing the characteristic 93 bp in-frame deletion within the *glpD* gene appear to have retain intact *glpFKX* operon. Taking into account that the Orientalis biovar likely evolved in China, the *glpFKX* intact variants potentially reflect natural maintenance of ancestral-type strains in which the clone that spread globally during the 3rd plague pandemic was derived [7].

Remarkably, two Chinese isolates (YN1683 and YN1065) are annotated as Orientalis biovar, despite possessing both intact *glpD* and *glpFKX* genes [122]. Likely, the phenotypic inability to ferment glycerol resulted in the formal classification of both isolates as Orientalis biovar. The existence of atypical glycerol non-fermenting isolates has been previously described in the literature. However, through subsequent culture of the atypical glycerol non-fermenting isolates, revertant colonies may develop which spontaneously display a positive glycerol fermentation phenotype. For example, a well-known Russian bivalent live plague vaccine 1-17 was comprised of a glycerol non-fermenting strain #1 and fermenting strain #17 [123]. Nevertheless, it was later found that the glycerol-negative phenotype of the strain #1 readily reverts to a glycerol-positive phenotype following several passages in liquid culture with extensive aeration [124].

In the absence of selective pressure, one could expect a random rate of mutation acquisition resulting in comparable degree of disruptions in *glpF* as observed in *glpK*. However, no mutations are present in the *glpF* gene of any biovar Orientalis isolate. Moreover, comparative analyses of strains available to date in GenBank revealed that *glpK* is intact in all other *Y. pestis* biovars, suggestive of *glpK* evolutionary bias in the absence of functional *glpD*. Thus, the acquisition of *glpK* mutations may reflect negative selection against GlpK activity in the presence of dysfunctional GlpD.

I sought to assess whether sole dysfunction of *glpD* in the presence of functional *glpK* may increase intracellular concentrations of G3P and thereby repress CRP activation. Contrary to expectations, sole dysfunction of *glpD* in the KIM6+ background decreased intracellular accumulation of G3P. Moreover, combined dysfunction of both *glpD* and *glpK* evident in biovar Orientalis isolates restores G3P accumulation to degree comparable to KIM6+. Restoration of *glpD* had no impact upon G3P concentration in the CO92 background. Thus, sole dysfunction of *glpD* in the presence of function *glpK* may provide a mechanism of regulatory feedback upon G3P.

My findings reveal that dysfunctional *glpD* in the presence of functional *glpK* in a KIM6+ background results in a slight, yet significant, decrease in biofilm formation when cultured in both peptide rich HIB as well as chemically defined BCS media supplemented with both 0.2% glucose and 0.2% glycerol. Moreover, expression of functional *glpD* in CO92L results in a substantial the stimulation of *Y. pestis* biofilm formation as a result of expressing functional *glpD*, both in the presence of functional as well as dysfunctional *glpK*. Therefore, regardless of *glpK* functionality, *glpD* enhances *Y. pestis* biofilm production. The mechanism by which functional GlpD promotes *Y. pestis* biofilm production has not been ascertained. However, since evoking *glpD* dysfunction in KIM6+ impairs G3P accumulation and the restoration of *glpD* has no impact upon G3P concentration in CO92, the alterations in biofilm production likely do not transpire through G3P-mediated regulation of CRP activation.

## **Chapter 3. The Carbon Storage Regulator Protein, CsrA, is Essential for Robust *Yersinia pestis* Biofilm Formation**

### **INTRODUCTION**

CRP has been characterized to control the expression of two competitive carbon storage system sRNA regulators, CsrB and CsrC. Studies with *Y. pseudotuberculosis* *crp*-deficient mutants demonstrate that CRP represses CsrB expression, yet enhances expression of CsrC [120]. Both CsrB and CsrC sRNA species bind and sequester the RNA-associating carbon storage regulator protein, CsrA [125,126]. Through association with mRNA 5' UTR GGA motifs, CsrA post-transcriptionally represses gene expression by preventing translation and/or disrupting the stability of target transcripts.

CsrA is a global regulator which has been shown to repress biofilm formation through a variety of modes in other members of family Enterobacteriaceae [127,128,129]. In *E. coli*, CsrA inhibits translation of the *Y. pestis* *hmsHFRS* homolog, *pgaABCD* [129]. Moreover, CsrA disrupts *E. coli* transcript stability of the diguanylate cyclase *ycdT* as well as the c-di-GMP-specific phosphodiesterase *yliE* mRNA [130]. In *E. coli*, translation of the glycogen synthesis operon *glgCAP* is repressed by CsrA [131]. Studies in *E. coli* demonstrate that glycogen production may confer dual roles upon biofilm regulation. Glycogen may serve as a stationary phase energy source, thus enhancing biofilm production [132]. Alternately, glycogen synthesis may compete for common metabolic intermediates, thereby repressing biofilm formation [127]. However, in accordance with the objective of this chapter, the impact of CsrA regulation of carbon metabolism and storage upon *Y. pestis* biofilm formation has not been ascertained.

CsrA is notably one of the most highly expressed factors during *Y. pestis* infection of the flea vector [101]. In Chapter 2, I have demonstrated that *Y. pestis* biofilm production is subject to carbon catabolite regulation. Since CsrA is tightly intertwined with carbon storage in other pathogens, CsrA may play a critical role in *Y. pestis* biofilm regulation. Therefore, the objective of this chapter is to ascertain the impact of CsrA upon *Y. pestis* biofilm production. Moreover, I seek to establish the regulatory role of CsrA upon *Y. pestis* glycogen synthesis in order to elucidate potential mechanisms of carbon catabolite regulation of biofilm formation.

## MATERIALS AND METHODS

### Bacterial Strains, Plasmids, and Oligonucleotides

Bacterial strains and plasmids used in this chapter are detailed in **Table 4**. Oligonucleotides are detailed in **Appendix B Table 1**.

**Table 4: Bacterial Strains and Plasmids**

<i>Y. pestis</i> strains	Characteristics*	Reference
CO92	Pgm+ pCD+	[112]
CO92 pgm-	Pgm- pCD+	Motin collection Unpublished
CO92 $\Delta$ <i>csrA</i> 5a	Scarless deletion of the <i>csrA</i> gene clone 5a	Motin collection Unpublished
CO92 $\Delta$ <i>csrA</i> 3b	Scarless deletion of the <i>csrA</i> gene clone 3b	Motin collection Unpublished

CO92 $\Delta$ <i>csrA</i> 5a <i>pgm</i> <sup>+</sup>	Pigmentation positive CO92 $\Delta$ <i>csrA</i> mutant derived from clone 5a Km <sup>R</sup> /Suc <sup>S</sup> intermediate	Motin collection Unpublished
CO92 $\Delta$ <i>csrA</i> <i>csrA</i> ' 5a	Scarless Restoration of the <i>csrA</i> gene of clone 5a	Motin collection Unpublished
CO92 $\Delta$ <i>csrA</i> <i>csrA</i> ' 3b	Scarless Restoration of the <i>csrA</i> gene of clone 3b	Motin collection Unpublished
CO92 $\Delta$ <i>glgCAP</i>	Scarless deletion of the <i>glgCAP</i> gene	Motin collection Unpublished
CO92 $\Delta$ <i>csrA</i> $\Delta$ <i>glgCAP</i>	Scarless deletion of the <i>glgCAP</i> gene from CO92 $\Delta$ <i>csrA</i> 5a	Motin collection Unpublished
CO92 $\Delta$ <i>hmsP</i>	Scarless deletion of the <i>hmsP</i> gene	Motin collection Unpublished
CO92 $\Delta$ <i>csrA</i> $\Delta$ <i>hmsP</i>	Scarless deletion of the <i>hmsP</i> gene from CO92 $\Delta$ <i>csrA</i> 5a	Motin collection Unpublished
KIM6 <sup>+</sup>	Pgm <sup>+</sup> pCD <sup>-</sup>	Brubaker collection
KIM6 <sup>+</sup> <i>pgm</i> <sup>-</sup>	Pgm <sup>-</sup> pCD <sup>-</sup>	Motin collection Unpublished
KIM6 <sup>+</sup> $\Delta$ <i>csrA</i> 2:14	Scarless deletion of the <i>csrA</i> gene clone 2:14	Motin collection Unpublished
KIM6 <sup>+</sup> $\Delta$ <i>csrA</i> 4:12	Scarless deletion of the <i>csrA</i> gene clone 4:12	Motin collection Unpublished

KIM6+ $\Delta$ <i>csrA</i> 2:14 K-g <i>pgm</i> +	Pigmentation positive revertant KIM6+ $\Delta$ <i>csrA</i> mutant clone 2:14 following serial transfer in BCS/0.2% K-gluconate/0.2% glucose	Motin collection Unpublished
KIM6+ $\Delta$ <i>csrA</i> <i>csrA</i> ' 2:6	Scarless Restoration of the <i>csrA</i> gene of clone 2:14	Motin collection Unpublished
<b>Plasmids</b>	<b>Characteristics</b>	<b>Reference</b>
pKD46	Mutagenesis helper plasmid, source of Lambda Red Recombinase, Ap <sup>R</sup>	[113]
pKD4_Km-sacB	Cloned <i>sacB</i> from pCVD442 in NgoMIV site of pKD4, source of <i>kan-sacB</i> cassette, Km <sup>R</sup> Ap <sup>R</sup> , Suc <sup>S</sup>	[111]

### Scarless Deletion and Chromosomal Restoration

Utilizing the procedure described in Chapter 2, the *csrA* gene was excised from *Y. pestis* KIM6+ and CO92 backgrounds in a scarless fashion. Moreover, subsequent additional recombination events were utilized to chromosomally restore the *csrA* gene via electroporation of a PCR fragment amplified with primers which encompass the *csrA* deletion region using CO92 DNA as a template, thereby circumventing the need for plasmid complementation. Verification of gene deletion and restoration was afforded by sequencing. Retention of the *pgm* locus was confirmed via PCR of the *hmsHF<sub>RS</sub>* operon.

Double deficient *glgCAP* or *hmsP* mutants were constructed in the CO92 $\Delta$ *csrA* 5a background were performed in an analogous fashion.

### Growth Kinetics and Crystal Violet Biofilm Quantification Assay

Bacterial growth curves were determined as previously described in Chapter 2. With the exception of the single CO92 $\Delta$ *hmsP* and double CO92 $\Delta$ *csrA* $\Delta$ *hmsP* mutants, biofilm production was assessed via crystal violet assay as detailed in Chapter 2. Due to the excessive biofilm production of the *hmsP*-deficient mutants, accurate optical density

readings could not be obtained during growth at 26°C. Therefore, biofilm quantification experimental pre-growth was modified to 37°C.

### **Congo Red Binding Assay**

Bacteria derived from glycerol stocks were cultured on Heart Infusion Agar (HIA) plates for 24-48 hours at 26°C. The bacteria were transferred to fresh HIA and incubated at 26°C for an additional 18-24 hours. Thereafter, 50 µL of fresh HIB was suspended to OD<sub>600</sub> = 0.3. Four microliters of this suspension was spotted on Congo red plates containing either 0.2% galactose or 0.2% K-gluconate. After 48 hours of inoculation at 26°C, phenotypic bacterial pigmentation was determined.

### **Whole Genome Sequencing**

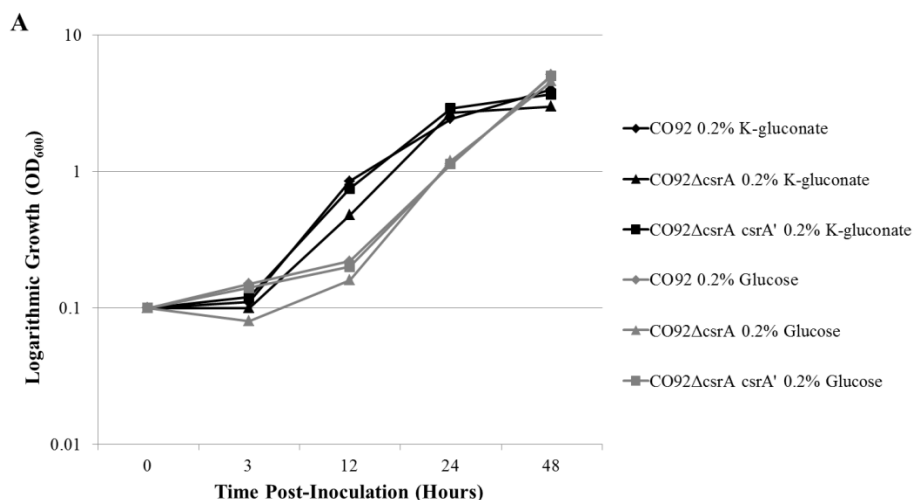
Whole-genome sequences of 4 *csrA*-deficient mutants were determined: CO92Δ*csrA* 5a, CO92Δ*csrA* 5a *pgm*+, KIM6+Δ*csrA* 2:14, and KIM6+Δ*csrA* 2:14 K-g *pgm*+. Bacteria derived from glycerol stocks were cultured on Heart Infusion Agar (HIA) plates for 24-48 hours at 26°C. The bacteria were transferred to fresh HIA and incubated at 26°C for an additional 18-24 hours. Genomic DNA was isolated via QIAmp DNA Mini kit (Qiagen) in accordance with manufacturer guidelines. Illumina MiSeq sequencing performed at Los Alamos National Laboratory yielded 7156350, 11128411, 8122124, and 9658052 251 bp reads for the respective aforementioned strains. The Illumina reads were *de novo* assembled by IDBA\_UD (v1.1.1) with parameter “--mink 27 --maxk 127 --step 20 --pre\_correction”. The assembled contigs were aligned to corresponding reference genomes (*Y.pestis* CO92, NC\_003143 and *Y.pestis* KIM 10, NC\_004088) by MUMmer (v3.23) with parameters “--maxmatch” and the uncovered reference regions were extract out using custom Perl script. Moreover, Illumina paired

reads were aligned to the corresponding reference genome (*Y.pestis* CO92 and *Y.pestis* KIM 10) by BWA (v0.7.10) aln algorithm with default parameters. The average depth of coverage and percent contig recovery were calculated from alignment results and the uncovered reference regions were extract out using custom Perl script. Population variation was judged from mapping result using SAMtools (v1.1) for conversion of BWA output format to BAM format and to perform SNP and Indel analysis. The SNP calls were filtered further by vcffilter.pl of SAMtools with following criteria: (i) minimum RMS mapping quality for SNPs {10}; (ii) minimum read depth {10}; (iii) maximum read depth {10000}; (iv) minimum number of alternate bases {3}; (v) SNP within INT bp around a gap to be filtered {3}; (vi) window size for filtering adjacent gaps {10}; (vii) min P-value for strand bias (given PV4) {0.0001}; (viii) min P-value for end distance bias {0.0001}; (x) variants in the repeats region of the reference are filtered.

## RESULTS

### CsrA is Essential for Robust *Y. pestis* Biofilm Production

Growth kinetics of the *csrA*-deficient mutant during incubation at 26°C was determined (**Fig. 17**).



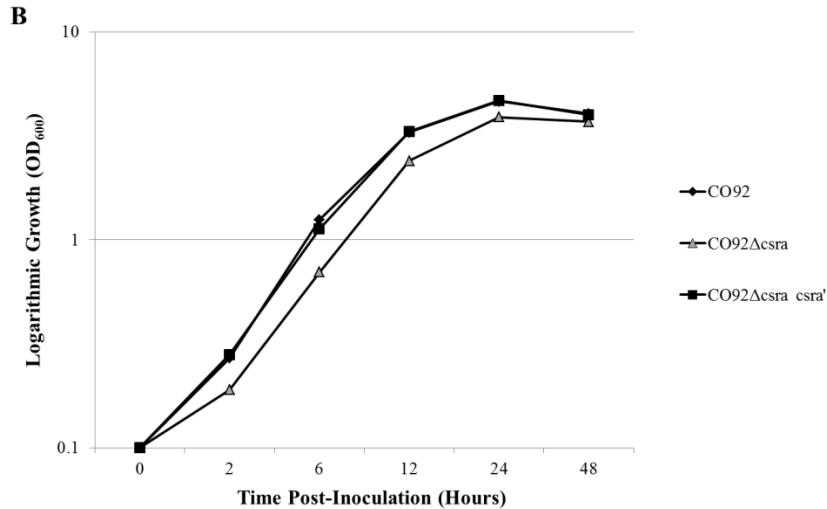


**Figure 17: 26°C Growth Kinetics of the CO92 *csrA*-deficient Mutant.**

Growth curves of CO92, CO92Δ*csrA*, and the chromosomal restoration mutant CO92Δ*csrA* *csrA*'.

**A.** Growth in BCS medium supplemented with either 0.2% glucose or 0.2% K-gluconate.

**B.** Growth kinetics when cultured in HIB medium.

No statistically significant alteration in 26°C growth kinetics was observed amongst the CO92 *csrA*-deficient mutant in comparison to the isogenic control and *csrA* chromosomal restoration mutant during growth in BCS medium supplemented with either 0.2% glucose or 0.2% K-gluconate (**Fig. 17A**). Similarly, there was no significant change in growth rate amongst the *csrA*-deficient mutant and the controls when cultured at 26°C in HIB (**Fig. 17B**). Therefore, considering there were no changes in growth rate as a result of *csrA* deletion, there is no need to normalize subsequent biofilm formation results to optical density.

Biofilm formation of the *csrA* deficient mutant was quantified by crystal violet assay during in BCS and HIB medium (**Fig. 18**).

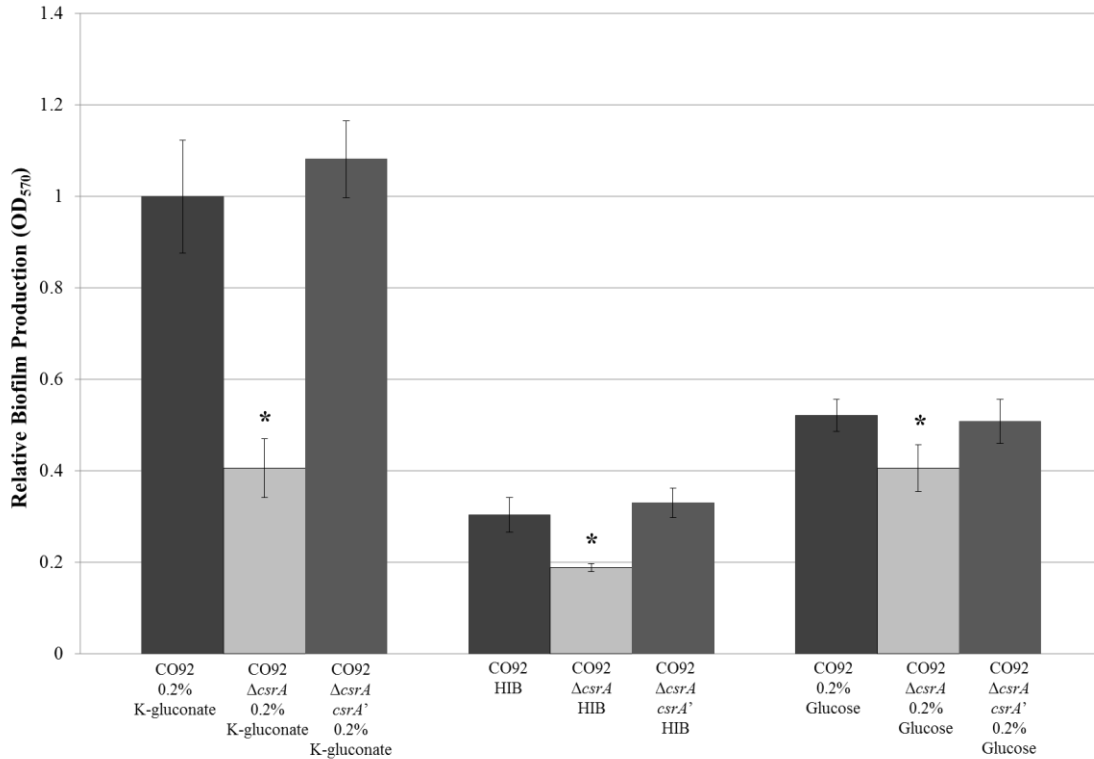


**Figure 18: CsrA is a Positive Regulator of *Y. pestis* Biofilm Formation.**

Relative biofilm production of CO92, CO92 $\Delta csrA$ , and the chromosomal restoration mutant CO92 $\Delta csrA csrA'$  when grown in BCS medium supplemented 0.2% K-gluconate, HIB medium, or BCS medium supplemented 0.2% glucose. Error bars reflect standard deviation from the mean of 2 independent experiments, each consisting of 6 technical replicates. \* P-value < 0.05 as determined by Student's T-test.

Loss of *csrA* resulted in a significant reduction in biofilm formation relative to the respective isogenic control and *csrA* genomic restoration mutants, regardless of available carbon source. After 24 hours post-inoculation, the relative biofilm production of the *csrA*-deficient mutant when cultured in BCS supplemented with 0.2% K-gluconate was >2-fold reduced relative to the control strains. In fact, the biofilm production of the *csrA* deletion mutant during growth in BCS supplemented with K-gluconate was comparable

to the biofilm production when cultured in the presence of glucose. Moreover, the biofilm formation was impaired by almost 2-fold for the CO92 $\Delta$ *csrA* mutant when grown in HIB.

To further evaluate the impact of CsrA upon *Y. pestis* biofilm production, I phenotypically assessed EPS production through Congo red binding assay (**Fig. 19**).

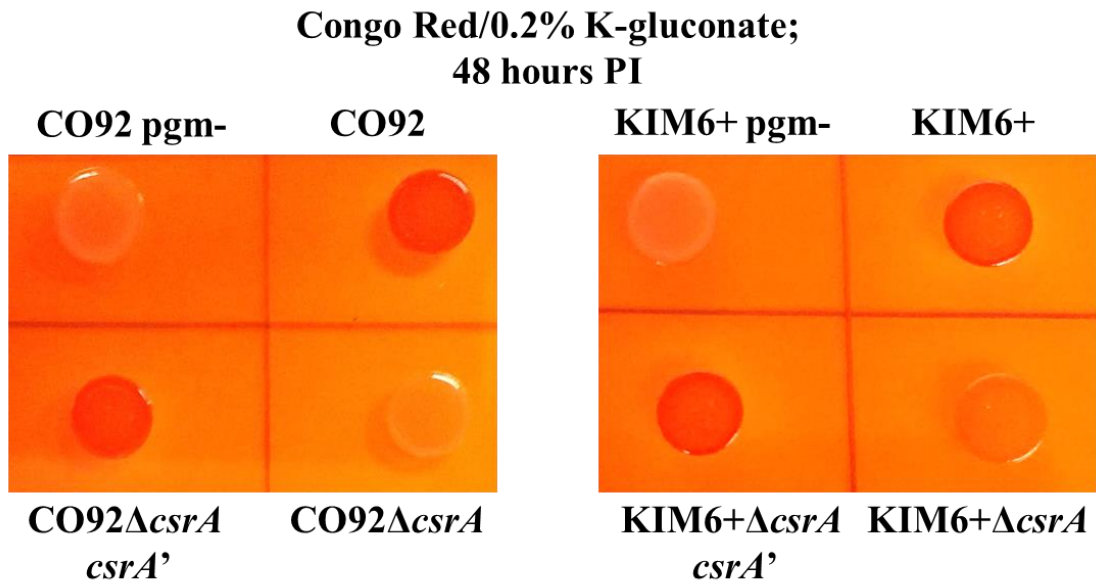


**Figure 19: Impaired Congo red Assimilation of *Y. pestis* *csrA*-deficient Mutants**

Congo red assimilation of the CO92 and KIM6+ *csrA*-deficient mutants, chromosomal *csrA* restoration mutants, parental isogenic controls, and *pgm* locus deficient mutants.

Loss of *csrA* in both the CO92 and KIM6+ genetic backgrounds drastically impaired Congo red assimilation. Up to 48 hours post-inoculation, the Congo red pigmentation of the *csrA*-deficient mutants were nearly identical to the biofilm-impaired *pgm* locus deficient strains. Complete chromosomal restoration of *csrA* in the *csrA*-deficient mutants reestablished wild-type Congo red pigmentation. Taken together, the biofilm quantification and Congo red assimilation assays demonstrate that *csrA* is essential for efficient *Y. pestis* biofilm formation.

## CsrA Stimulates *Y. pestis* Biofilm Production Independent of Glycogen Regulation

In *E. coli*, CsrA is known to inhibit glycogen synthesis by impairing translation of the *glgCAP* operon. Therefore, I sought to determine if CsrA promotes *Y. pestis* biofilm production through regulation of glycogen formation. To do so, biofilm production was compared amongst a *glgCAP* deletion mutant, a double deficient *csrA* and *glgCAP* mutant, and the appropriate controls (**Fig. 20**).

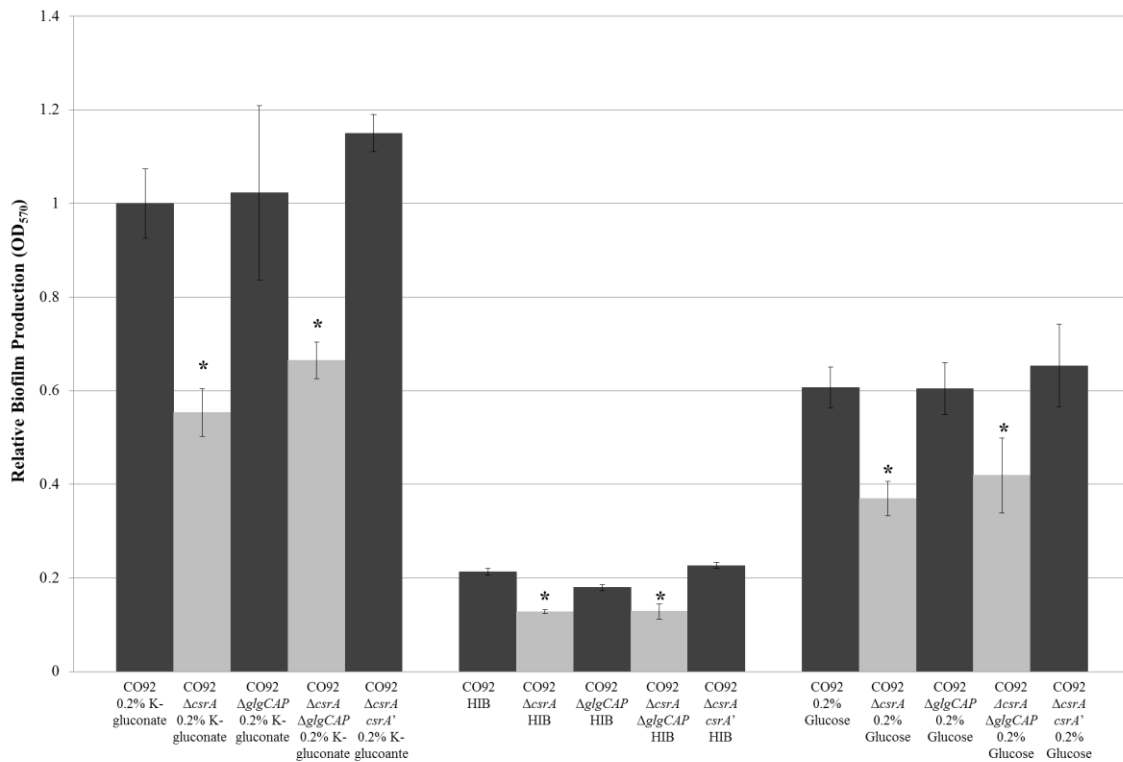


**Figure 20: CsrA Enhances *Y. pestis* Biofilm Production Independent of Glycogen Regulation.**

Relative biofilm production 24 hours post-inoculation of CO92, CO92 $\Delta csrA$ , CO92 $\Delta glgCAP$ , CO92 $\Delta csrA \Delta glgCAP$ , and the *csrA* chromosomal restoration mutant when grown in BCS medium supplemented 0.2% K-gluconate, HIB medium, or BCS medium supplemented 0.2% glucose. Error bars reflect standard deviation from the mean of 2 independent experiments, each consisting of 4 technical replicates. \* P-value < 0.05 as determined by Student's T-test.

My findings demonstrate that deletion of *glgCAP* in a *csrA*-deficient background was insufficient to restore wild-type biofilm production as demonstrated by crystal violet assay. Moreover, sole deletion of *glgCAP* had no discernable impact upon *Y. pestis* biofilm production, regardless of media composition or available carbon source.

Congo red binding assay was utilized to support the biofilm quantification results (Fig. 21).

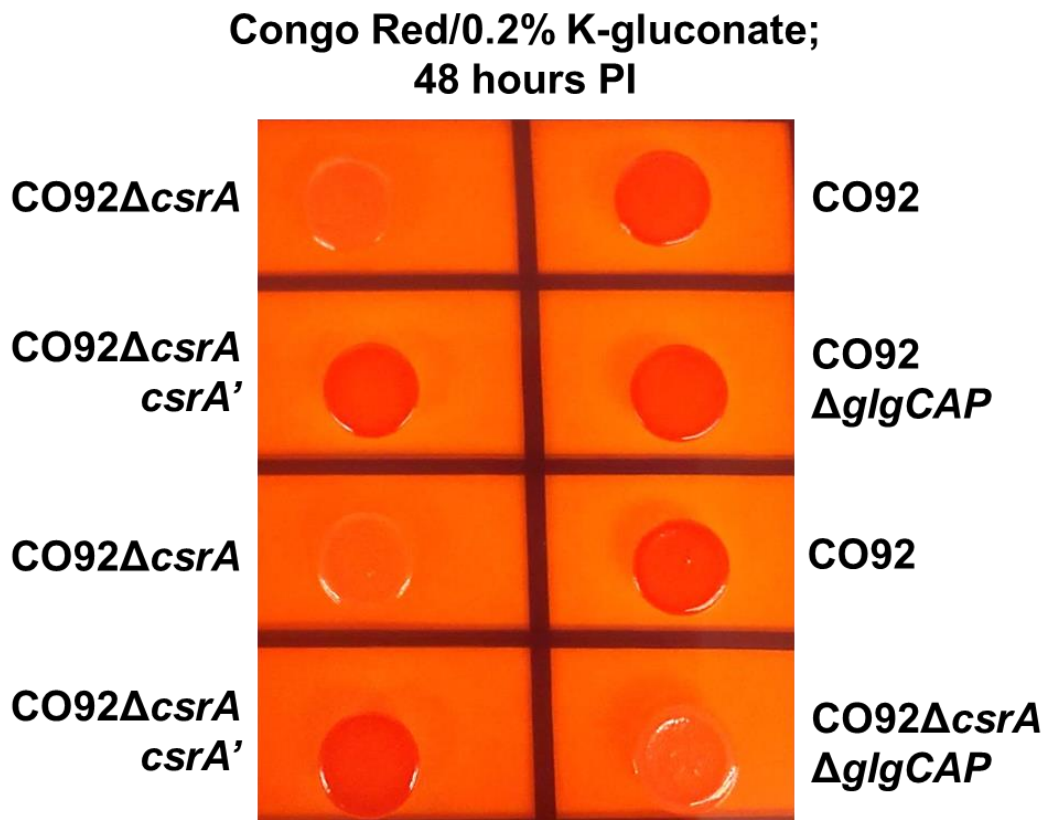


**Figure 21: Congo Red Binding of *Y. pestis* *csrA*-deficient Mutant is not Restored by Loss of the *glgCAP* Operon.**

Congo red assimilation of the CO92, CO92Δ*csrA*, CO92Δ*glgCAP*, CO92Δ*csrA*Δ*glgCAP*, and the *csrA* chromosomal restoration mutant.

In accordance with the biofilm quantification results, sole deletion of *glgCAP* did not alter Congo red binding. Furthermore, loss of *glgCAP* in the *csrA*-deficient mutant was insufficient to restore wild-type pigmentation. Taken together, these findings demonstrate that glycogen formation is dispensable for *Y. pestis* biofilm production. In a similar note, the potential regulation of glycogen synthesis by CsrA has no bearing upon biofilm production in *Y. pestis*. Thus, the mechanism by which CsrA enhances *Y. pestis* biofilm production must occur through an alternate means.

### **Deletion of *hmsP* Restores Biofilm Production of the *csrA*-deficient Mutant**

CsrA has been shown to alter the transcript stability of factors which regulate the cyclic diguanylate small molecule activator of PNAG biofilm production in *E. coli*; and therefore, may stimulate *Y. pestis* biofilm production via a similar mode of action. To assess this hypothesis, the *hmsP* gene encoding a diguanylate phosphodiesterase biofilm inhibitor was deleted from both wild-type CO92 and the CO92 *csrA*-deficient mutants. Through crystal violet assay (**Fig. 22**) and Congo Red binding (**Fig. 23**), deletion of *hmsP* was found to restore biofilm production in the *csrA*-deficient mutant. Deletion of *hmsP* significantly enhanced biofilm production of the *csrA*-deficient mutant by >2.5 fold. Furthermore, loss of *hmsP* restored Congo red binding of the *csrA*-deficient mutant, indicative of enhanced EPS production. These results demonstrate that deletion of HmsP, a characterized negative regulator of *Y. pestis* biofilm production, is sufficient to compensate for the defect in biofilm production caused by *csrA* deficiency. Therefore, CsrA may promote *Y. pestis* biofilm production through regulation of cyclic diguanylate activator.

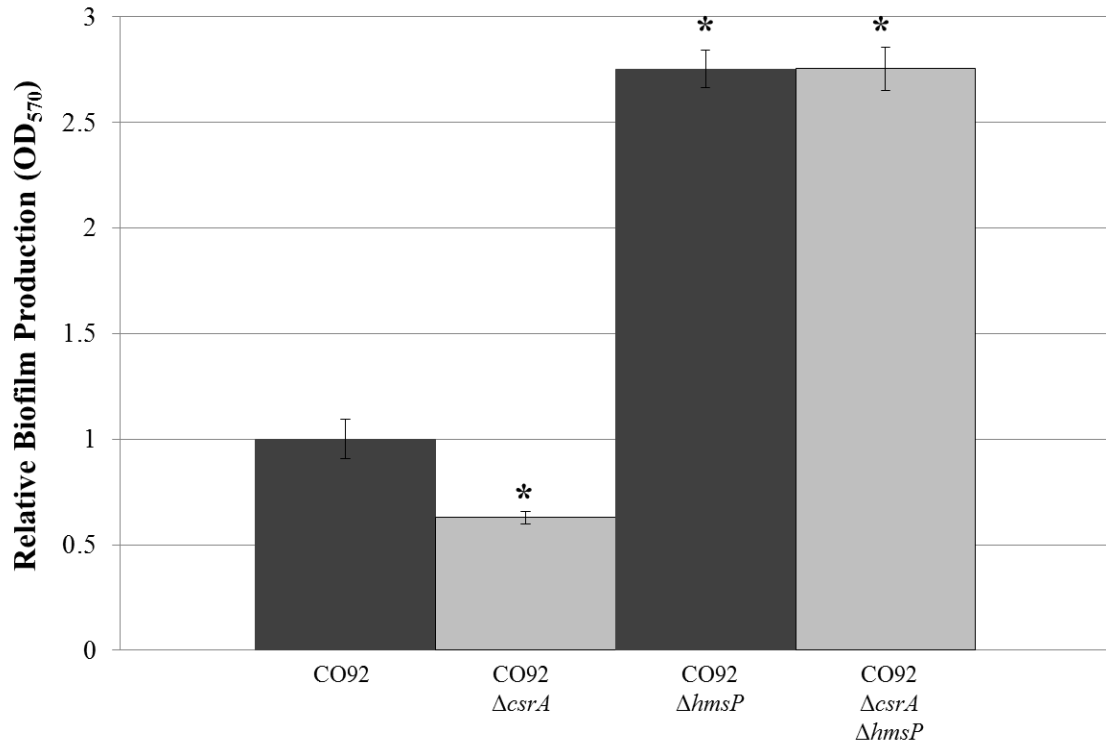


**Figure 22: Deletion of *hmsP* in a CO92 $\Delta csrA$  Mutant Enables Excessive Biofilm Production.**

Relative biofilm production of CO92, CO92 $\Delta csrA$ , CO92 $\Delta hmsP$ , and CO92 $\Delta csrA \Delta hmsP$  following 24 hours post-inoculation in HIB medium. Error bars reflect standard deviation from the mean of 2 independent experiments, each consisting of 6 technical replicates. \* P-value < 0.05 as determined by Student's T-test.

**Congo Red/0.2% K-gluconate;  
48 hours PI**

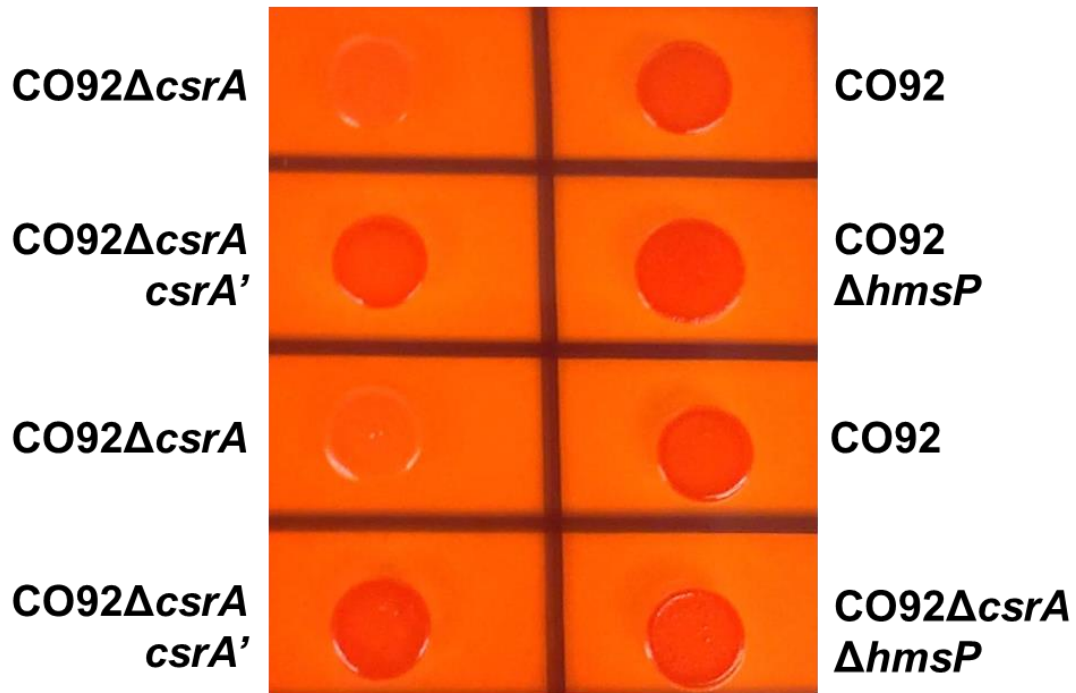


**Figure 23: Loss of *hmsP* Restores Congo Red Pigmentation of the CO92 *csrA*-deficient Mutant.**

Congo red assimilation of the CO92, CO92Δ*csrA*, CO92Δ*hmsP*, CO92Δ*csrA*Δ*hmsP*, and the *csrA* chromosomal restoration mutant.

**Spontaneous Pigmentation Reversions of *csrA*-deficient Mutants**

At a relatively low frequency, *csrA*-deficient *Y. pestis* mutants constructed in either the KIM6+ or CO92 backgrounds spontaneously revert to a positive Congo red pigmentation phenotype (Table 5).

**Table 5: Frequency of *csrA*-deficient Congo Red Pigmentation Revertants**

<i>Y. pestis</i> $\Delta csrA$ strain, Dilution	Pigmentation Positive Revertant Colonies	Pigmentation Impaired/Negative Colonies
KIM6+ $\Delta csrA$ 2:14, $10^{-5}$ <sup>A</sup>	3	337
KIM6+ $\Delta csrA$ 2:14, $10^{-5}$ <sup>A</sup>	6	396
KIM6+ $\Delta csrA$ 2:14, $10^{-5}$ <sup>B</sup>	3	159
KIM6+ $\Delta csrA$ 2:14, $10^{-5}$ <sup>B</sup>	1	123
CO92 $\Delta csrA$ 5a, $10^{-5}$ <sup>C</sup>	2	416
CO92 $\Delta csrA$ 3b, $10^{-5}$ <sup>C</sup>	1	544
CO92 $\Delta csrA$ 5a, $10^{-6}$ <sup>C</sup>	0	36
CO92 $\Delta csrA$ 3b, $10^{-6}$ <sup>C</sup>	0	44

<sup>A</sup> Congo red assimilation determined after 24 hours incubation at 37°C and subsequent temperature shift to 26°C during growth in BCS supplemented with 0.2% K-glucoante.

<sup>B</sup> Congo red assimilation determined after 24 hours incubation at 37°C and subsequent temperature shift to 26°C during growth in BCS supplemented with 0.2% K-gluconate and 0.2% glucose.

<sup>C</sup> Congo red assimilation determined after 48 hours incubation at 26°C during growth in BCS supplemented with 0.2% K-gluconate.

The positive Congo red pigmentation phenotype of the revertant clones is stable upon subsequent serial passage. Subsequent to initial identification of the pigmentation revertants on Congo Red/0.2% galactose, glycerol stocks were created with after a single transfer upon HIA plates. Thereafter, both the CO92 $\Delta csrA$  5a pgm+ and KIM6+ $\Delta csrA$  2:14 K-g pgm+ strains were serial transferred twice on HIA plates prior to phenotypic assessment of pigmentation (**Fig. 24**).

**Congo Red/0.2% K-gluconate  
72 hours Post-Inoculation**

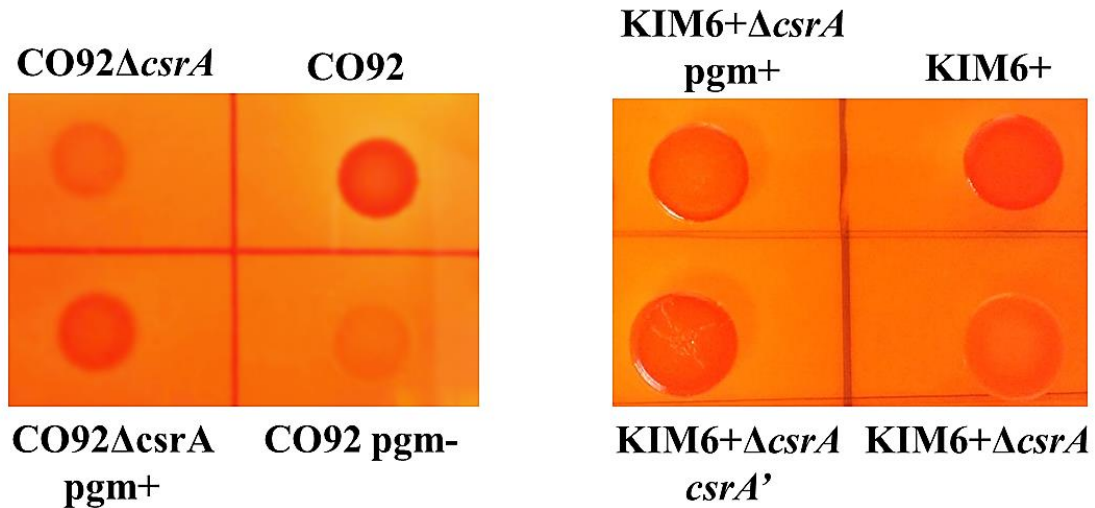


**Figure 24: *csrA*-deficient Congo Red Pigmentation Positive Revertant Clones.**

Phenotypic Congo red absorption following 72 hours of incubation at 26°C on Congo Red plates supplemented with 0.2% K-gluconate of spontaneous pigmentation positive revertant *csrA*-deficient clones derived in both CO92 and KIM6+ mutants.

In order to ascertain a potential genetic basis for the pigmentation reversions, whole genome sequences were determined for KIM6+ and CO92 *csrA*-deficient mutants exhibiting impaired pigmentation phenotype as well as corresponding pigmentation revertant clones. Sequencing results demonstrated nearly complete reference map coverage (99.9%) for each strain with a range of 244X to 408X depth of the genome (Table 6).

**Table 6: Whole Genome Sequencing Coverage of *csrA*-deficient Congo Red Pigmentation Impaired and Pigmentation Positive Revertants**

	Mapped reads	Reference Recovery (%)	Average Fold Coverage (x)	Fold Standard Deviation
<b>Ref:</b>				
<b>NC_003143</b>				
CO92Δ <i>csrA</i> 5a	4831565 (67.5%)	99.99	244.63	109.35
CO92Δ <i>csrA</i> 5a pgm+	8072320 (72.5%)	99.99	408.97	191.89
<b>Ref:</b>				
<b>NC_004088</b>				
KIM6Δ <i>csrA</i> 2:14	6084441 (74.9%)	99.99	312	83.14
KIM6+Δ <i>csrA</i> 2:14 K-g pgm+	7629419 (78.9%)	99.99	390.65	151.62

Of the uncovered reference regions, no conserved gap was identified aside from the 184 bp excision of the *csrA* gene (Table 7).

**Table 7: Whole Genome Sequencing Contig Mapping of *csrA*-deficient Congo Red Pigmentation Impaired and Pigmentation Positive Revertants**

Sample	Gap Start*	Gap End*	Gap Size	CDS Start*	CDS End*	CDS Product
<b>Ref:</b>						
<b>NC_003143</b>						
CO92Δ <i>csrA</i> 5a	2293680	2293697	18			
CO92Δ <i>csrA</i> 5a	3683281	3683464	184	3683279	3683464	YPO3304: carbon storage regulator
CO92Δ <i>csrA</i> 5a pgm+	2027730	2027836	107			
CO92Δ <i>csrA</i> 5a pgm+	2293680	2293697	18			
CO92Δ <i>csrA</i> 5a pgm+	3548487	3548533	47			
CO92Δ <i>csrA</i> 5a pgm+	3683281	3683464	184	3683279	3683464	YPO3304: carbon storage regulator

<b>Ref:</b>						
<b>NC_004088</b>						
KIM6 $\Delta$ <i>csrA</i> 2:14	54345	54359	15	53277	54503	y0040: hypothetical protein
KIM6+ $\Delta$ <i>csrA</i> 2:14	995115	995298	184	995115	995300	y0884: carbon storage regulator
KIM6+ $\Delta$ <i>csrA</i> 2:14	2870463	2870485	23	2867409	2870561	y2605: adhesin
KIM6+ $\Delta$ <i>csrA</i> 2:14 K-g pgm+	995115	995298	184	995115	995300	y0884: carbon storage regulator
KIM6+ $\Delta$ <i>csrA</i> 2:14 K-g pgm+	4240992	4240995	4			

\* Coordinate of the reference genome.

Moreover, no discernable conserved SNP or INDEL genetic alteration was exclusively acquired in the pigmentation revertant *csrA*-deficient mutants (**Table 8**).

**Table 8: Unique Genetic Variants Amongst the *csrA*-deficient Congo Red Pigmentation Impaired and Pigmentation Positive Revertants**

Sample	Ref. Position *	Ref. Seq.	Var. Seq.	Type	CDS Start *	CDS End *	Product
CO92 $\Delta$ <i>csrA</i> 5a	1234971	G	GA	Ins.	1234752	1235063	YPO1087: putative prophage protein
KIM6 $\Delta$ <i>csrA</i> 2:14	2006621	TAA	TA	Del.			Intergenic region
KIM6 $\Delta$ <i>csrA</i> 2:14	2959406	CGGG	CGG	Del.	2959360	2959551	y2681: hypothetical protein
KIM6 $\Delta$ <i>csrA</i> 2:14	2006616	T	C	SNP			Intergenic region
KIM6 $\Delta$ <i>csrA</i> 2:14	3787395	T	C	SNP			Intergenic region
KIM6+ $\Delta$ <i>csrA</i> 2:14 K-g pgm+	1830492	ACC	AC	Del.			Intergenic region
KIM6+ $\Delta$ <i>csrA</i> 2:14 K-g pgm+	2006613	GCC	GCCC	Ins.			Intergenic region

KIM6+ $\Delta csrA$ 2:14 K-g <i>pgm</i> +	2018832	CAAA	CAA	Del.	2018786	2021923	y1834: hypothetical protein
KIM6+ $\Delta csrA$ 2:14 K-g <i>pgm</i> +	2253704	CG	C	Del.	2253591	2254466	y2047: tryptophan synthase subunit alpha

\* Coordinate of the reference genome. CO92: NC\_003142; KIM10: NC\_004088.

Ref.: reference genome; Var.: Variant; Seq.: Sequence; Ins.: Insertion; Del.: Deletion

Ultimately, the whole genome sequencing data confirmed the deletion of *csrA* in all mutants. Sequencing revealed complete retention of the pigmentation locus, including the *hmsHF<sub>RS</sub>* biofilm synthesis operon, regardless of pigmentation phenotype. Genomic integrity was maintained for previously characterized biofilm regulatory factors, notably *hmsP*, *hmsT*, *hmsB*, *hmsC/N*, *hmsD*, *hmsE/A*, and *fur*. Moreover, the capacity to assimilate Congo red pigmentation by the *csrA*-deficient pigmentation positive revertants does not result from loss of genetic material as a consequence of IS element excision.

## DISCUSSION

The carbon storage regulator protein, CsrA, is known to post-transcriptionally inhibit *E. coli* biofilm formation via multiple modes of action [129,130]. My findings reveal that *Y. pestis* biofilm formation, contrary to what has been described for *E. coli*, is enhanced by CsrA. *Y. pestis* mutants deficient in *csrA* demonstrate significantly impaired biofilm formation, regardless of available carbon source or media composition. Moreover, phenotypic assessment of the *csrA* deletion mutants indicate severely repressed Congo red assimilation which is comparable to biofilm-deficient *pgm* locus excision (*hmsHF<sub>RS</sub>* negative) *Y. pestis* after 48 hours incubation at 26°C, reflective of impaired PNAG production. Considering *csrA* is one of the most highly expressed genes

during *Y. pestis* infection of the flea midgut, CsrA may function as a crucial promoter of *Y. pestis* biofilm-mediated transmission.

Dissimilar to the *E. coli pgaA* 5' UTR, the predicted *Y. pestis hmsH* 5' UTR does not contain an abundance of putative CsrA binding (GGA) motifs (**Fig. 25**) [129]. This observation suggests CsrA may not readily associate with and impair *hmsHFRS* translation; however, does not address the mechanism by which CsrA enhances *Y. pestis* biofilm formation.

<i>E. coli</i> <i>pgaABCD</i> ( <i>hmsHFRS</i> homolog) 5' UTR	<i>Y. pestis</i> Predicted <i>hmsHFRS</i> 5' UTR
AGGCAUUGGGAUUUAUGCCGUUUUCC	<b>UUGCAU</b> UUUAAUUAACGUCUU <b>UGUU</b>
UGAAGAUCUCAUCAUUGGAAUGGAU	<b>ACAUU</b> UUCACCUCCAUAUAUCGCGC
UUUCGGGCGAGAAA <b>GGA</b> UUUUUAU	AAUAACAAUAUCCUAUAUAUGACUUUG
<b>GGA</b> CACUCUGCUUCAUUUCUUCUUC	CAACAUAUCCCUUUCAGCUAACCUA
UCAUCAACAUAUCACGUCUCUCUU	UAUGGCAUGGUAAUACAUCUAAG
CCGCGUUUAAUAAC <b>GGA</b> UUAUGAGGU	AAUCCAUUUCAUUCAUUCCAUAA
GCAAAAUAUCUUUCUUUCAGUUACC	UGAAAAAUGUACGUUCA <b>GGA</b> AGUCGC
UGUAAUUAGAUACAGAG <b>GAGAG</b> AUUUU	UUUCCUUGAUCAUCAAACAAGUUGCU
GGCAAUACA <b>GGA</b> GUAUAAC <b>GGAUG</b>	GGCUUAAGGGUUAUAUAUG

**Figure 25: *E. coli* and *Y. pestis* PNAG biosynthesis operon 5' UTR Comparison.**

Comparison of *E. coli pgaABCD* 5' UTR and *Y. pestis hmsHFRS* leader predicted (BPROM score 6.05; theoretical -35 and -10 TSS boxes in **bold** [133]) PNAG biosynthesis operons. Numerals I-VI indicate experimentally characterized CsrA interaction sites [129]. Yellow highlights reflect putative CsrA binding motifs. Dissimilar to the *E. coli pgaA* 5' UTR, the predicted *Y. pestis hmsH* 5' UTR does not appear to encompass an abundance of putative CsrA binding motifs.

CsrA has been well-documented to regulate gene expression via disruption of transcript stability and translational inhibition [129,130,131]. Therefore, I postulate that

CsrA stimulates *Y. pestis* PNAG production by repressing the gene expression of an inhibitor of *Y. pestis* biofilm formation (**Fig. 26**).

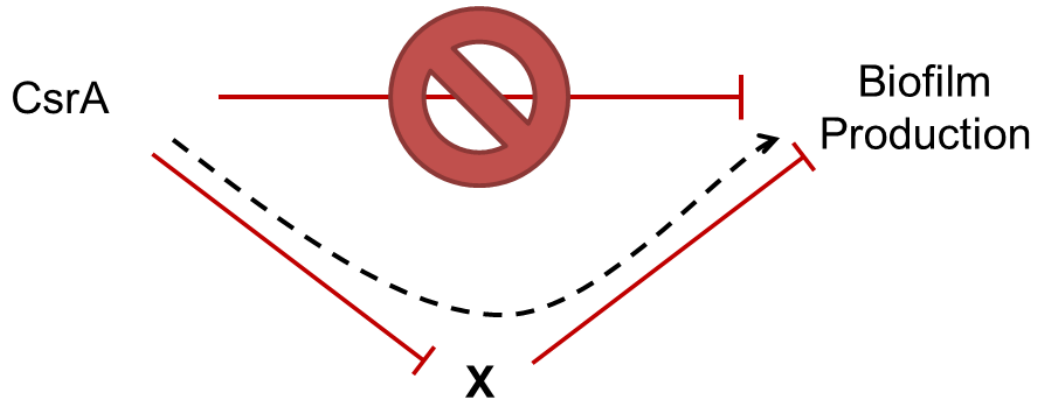


**Figure 26: Proposed Mechanism of *Y. pestis* CsrA Biofilm Regulation.**

Contrary to what has been described in *E. coli*, CsrA promotes *Y. pestis* biofilm production. Since CsrA is a well-documented post-transcriptional repressor, I postulate CsrA indirectly enables robust biofilm production by inhibiting the expression of an uncharacterized repressor of *Y. pestis* biofilm formation (denoted as “X”).

To provide insight into the mechanism by which CsrA enhances *Y. pestis* biofilm production, the predicted 5' UTR of potential repressors of *Y. pestis* biofilm were assessed for putative CsrA binding sites. Foremost, I analyzed the glycogen synthesis *glgCAP* operon which has been demonstrated to be repressed by CsrA in *E. coli* [127]. However, other studies indicate that glycogen formation may also compete for PNAG synthesis intermediates, thus impairing *E. coli* biofilm formation [132]. The impact of glycogen formation upon *Y. pestis* biofilm production has not been ascertained. Comparison of the *glgC* 5' UTR amongst *E. coli* and *Y. pestis* does not reveal any stark alterations in putative CsrA binding sites, suggestive of a conserved mechanism of CsrA-mediated regulation of glycogen production amongst these pathogens (**Fig. 27**).

<i>E. coli</i> <i>glgCAP</i> major transcript 5' UTR	<i>Y. pestis</i> <i>glgCAP</i> predicted 5' UTR
AUUGUUUUACCUGCUGG <b>GGAG</b> UGGC	<b>CUGCCAGCAGCAACUACAGAUUUUGU</b>
ACGCCAUUCCCCAUUCGCUGGAGAG <b>G</b>	<b>UAUCUCAGCGCUGGUUGGUGCUC</b> AUC
<b>GA</b> UAACCCAGUGAUUACGGCUGUCUG	AAUGCCACUGAUCACGAGUGUGAAAU
GCAG <b>GGACCUGCACACGGAU</b> UGUGUG	GCACUUACCUGAAGG <b>GGAAUGGGAGG</b>
UGUCCAGAGAUGAUAAAAA <b>GGAGU</b>	<b>GGAU</b> UCCUCCUUUGGGGUGUCAGAC
UAGUCAUG	CAUGC <b>GGAGCG</b> GAUUAACCACAUGGCG
	CGGGUCCGCGCAUACCAUUUGUGUGC
	UCAUAAAGAGAGAUUAA <b>GGAG</b> CUUUU
	<u>AUG</u>

**Figure 27: *E. coli* and *Y. pestis glgCAP* biosynthesis operon 5' UTR Comparison.**

Comparison of the *E. coli glgCAP* major transcript 5' UTR and the predicted *Y. pestis glgCAP* 5' UTR (BPROM score 2.2; theoretical -35 and -10 TSS boxes in **bold** [133]) glycogen synthesis operons. Numerals I and II indicate experimentally characterized CsrA interaction sites [131]. Yellow highlights reflect putative CsrA binding motifs. The *glgC* 5' UTR of *E. coli* and *Y. pestis* demonstrate multiple putative CsrA binding sites, suggesting a similar mode of CsrA-mediated repression of glycogen synthesis amongst the two pathogens.

My results demonstrate that deletion of the *glgCAP* operon does not significantly alter *Y. pestis* biofilm formation, thereby establishing glycogen formation is dispensable for *Y. pestis* biofilm production. As such, deletion of the *glgCAP* glycogen synthesis operon from the CO92 *csrA*-deficient mutant was insufficient to restore Congo red pigmentation or biofilm production. Therefore, the mechanism by which CsrA enables *Y. pestis* biofilm production transpires through a mode of action independent of glycogen regulation.

*Y. pestis* PNAG production is dependent upon the cyclic diguanylate small molecule activator. There are two characterized inhibitors of *Y. pestis* biofilm production

which function through conserved mode of cyclic diguanylate regulation: 1) the Fur transcriptional regulator which impairs transcription of *hmsT* encoding a diguanylate cyclase and 2) the HmsP phosphodiesterase which enables cyclic diguanylate degradation [61,62,134]. Carbon catabolite regulation of *Y. pestis* biofilm production, as detailed in Chapter 2, is not associated with transcriptional alterations of *hmsT*, and therefore, is unlikely to be mediated by CsrA regulation of Fur. Interestingly, the predicted 5' UTR of *Y. pestis hmsP* indicates multiple putative CsrA binding sites (**Fig. 28**).

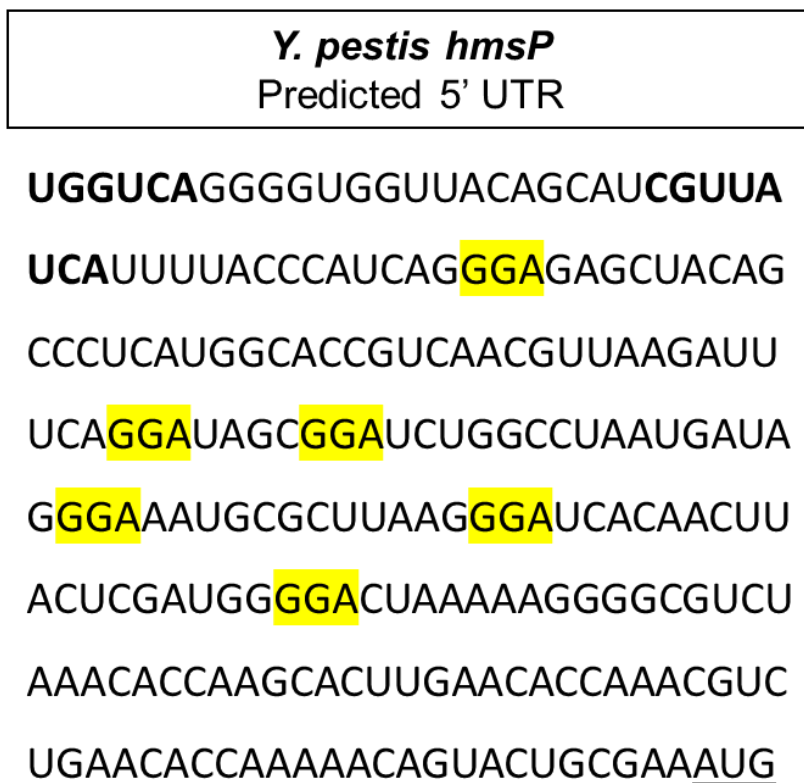


**Figure 28:** *Y. pestis hmsP* 5' UTR Predicted CsrA-binding Sites.

The predicted *Y. pestis hmsP* 5' UTR (BPROM score 3.68; theoretical -35 and -10 TSS boxes in **bold** [133]) encoding a diguanylate cyclase phosphodiesterase. Yellow highlights indicate putative CsrA binding motifs. The *hmsP* 5' UTR demonstrates various putative CsrA binding sites, potentially reflecting CsrA-mediated repression cyclic diguanylate turnover in *Y. pestis*.

Upon deletion of *hmsP* from the CO92 *csrA*-deficient mutant, Congo red assimilation was restored. Moreover, the *csrA* and *hmsP* double deficient mutant produced excessive biofilms as demonstrated by crystal violet assay. Therefore, CsrA may indirectly promote *Y. pestis* biofilm production by promoting biosynthesis and/or preventing degradation of cyclic diguanylate biosynthesis. However, further studies are necessary to confirm the role of CsrA upon *Y. pestis* cyclic diguanylate regulation.

CRP-mediated modulation of CsrA may contribute to carbon catabolite regulation of *Y. pestis* biofilm production. It has been demonstrated that CsrB and CsrC sRNA inhibitors of CsrA are not readily expressed in *Y. pestis* at 26°C relative to 37°C [120]. Therefore, sequestration of CsrA may be repressed during *Y. pestis* infection of the flea vector. The differential modulation of CsrB and CsrC sRNA species by CRP may confer optimal CsrA activation during infection of the flea midgut. Perhaps CRP-induced CsrC does not sequester CsrA as efficiently as CRP-repressed CsrB. It is important to note that *Y. pestis* CsrC, contrary to *E. coli* CsrC, contains a 3' terminal poly(U)-rich region. Such sites have been shown to facilitate interaction with the sRNA chaperone molecule, Hfq [69]. Thus, the modification of *Y. pestis* CsrC may promote Hfq-mediated sequestration, thereby preventing CsrA inhibition. Alternately, the expression other uncharacterized factors subject to CsrA regulation may be repressed in active CRP active conditions, thereby reducing CsrA sequestration and enhancing *Y. pestis* biofilm production.

At a relatively low frequency, similar to what has been described for *en bloc* excision of the Pgm locus, the *csrA*-deficient mutants spontaneously revert to a positive pigmentation phenotype. Thus, I sought to assess whether the revertant clones have lost an IS element containing a CsrA-repressed negative regulator of *Y. pestis* biofilm production. However, whole genome sequencing of CO92 and KIM6+ *csrA*-deficient pigmentation revertant clones along with the respective impaired pigmentation phenotype *csrA* deletion progenitors demonstrated retention of all IS elements. Moreover, no conserved unique sequence variations were identified amongst the both sets of *csrA*-

deficient pigmentation impaired and the pigmentation positive revert clones. Therefore, pigmentation reversion of the  $\Delta csrA$  mutants is not a consequence of single-nucleotide polymorphism, frameshift, or loss of IS elements or recombinatorial deletions. However, one potential limitation of the reference alignment approach may be the masking of additional IS element insertions or direct repeats which may confer a compensatory effect or disrupt relevant genes/sRNA. Alternately, plasmid copy number may vary amongst the pigmentation impaired and pigmentation positive mutants; however, this scenario is less likely considering the revertant phenotype is stable through serial passage.

## **Chapter 4. Elucidating the Involvement of sRNA upon *Y. pestis* Carbon Catabolite Regulation of Biofilm Formation**

### **INTRODUCTION**

Various RNA sequencing studies conducted by multiple investigative groups have been identified a plethora of sRNA species expressed in *Yersinia* [65,66,67,134]. Many of which are highly conserved amongst other members of family Enterobacteriaceae; however, certain sRNA species are novel to *Y. pestis* or have been lost during the divergence from the *Y. pseudotuberculosis* ancestor. Notably, two putative sRNA species, sR084 and Ysr172, are not present in the atypical, non-epidemic *Y. pestis* strain Pestoides F. Contrary to *Y. pestis* strains CO92 and KIM6+ which are subject to carbon catabolite regulation of biofilm production, Pestoides F is a more ancestral biovar Microtus isolate [23,136,137]. The acquisition of novel sRNA species in the more evolutionary divergent *Y. pestis* isolates may be reflective of sRNA-mediated *Y. pestis* microevolution. However, biofilm production of Pestoides F in response to available carbon sources has not been characterized.

The physiological function of the overwhelming majority of *Y. pestis* predicted sRNA species has not been ascertained. Recently, HmsB (sR035/ysr104) sRNA has been identified as a critical regulator of *Y. pestis* biofilm formation which stimulates the expression of *hmsB*, *hmsCDE/NDA*, *hmsT*, and *hmsHFRS*, yet represses expression of *hmsP* [67,138]. However, the mechanism by which HmsB promotes *Y. pestis* biofilm formation has not been ascertained. The putative upstream promoter region of HmsB contains an RcsAB box sequence. The RcsA response regulator is not functional in *Y. pestis*; nonetheless, the DNA-binding response regulator RcsB may function independent of RcsA, thus promoting the expression of HmsB [134].

Bioinformatics predictions indicate theoretical CRP binding sites in the putative sRNA up-stream promoter regions of multiple sRNA species, including HmsB (BPROM score = 9) [133, 67, 138]. Moreover, the expression profiles of certain sRNA species have been shown to be differentially modulated in the presence or absence of CRP [67]. CRP may control the expression of sRNA species involved in biofilm production, thereby facilitating carbon catabolite regulation of *Y. pestis* biofilm formation. Furthermore, many sRNA species are differentially modulated in response to growth temperatures reflective of different aspects of the *Y. pestis* infectious cycle (**Table 9**). Central aspects of *Y. pestis* pathogenesis, possibly encompassing carbon catabolite regulation of biofilm production, may be facilitated by sRNA-mediated regulation.

**Table 9: *Y. pestis* Thermo-regulated sRNA Species**

<b>sRNA</b>	<b>Characteristics</b>	<b>Reference</b>
CsrC Ysr186/sR003	Homology to all <i>Yersinia</i> sp. Induced by CRP Down-regulated at 37°C	[66][67] [120]
CyaR/RyeE Ysr159/sR012	Homology to all <i>Yersinia</i> sp. Induced by CRP	[66] [67]
CsrB Ysr179/sR026	Homology to all <i>Yersinia</i> sp. Repressed by CRP Down-regulated at 37°C	[66] [67] [120]
Ysr110/sR065	Homology to all <i>Yersinia</i> sp. Up-regulated at 37°C Induced by CRP	[67] [135]
Yp-sR32	Homology to all <i>Yersinia</i> sp. Down-regulated 37°C Putative CRP-binding site	[65]
sR034/Ysr59 (2 size variants)	Homology to all <i>Yersinia</i> sp. Temperature Regulation	[67] [135]
HmsB sR035/Ysr104 (3 size variants)	Homology to all <i>Yersinia</i> sp. Temperature Regulation Putative CRP-binding site	[67] [133] [135] [138]
sR066	Homology to all <i>Yersinia</i> sp. Repressed by CRP	[67]
sR084	<i>Y. pestis</i> pPCP plasmid: Not in Pestoides F Induced by CRP Up-regulated at 37°C Putative CRP-binding site	[67]
Ysr172	<i>lacY</i> IS285 interruption: Not in Pestoides F Down-regulated at 37°C Putative CRP-binding site	[66]

Hfq is a chaperone molecule which facilitates interaction amongst sRNA species and target mRNA. Hfq has been described to differentially modulate biofilm formation of many bacterial species; however, the role of Hfq upon *Y. pestis* biofilm regulation is not fully understood considering two independent studies with *hfq*-deficient *Y. pestis* mutants have demonstrate conflicting findings. Foremost, deletion of *hfq* in a CO92 (pCD1+) background during growth in dextrose-rich BHI medium indicated Hfq impairs biofilm production [139]. Alternately, deletion of *hfq* in a KIM6+ (pCD1-) background during growth in TMH supplemented with 0.2% galactose demonstrated Hfq stimulates biofilm production [140]. Thus, there are two principal confounding variables evident amongst these studies: 1) discrepancies amongst *Y. pestis* genetic backgrounds, most notably the presence or absence of pCD1, and 2) inconsistencies in media composition which contain either primary or alternate carbon sources. CsrA has been shown to repress translation of Hfq in *E. coli*, further suggesting potential interplay amongst *Y. pestis* biofilm production and sRNA regulation [141].

The objective of this Chapter is to discern whether the acquisition of the sR084 and Ysr172 sRNA species, which contain putative CRP-binding sites and are uniquely expressed by *Y. pestis*, are involved in biofilm regulation. Furthermore, I seek to establish the role of Hfq in respect to carbon catabolite regulation of *Y. pestis* biofilm formation.

## **MATERIALS AND METHODS**

### **Bacterial Strains, Plasmids, and Oligonucleotides**

Bacterial strains and plasmids used in this chapter are detailed in **Table 10**. Oligonucleotides are detailed in **Appendix C Table 1**.

**Table 10: Bacterial Strains and Plasmids**

<i>Y. pestis</i> strains	Characteristics*	Reference
CO92	Pgm+ pCD+ pMT+ pPCP+	[112]
CO92 pPCP-	Pgm+ pCD+ pMT+ pPCP-	Motin collection Unpublished
CO92 pCD1- (CO92L)	Pgm+ pCD- pMT+ pPCP+	Motin collection [111]
CO92 $\Delta$ <i>hfq</i>	Scarless deletion of the <i>hfq</i> gene	Motin collection Unpublished
CO92 $\Delta$ <i>hfq</i> v2	Independently Constructed scarless deletion of the <i>hfq</i> gene	Motin collection Unpublished
CO92 $\Delta$ <i>hfq hfq'</i>	Scarless restoration of the <i>hfq</i> gene	Motin collection Unpublished
CO92 $\Delta$ <i>hfq</i> v2 <i>hfq'</i>	Scarless restoration of the <i>hfq</i> gene in <i>hfq</i> -deficient clone v2	Motin collection Unpublished
CO92 $\Delta$ Ysr172	Scarless deletion of the Ysr172 sRNA	Motin collection Unpublished
CO92 $\Delta$ Ysr172 Ysr172'	Scarless restoration of Ysr172 sRNA	Motin collection Unpublished
Pestoides F	Pgm+ pCD+ pMT+ pPCP-	CDC Collection
KIM6+	Pgm+ pCD <sup>-</sup> pMT+ pPCP+	Brubaker collection

KIM6+ : pCD1Ap	Pgm+ pCD1+ pMT+ pPCP+	[111]
<b>Plasmids</b>	<b>Characteristics</b>	<b>Reference</b>
pKD46	Mutagenesis helper plasmid, source of Lambda Red Recombinase, Ap <sup>R</sup>	[113]
pKD4_Km-sacB	Cloned <i>sacB</i> from pCVD442 in NgoMIV site of pKD4, source of <i>kan-sacB</i> cassette, Km <sup>R</sup> Ap <sup>R</sup> ,Suc <sup>S</sup>	[111]
pCD1Ap	Virulence plasmid pCD1 of <i>Y. pestis</i> KIM labeled with Ap <sup>R</sup> marker	Provided by R. Perry

### Scarless Deletion and Chromosomal Restoration

Utilizing the procedure described in Chapter 2, the *hfq* gene or the putative Ysr172 sRNA were independently excised from the *Y. pestis* CO92 background in a scarless fashion. Moreover, subsequent additional recombination events were employed to chromosomally reconstitute the original *hfq* gene or Ysr172 sRNA sequence via electroporation of a PCR fragment amplified with primers encompassing the deleted region using CO92 DNA as a template, thus chromosomally restoring the wild-type sequence. Verification of gene deletion and restoration was afforded by sequencing. Retention of the *pgm* locus was confirmed via PCR of the *hmsHFERS* operon.

### Growth Kinetics and Crystal Violet Biofilm Quantification Assay

Bacterial growth curves and crystal violet biofilm quantification were determined as previously described in Chapter 2.

## RESULTS

### Pestoides F is not Subject to Carbon Catabolite Regulation of Biofilm Production

The relative biofilm production of *Pestoides F* during growth in either HIB medium or BCS medium supplemented with either 0.2% K-gluconate or 0.2% glucose was quantified via crystal violet assay (**Fig. 29**).

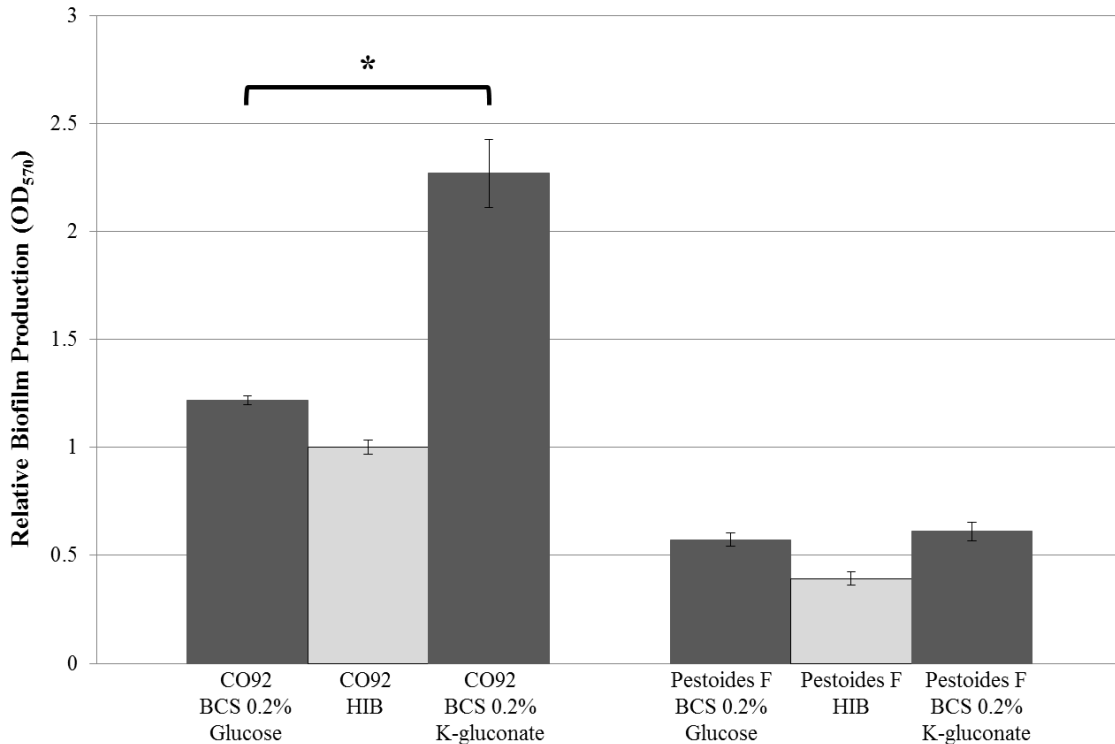


**Figure 29: *Pestoides F* Lacks Biofilm Carbon Catabolite Regulation**

Crystal violet relative biofilm quantification of CO92 and *Pestoides F* 24 hours post-inoculation of HIB and BCS containing either 0.2% glucose or 0.2% K-gluconate. Error bars reflect standard deviation from the mean of 2 independent experiments, each consisting of 4 technical replicates. \* P-value < 0.05 as determined by two-tailed Student’s T-test.

Contrary to what has been previously documented in Chapter 2 for *Y. pestis* strains CO92 and KIM6+, *Pestoides F* does not demonstrate differential modulation of biofilm formation in response to available primary or alternate carbon sources. Moreover, *Pestoides F* biofilm production is notably compromised regardless of media composition.

In order to elucidate the underlying mechanism defining the meager biofilm production of Pestoides F, I sought to elucidate the role of sR084 and Ysr172 sRNA species, which are not present in Pestoides F, upon *Y. pestis* biofilm regulation.

### ***Y. pestis* pPCP1, Encoding sR084 sRNA, is Dispensable for Biofilm Formation**

To determine the physiological impact of sR084 upon *Y. pestis* biofilm production, the biofilm production was compared amongst wild-type CO92 and a pPCP1-cured mutant (**Fig. 30**).

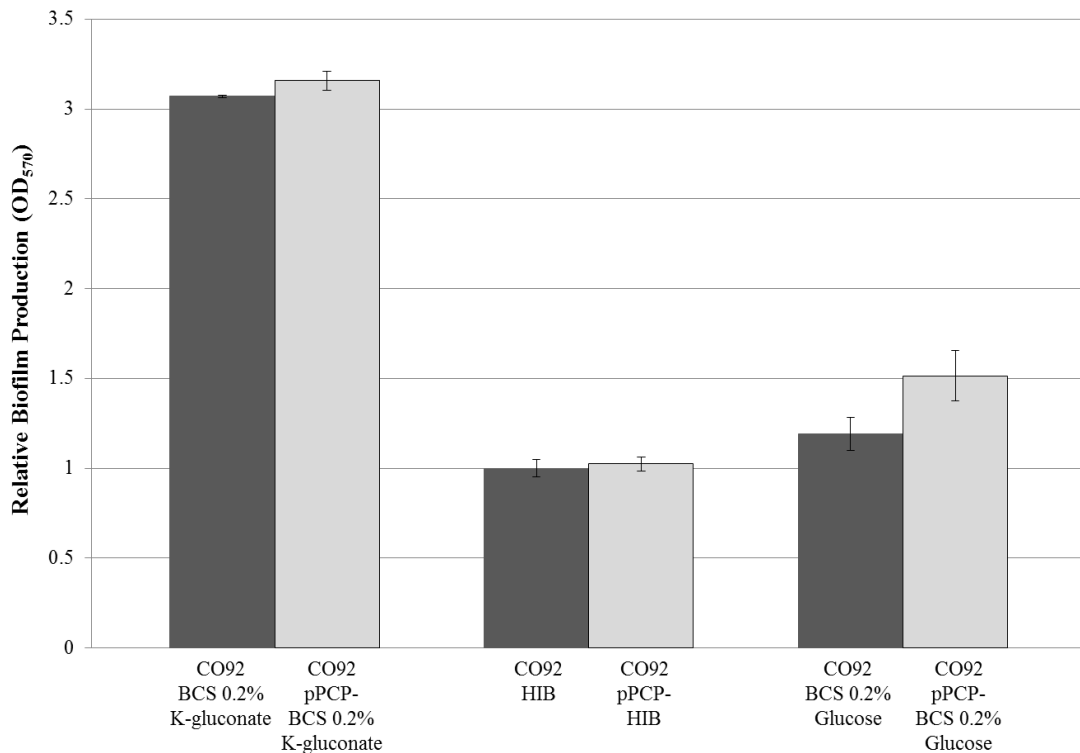


**Figure 30: pPCP, encoding sR084, does not alter CO92 Biofilm Production**

Relative biofilm formation of wild-type CO92 and a pPCP deficient mutant 24 hours post-inoculation of HIB and BCS containing either 0.2% glucose or 0.2% K-gluconate. Error bars reflect standard deviation from the mean of 2 independent experiments, each consisting of 4 technical replicates. \* P-value < 0.05 as determined by Student's T-test.

Irrespective of media composition, no significant alteration in biofilm production was identified amongst wild-type CO92 and the pPCP-negative variant. Therefore, my findings establish that the pPCP plasmid is dispensable for *Y. pestis* biofilm production. Moreover, these findings indirectly demonstrate that sR084 does not contribute to *Y. pestis* biofilm production.

### ***Y. pestis* Ysr172 does not Contribute to Biofilm Carbon Catabolite Regulation**

To elucidate the role of Ysr172 upon *Y. pestis* biofilm regulation, biofilm production of a Ysr172 sRNA scarless deletion mutant was quantified (**Fig. 31**).

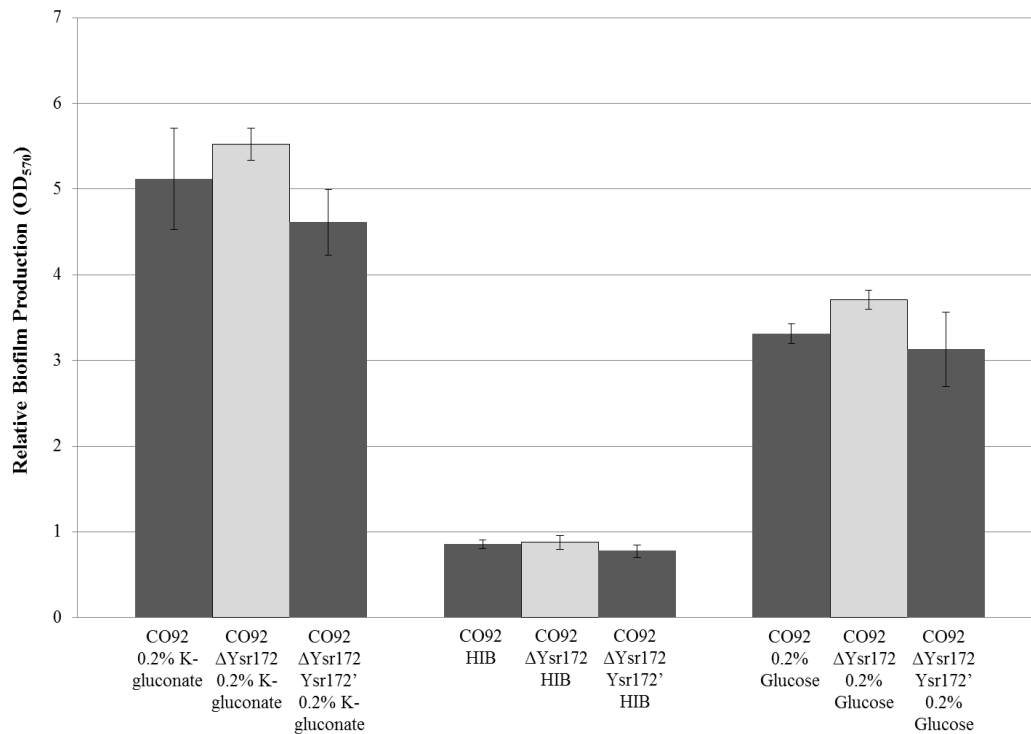


**Figure 31: Ysr172 has not Impact upon CO92 Biofilm Production**

Relative biofilm production of CO92, the CO92ΔYsr172 deletion mutant, and the chromosomally restored CO92ΔYsr172 Ysr172' following 24 hours post-inoculation of BCS medium supplemented with 0.2% K-gluconate, HIB medium, or BCS medium supplemented with 0.2% glucose. Error bars reflect standard deviation from the mean of 2 independent experiments, each consisting of 4 (BCS) or 6 (HIB) technical replicates. \* P-value < 0.05 as determined by Student's T-test.

Deletion of Ysr172 did not result in a significant change in biofilm formation relative to the isogenic control and chromosomal restoration clone during growth in either BCS or HIB medium. Therefore, the Ysr172 sRNA is not involved in *Y. pestis* biofilm regulation.

### **pCD1 does not contribute to *Y. pestis* Biofilm Production**

Prior studies by other investigators have suggested involvement of the pCD1 plasmid upon *Y. pestis* biofilm production. To discern the potential contribution of the *Y. pestis* pCD1 biofilm formation, wild-type CO92 (pCD1+), pCD1-cured CO92, KIM6+ (pCD1-), and KIM6+ transformed with pCD1Ap (kindly provided by Dr. Robert Perry) were compared via crystal violet biofilm quantification assay (**Fig. 32**).

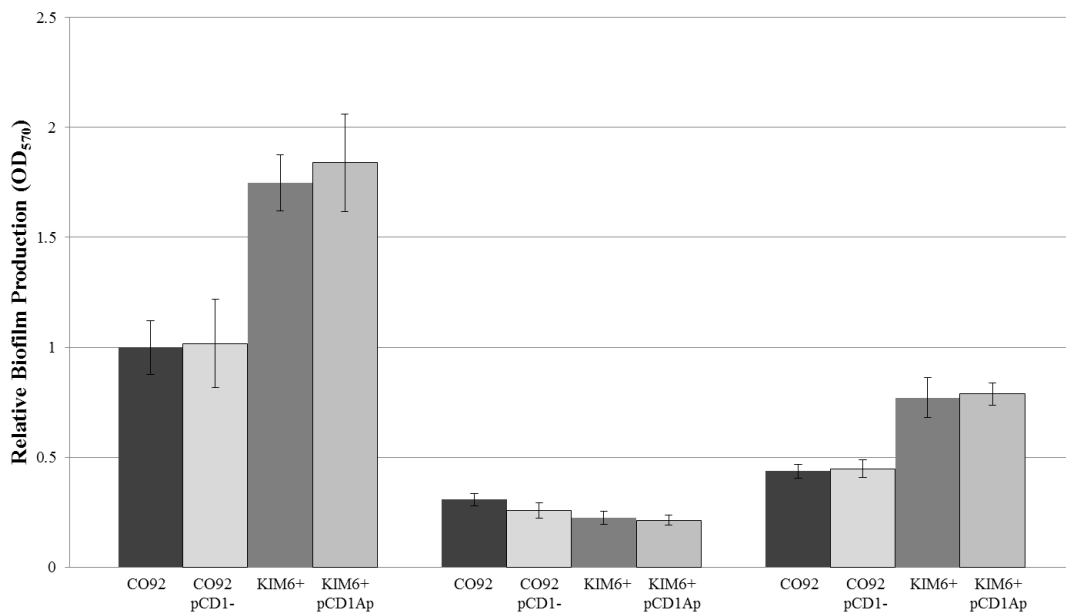


**Figure 32: pCD1 has no influence upon *Y. pestis* Biofilm Production**

Relative biofilm production of CO92, CO92 pCD1-, KIM6+, and KIM6+ : pCD1Ap following 24 hours post-inoculation of BCS medium supplemented with 0.2% K-gluconate, HIB medium, or BCS medium supplemented with 0.2% glucose. Error bars reflect standard deviation from the mean of 1 experiment consisting of 6 technical replicates. \* P-value < 0.05 as determined by Student's T-test.

Both the loss of pCD1 in CO92 and the transformation of pCD1Ap in KIM6+ did not significantly alter biofilm production relative to the respective parental strains. These findings demonstrate that pCD1 has no impact upon biofilm formation for both CO92 and KIM6+ strains of *Y. pestis*.

### Hfq, Dependent upon Available Carbon Sources, Differentially Modulates *Y. pestis* CO92 Biofilm Production

To identify the interplay amongst Hfq and *Y. pestis* carbon catabolite regulation of biofilm production, two independent *hfq*-deficient mutants were constructed in the CO92 background. Moreover, to circumvent variable complementation efficacy afforded by plasmid-based expression, the *hfq* gene was scarlessly restored in the deficient mutants to provide complete complementation. Growth kinetics in BCS medium supplemented with 0.2% glucose or 0.2% K-gluconate incubated at 26°C were determined (**Fig. 33**).

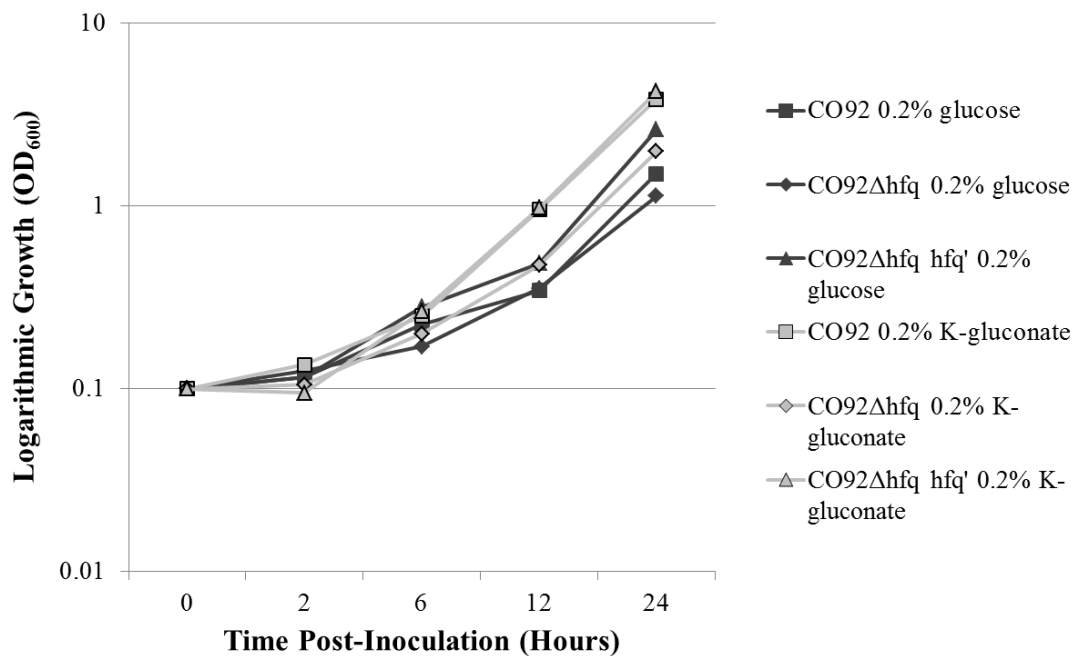


**Figure 33: Impaired Growth of the CO92 $\Delta hfq$  mutant**

Growth kinetics of CO92, CO92 $\Delta hfq$ , and CO92 $\Delta hfq hfq'$  when grown in BCS medium supplemented with either 0.2% K-gluconate or 0.2% glucose. Results reflect the average of two independent *hfq* deletion mutants and respective chromosomal restoration clones.

Deletion of *hfq* resulted in an approximate 1.5 to 2-fold decrease in growth relative to the isogenic control and the chromosomally complemented mutant after 24 hours post-inoculation of BCS medium supplemented with 0.2% glucose or 0.2% K-gluconate, respectively. Therefore, to distinguish the direct regulatory involvement of Hfq upon *Y. pestis* biofilm formation, subsequent biofilm formation findings require growth density normalization.

The impact of *hfq*-deficiency upon *Y. pestis* biofilm production was quantified by crystal violet assay (**Fig. 34**).

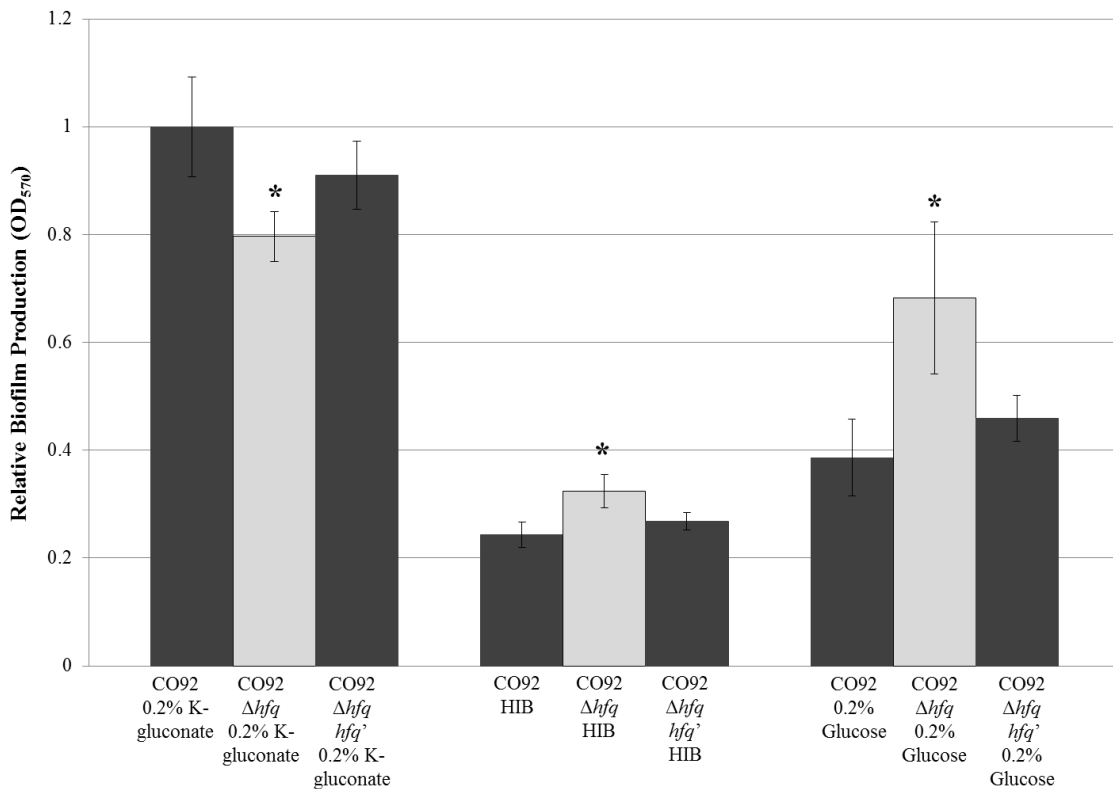


**Figure 34: Hfq Differentially Modulates *Y. pestis* Biofilm Production Dependent upon Available Carbon Sources.**

Relative biofilm production of CO92, CO92 $\Delta$ *hfq*, and CO92 $\Delta$ *hfq hfq'* when grown in BCS medium supplemented with 0.2% K-gluconate, HIB medium, or BCS medium supplemented with 0.2% glucose. Results reflect the average 3 experiments, each consisting of 4 technical replicates. Moreover, CO92 $\Delta$ *hfq*, and CO92 $\Delta$ *hfq hfq'* reflect the average of two independently derived *hfq* deletion mutants and respective chromosomal restoration clones.  
\* P-value <0.05 as determined by two-tailed Student's T test.

When grown in BCS medium supplemented with 0.2% K-gluconate, the biofilm production of the CO92 $\Delta$ *hfq* mutants was impaired. Conversely, when grown in BCS medium supplemented with 0.2% glucose, the biofilm production of the *hfq*-deficient mutants was enhanced. Therefore, these findings demonstrate that Hfq represses biofilm production in the presence of primary carbon sources, but enhances biofilm production upon sole utilization of alternate carbon sources. Upon normalization to growth density when cultured in BCS solely supplemented with 0.2% K-gluconate, there is no discernable change in biofilm production. Therefore, primarily as a consequence of growth rate, Hfq promotes *Y. pestis* biofilm production during the metabolism of alternate carbon sources. Alternately, biofilm normalization to optical density when grown in the presence of glucose further augments biofilm production of the *hfq*-deficient mutants. Therefore, Hfq negatively regulates biofilm production during the metabolism of primary carbon sources.

## **DISCUSSION**

In order to evaluate the evolution of *Y. pestis* carbon catabolite regulation of biofilm production, I sought to characterize the biofilm formation of Pestoides F (biovar Microtus), a phylogenetically ancestral isolate of *Y. pestis*. My findings demonstrate that, contrary to the more recent evolutionary divergents KIM6+ (biovar Medievalis) and CO92 (biovar Orientalis), Pestoides F does not differentially modulate biofilm production

in response to primary or alternate carbon sources. No significant change in Pestoides F biofilm production is detected when cultured in BCS medium supplemented with either 0.2% K-gluconate or 0.2% glucose. Moreover, regardless of media composition, Pestoides F biofilm production is relatively impaired in respect to the more evolutionarily recent isolates. Since CRP is known to be involved in sRNA regulation, I sought to assess whether the presence of unique sRNA molecules not present in Pestoides F contribute to carbon catabolite regulation of *Y. pestis* biofilm production.

There are two sRNA species, sR084 and Ysr172, identified by independent studies by other investigators that are not expressed in Pestoides F and contain upstream putative CRP-binding sites [66,67,133]. Foremost, sR084 is encoded on the pPCP1 plasmid which is absent in Pestoides F. Alternately, the Ysr172 sRNA is the product of IS285 element interruption of the *lacY* gene which is present in both KIM6+ and CO92, but not in Pestoides F. As an indirect measure to determine the contribution of sR084 upon *Y. pestis* biofilm production, CO92 and an isogenic pPCP1 cured mutant were compared. To determine the impact of Ysr172, the sRNA was scarlessly deleted from the CO92 background. Regardless of BCS or HIB media type, no change in biofilm formation was identified amongst the CO92 pPCP1 positive and negative strains. Furthermore, no significant alteration in biofilm production was observed in the presence of available primary or alternate carbon source. Therefore, these findings demonstrate the entire pPCP1 plasmid, including sR084, is dispensable for *Y. pestis* biofilm production. This observation coincides with studies showing the pPCP plasmid does not affect *Y. pestis X. cheopis* colonization, blockage, or transmission [142]. My findings also establish no change in biofilm production amongst the Ysr172-deficient mutant and the isogenic parent/chromosomal restoration controls. The presence of Ysr172 sRNA may simply reflect an arbitrary artifact of IS element recombination or may serve an alternate function, independent of biofilm regulation, during *Y. pestis* pathogenesis.

Therefore, the mechanism by which Pestoides F biofilm production, void of carbon catabolite regulation, is compromised relative to KIM6+ and CO92 must transpire through alternate means. It is crucial to note that the genome of Pestoides F contains multiple missense mutations within previously characterized biofilm related factors (Table 11) [136].

**Table 11: Pestoides F Biofilm Synthesis/Regulation Missense Mutations**

<b>Protein</b>	<b>Missense Mutation</b>
HmsF	L260Q
HmsP	L288M
HmsT	F15L
HmsT	N313S*

\* *Y. pseudotuberculosis* ancestral-type sequence.

As such, the poor capacity to produce biofilms by Pestoides F may be a consequence of genetic mutation which disrupts PNAG biosynthesis and/or excretion. Although it is uncertain whether these mutations are naturally acquired or laboratory derived, additional studies are necessary to discern the potential impact of the point mutations upon biofilm production. Characterization of the Pestoides F missense mutations may provide key insight regarding the mechanism defining *Y. pestis* carbon catabolite regulation of biofilm formation.

As described in Chapter 3, CsrA was shown to be a crucial positive regulator of *Y. pestis* biofilm production. In *E. coli*, CsrA has been shown to repress translation of the sRNA chaperone molecule, Hfq [141]. Studies in *Y. pestis* have demonstrated conflicting contributions regarding the impact of Hfq upon biofilm formation [139,140]. However, one of the confounding variables amongst these studies is the presence or absence of the

pCD1 plasmid. Thus, I sought to assess the impact of pCD1 upon *Y. pestis* biofilm production. To do so, I compared wild-type CO92 to a pCD1-cured variant as well as KIM6+ to an isogenic mutant transformed with pCD1Ap. My findings revealed no alteration in biofilm formation regardless of the presence or absence of pCD1 in either genetic background. Therefore, pCD1 is dispensable for *Y. pestis* biofilm production and is not responsible for the conflicting findings demonstrating variable contributions of Hfq upon *Y. pestis* biofilm formation.

Another confounding variable amongst the independent biofilm assessments of *hfq*-deficient mutants pertains to media composition. The study by Bellows et al., 2012 utilized BHI which is supplemented with dextrose, a primary carbon source. Alternately, the study by Rempe et al., 2012 utilized TMH supplemented with 0.2% galactose, an alternate carbon source. Thus, the conflicting contributions regarding of Hfq upon *Y. pestis* biofilm formation by be dependent upon available carbon sources. My findings demonstrate that growth of an *hfq*-deficient mutant in the presence of glucose stimulates biofilm production. Conversely, when the *hfq* deletion mutant is grown in culture media solely supplemented with alternate carbon sources, biofilm formation is impaired. Therefore, my results independently verify the findings procured by the other investigators which demonstrate the involvement of Hfq upon carbon catabolite regulation of *Y. pestis* biofilm formation.

It is interesting to note that, regardless of media composition or available carbon source, deletion of *hfq* results in stunted growth kinetics. Upon normalization of biofilm formation to growth kinetics when cultured in media solely supplemented with alternate carbon sources, the defect in biofilm formation of the *hfq*-deficient mutant is diminished. Therefore, rather than conferring a direct regulatory effect, Hfq likely enhances *Y. pestis* biofilm production during the metabolism of alternate carbon sources by stimulating growth. However, when biofilm production of the *hfq* deletion mutant is normalized to optical density when grown in BCS medium supplemented with glucose or in HIB

medium, the observed enhancement of biofilm formation is further amplified. Thus, Hfq represses biofilm production during both peptide catabolism as well as during the metabolism of primary carbon sources. These findings suggest that Hfq may facilitate the interaction amongst sRNA species and/or target mRNA species which in turn regulate *Y. pestis* biofilm production. Many sRNA species identified in *Y. pestis* have been shown to be differentially expressed in the presence or absence of Hfq. However, further work is necessary to characterize the specific sRNA/mRNA species which interact with Hfq to enable the differential regulation of *Y. pestis* biofilm production.

## **Chapter 5. Carbon Catabolite Regulation of *Y. pestis* Pathogenesis**

### **INTRODUCTION**

The CRP global regulator has been shown to differentially modulate greater than 6% of the total protein encoding capacity of *Y. pestis*, including prominent virulence factors [103]. CRP directly enhances the gene expression of *pla*, encoding a plasminogen activator protease, which promotes *Y. pestis* dissemination during pneumonic and bubonic forms of plague [143]. Conversely, CRP negatively regulates transcription of the *sycO-ypkA-ypoJ* operon, thereby repressing the expression of T3SS chaperone and effector molecules [103]. *Y. pestis* mutants deficient in *crp* have been shown to be attenuated for virulence [103,144].

Studies in *E. coli* have demonstrated that G3P indirectly inhibits the activation of CRP [105]. However, as described in Chapter 2, *Y. pestis* biovar Orientalis isolates have lost the capacity to ferment glycerol as consequence of a uniform deletion in *glpD* [110]. The inability to ferment glycerol is notably ensured by a variety of disruptive mutations in *glpK* [111]. Interestingly, sole dysfunction of *glpD* in the presence of functional *glpK* suppresses *Y. pestis* intracellular concentrations of G3P [111]. Prior transcriptomics

analyses have indicated components of the aerobic glycerol metabolic pathway are simulated during temperature shifts representing the transition from the flea vector (26°C) to the human host (37°C) and amid survival in the macrophage intraphagosomal environment [145,146]. Therefore, the acquired defect in *Y. pestis* aerobic glycerol metabolism may reflect evolutionary modification of adaptive responses which promote CRP activation during mammalian infection. However, the interplay amongst glycerol metabolism and CRP activation in respect to mammalian pathogenesis has not been assessed in *Y. pestis*.

CRP differentially modulates the expression of CsrB and CsrC sRNA inhibitors of the carbon storage regulator protein, CsrA [120]. CsrA has been shown to inhibit expression of the RovA transcriptional regulator in *Y. pseudotuberculosis* [120]. Recent studies indicate the CRP/CsrA/RovA regulatory network facilitates the expression profile consistent with persistent *Y. pseudotuberculosis* infection [147]. Furthermore, the primary cell entry factor invasin, InvA, is activated by RovA in both *Y. enterocolitica* and *Y. pseudotuberculosis* [148,149]. Although *invA* is dysfunctional in *Y. pestis*, *rovA*-deficient *Y. enterocolitica* is significantly less virulent than an *inv* mutant, indicating RovA regulates additional virulence determinants [148,150]. To further support this notion, deletion of *rovA* has been shown to significantly attenuate *Y. pestis* virulence in a bubonic model of plague [116]. Therefore, I seek to elucidate the impact of CsrA regulation during *Y. pestis* in environments reflective of the mammalian host.

## **MATERIALS AND METHODS**

### **Bacterial Strains, Plasmids, and Oligonucleotides**

Bacterial strains and plasmids used in this chapter are detailed in **Table 12**. Oligonucleotides are detailed in **Appendix D Table 1**.

**Table 12: Bacterial Strains and Plasmids**

<i>Y. pestis</i> strains	Characteristics*	Reference
CO92	Pgm+ pCD+ Gly <sup>-</sup>	[112]
CO92L	Pgm+ pCD- Gly <sup>-</sup>	Motin collection Unpublished
CO92L <i>glpD</i> +	Pgm+ pCD <sup>-</sup> Gly <sup>-</sup> (defective <i>glpD</i> ' allele replaced with functional <i>glpD</i> gene in the chromosome)	[111]
CO92Δ <i>csrA</i> 5a	Scarless deletion of the <i>csrA</i> gene clone 5a	Motin collection Unpublished
CO92Δ <i>csrA</i> 3b	Scarless deletion of the <i>csrA</i> gene clone 3b	Motin collection Unpublished
CO92Δ <i>csrA</i> <i>csrA</i> ' 5a	Scarless Restoration of the <i>csrA</i> gene of clone 5a	Motin collection Unpublished
CO92Δ <i>csrA</i> Δ <i>glgCAP</i>	Scarless deletion of <i>glgCAP</i> operon from <i>csrA</i> -deficient clone 5a	Motin collection Unpublished
CO92Δ <i>csrA</i> Δ <i>nhaR</i>	Scarless deletion of <i>nhaR</i> gene from <i>csrA</i> -deficient clone 5a	Motin collection Unpublished
CO92Δ <i>csrA</i> <i>csrA</i> ' 3b	Scarless Restoration of the <i>csrA</i> gene of clone 3b	Motin collection Unpublished
CO92Δ <i>phoQP</i>	FRT recombinatorial deletion of <i>phoQP</i>	Motin collection
KIM6+	Pgm+ pCD <sup>-</sup> Gly+	Brubaker collection
KIM6+ : pCD1Ap	Pgm+ pCD+ Gly+	[111]

KIM5 (D27)	Pgm <sup>-</sup> pCD <sup>+</sup> Gly <sup>+</sup>	Brubaker collection
KIM 6+ <i>glpD'</i> :pCD1Ap	Pgm <sup>+</sup> pCD <sup>+</sup> Gly <sup>-</sup> (functional <i>glpD</i> gene replaced with defective <i>glpD'</i> allele in the chromosome)	[111]
KIM6+ $\Delta$ <i>glpABC</i> :pCD1Ap	Pgm <sup>+</sup> pCD <sup>+</sup> Gly <sup>+</sup> FRT recombinatorial deletion of the <i>glpABC</i> operon	[111]
KIM6+ <i>glpD'</i> $\Delta$ <i>glpABC</i> :pCD1Ap	Pgm <sup>+</sup> pCD <sup>+</sup> Gly <sup>-</sup> (functional <i>glpD</i> gene replaced with defective <i>glpD'</i> allele in the chromosome) FRT recombinatorial deletion of the <i>glpABC</i> operon	[111]
KIM 6+ $\Delta$ <i>crp</i> :pCD1Ap	Pgm <sup>+</sup> pCD <sup>+</sup> Gly <sup>+</sup> Scarless deletion of the <i>crp</i> gene	Motin collection Unpublished
KIM6+ $\Delta$ <i>csrA</i> 2:14	Scarless deletion of the <i>csrA</i> gene clone 2:14	Motin collection Unpublished
KIM6+ $\Delta$ <i>csrA</i> <i>csrA'</i> 2:6	Scarless Restoration of the <i>csrA</i> gene of clone 2:14	Motin collection Unpublished
<b>Plasmids</b>	<b>Characteristics</b>	<b>Reference</b>
pKD46	Mutagenesis helper plasmid, source of Lambda Red Recombinase, Ap <sup>R</sup>	[113]
pKD4	Source of <i>kan</i> cassette, Km <sup>R</sup> Ap <sup>R</sup>	[113]
pCD1Ap	Virulence plasmid pCD1 of <i>Y. pestis</i> KIM labeled with Ap <sup>R</sup> marker	Provided by R. Perry

### Deletion of the *glpABC* operon

The *glpABC* operon which facilitates the anaerobic metabolism of glycerol was deleted from KIM6+ and KIM6+ *glpD'* [111,113]. Briefly, a single crossover recombination event replaced the *glpABC* operon with a kanamycin-resistant deletion construct amplified from pKD4 in electrocompetent *Y. pestis* expressing Lambda Red

Recombinase encoded by the pKD46 helper plasmid. FLP-mediated recombination was utilized for excision of the *glpABC* deletion cassette.

### **37°C Growth Kinetics**

Growth kinetics of the glycerol metabolism and carbon storage regulator mutants were performed as previously described in Chapter 2. However, to assess conditions reflective of the mammalian host system, growth kinetics were determined during incubation at 37°C [111]. Additionally, to circumvent prolonged lag phase and prevent potential cell death/bacteriostasis during K-phosphate wash, growth of the *csrA* mutants and respective controls were also assessed following two experimental pre-growth transfers in BCS medium supplemented with 0.2% K-gluconate during incubation at 26°C whilst shaking at 250 rpm. Thereafter, a direct transfer yielding a final OD<sub>600</sub> = 0.1 was inoculated in BCS medium supplemented with either 0.2% K-gluconate or a combination of both 0.2% K-gluconate and 0.2% glucose inoculated at 37°C while shaking at 250 rpm. Optical density readings were determined at 0, 3, 6, 12, and 24 hours post-inoculation. After 24 hours of growth at 37°C, the entire culture was transferred to 26°C. Additional optical density readings were determined at 0, 6, 18, 24, and 48 hours post-transfer to 26°C. To support optical density readings, CFU statistics were determined at each time point post-inoculation via plating dilution series on either HIA or Congo red agar supplemented with 0.2% K-gluconate.

### **Semi-quantitative RT-PCR**

*Y. pestis* KIM5 (D27) derived from glycerol stock was streaked on HIA plates and incubated at 26°C for 36 hours. An initial OD<sub>600</sub> = 0.1 was inoculated in 50 ml of chemically defined BCS medium supplemented with 0.2% K-gluconate in a 500 ml flask

at for 12 hours at 26°C whilst shaking at 250 rpm. 170 ml of chemically defined BCS medium supplemented with 0.2% K-gluconate was again inoculated with  $OD_{600} = 0.1$  of pre-grown bacteria in 1 L flask and incubated for 4 hours at 26°C while shaking at 250 rpm. Twenty-five milliliters of chemically defined BCS media with 4 mM  $CaCl_2$  containing either 0.2% K-gluconate; 0.2% K-gluconate and 0.2% glycerol; or 0.2% K-gluconate, 0.2% glycerol, and 0.2% glucose were inoculated with  $OD_{600} = 0.3$  in 250 ml flasks and incubated at 26°C or 37°C. Approximately  $8 \times 10^8$  total cells as determined by optical density were extracted at 1 and 4 hours post-inoculation and immediately added to an equal volume of cold (4°C) RNeasy Lysis Solution (Qiagen). RNA isolation, DNase treatment, RT-PCR amplification, and product visualization were all performed as described in Chapter 2 (**Appendix D Figs. 1 & 2**). Semi-quantitative analyses were performed by ImageJ v1.47 (<http://rsb.info.nih.gov/ij/>) with normalization to the *gyrB* gene [111,115,116,117].

### **Murine-like Macrophage Challenge**

RAW 264.7 murine macrophage-like cells (ATCC, Manassas, VA) seeded at  $2 \times 10^5$  cells per well were grown in Dulbecco's modified Eagle medium (DMEM, Gibco BRL, Grand Island, NY) supplemented with glutamine, 10% (v/v) FBS and 1 mM sodium pyruvate (tissue culture medium) at 37° C in the presence of 5%  $CO_2$ . Following overnight incubation, the cells were washed twice with Dulbecco's Phosphate-Buffered Saline lacking calcium and magnesium (DPBS, Corning, Manassas, VA) and reconstituted with 250  $\mu$ l/well fresh tissue culture medium. *Y. pestis* strains CO92, CO92 $\Delta$ *csrA* 5a, CO92 $\Delta$ *csrA* 3b, CO92 $\Delta$ *csrA csrA'* 5a, CO92 $\Delta$ *csrA csrA'* 3b, CO92L, CO92L *glpD*<sup>+</sup>, KIM6<sup>+</sup>, KIM6<sup>+</sup> *glpD*<sup>'</sup>, KIM6<sup>+</sup> $\Delta$ *glpABC*, KIM6<sup>+</sup> *glpD*<sup>'</sup> $\Delta$ *glpABC*, and CO92 $\Delta$ *phoQP* were grown overnight at 26°C in DMEM containing glutamine, 1% (v/v) FBS, 1 mM sodium pyruvate, and 30 mM HEPES (bacterial growth medium). Overnight

cultures were then diluted and the bacteria were grown to the exponential phase. Macrophages were inoculated with an MOI = 0.1 of the bacterial suspension, and uptake was allowed for 1 hour at 37°C. The monolayer was washed twice with DPBS and then was incubated for an additional hour at 37°C with 1 ml of fresh tissue culture medium supplemented with 15 µg/ml gentamicin (Corning). Thereafter, coinciding with the 0 hour time point, the monolayer was washed twice with DPBS. The 18 hour time point samples were incubated at 37°C with tissue culture medium supplemented with 4 µg/ml gentamicin. Macrophages were lysed with 0.2 ml of 0.1% sodium deoxycholate in DPBS. The lysate was suspended in 1.8 ml of bacterial growth medium, serial dilutions were prepared in bacterial growth medium and plated onto HIA supplemented with 0.5% (v/v) FBS in duplicate. Results reflect the average of two biological replicates [111].

### ***Y. pestis* Glycerol Mutant Murine Challenge**

*Y. pestis* strains derived from glycerol stocks were cultured on HIA plates and grown at 26°C for 18-24 hours. Bacteria were streaked on fresh HIA plates and incubated again at 26°C for 12-18 hours. Strains were suspended and diluted in 0.033M K-phosphate buffer at 4°C. Groups of 5 Female 8 week Swiss Webster mice (Taconic Farms, Germantown, NY) were challenged by the subcutaneous (s.c.) route with 500 CFU (KIM6+ : pCD1Ap s.c. LD<sub>50</sub> = ~10 CFU) or by the intranasal (i.n.) route with 4,000 CFU (KIM6+ : pCD1Ap i.n. LD<sub>50</sub> = ~400 CFU) of each *Y. pestis* strain. Verification of proper inoculum concentration was ascertained by CFU determination on HIA plates. Experimental observation progressed for the course of four weeks. To discern more subtle changes in virulence, the experiment was replicated utilizing lower inoculum. Ten mice per group were challenged by the s.c. route with 200 CFU and 5 mice per group were challenged by the i.n. route with 2,000 CFU for each *Y. pestis* strain. The experiment was terminated at 16 days post-inoculation. Kaplan–Meier survival

curves were generated, and statistical significance was determined by log-rank test (IBM SPSS Statistics v20).

All animal experiments were conducted in ABSL-3 facilities within the Galveston National Lab under a protocol approved by the Institutional Animal Care and Use Committee at UTMB. The experimental duration progressed to a humane endpoint in which case surviving mice were euthanized [111].

## RESULTS

### Disruption of Aerobic Glycerol Metabolism does not affect 37°C Growth

Growth kinetics of the KIM6+ *glpD*' allelic exchange mutant were comparable to the parent strain during growth at 37°C when cultured in BCS chemically defined medium utilizing glucose as the sole carbon source (Fig. 35).

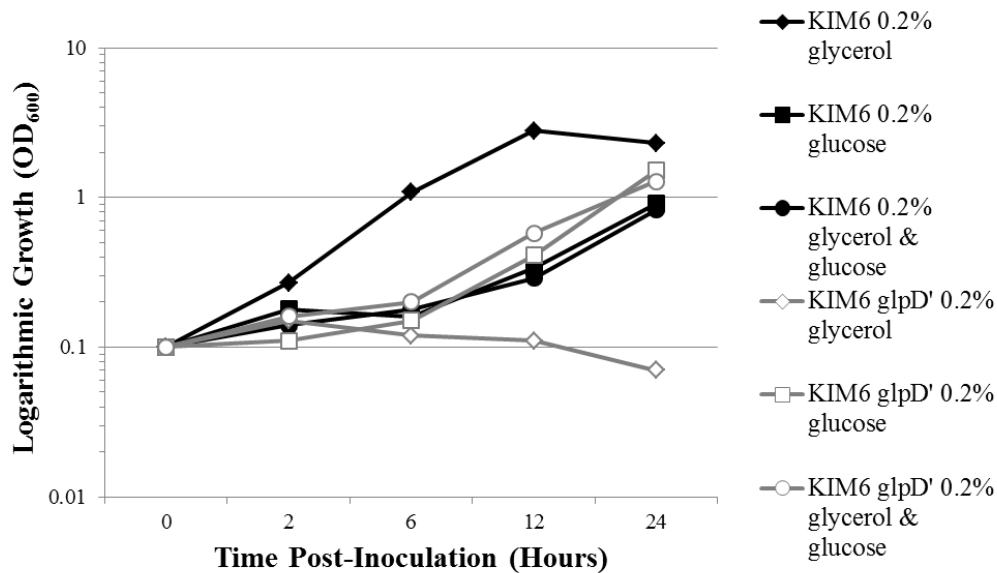


**Figure 35: 37°C Growth Kinetics of the *glpD*-impaired KIM6+**

Semi-logarithmic 37°C growth curve comparing KIM6+ and the KIM6+ *glpD*' mutant when cultured in BCS supplemented with either 0.2% glycerol, 0.2% glucose, or a combination of both 0.2% glycerol and 0.2% glucose. Reproduced with permission [111].

In accordance with the 26°C growth kinetics detailed in Chapter 2, the KIM+ *glpD*-dysfunctional mutant was incapable of proliferating in BCS medium solely supplemented with glycerol. Interestingly, the 37°C growth rate of KIM6+ in BCS medium supplemented with glycerol alone was superior relative to growth in BCS medium either solely supplemented with glucose or supplemented with a combination of both glucose and glycerol. This observation may indicate that *Y. pestis* metabolism of alternate carbon sources is more efficient than the utilization of glucose during growth at 37°C. Alternately, the presence of glucose may impart an inhibitory effect upon *Y. pestis* growth at 37°C. The growth rate of the KIM6+ and the *glpD*-dysfunctional mutant were nearly identical when cultured in medium solely supplemented with glucose in respect to medium simultaneously supplemented with both glucose and glycerol. Thus, *Y. pestis* preferentially utilize glucose indicative of carbon catabolite repression effect at 37°C.

### **Temperature Shift from 26°C to 37°C Prompts a Rapid Transient Up-Regulation of Aerobic Glycerol Metabolism**

Expression patterns of the aerobic glycerol metabolic pathway during transition from 26°C to 37°C in the presence of different carbon sources were evaluated via semi-quantitative RT-PCR (**Fig. 36**).

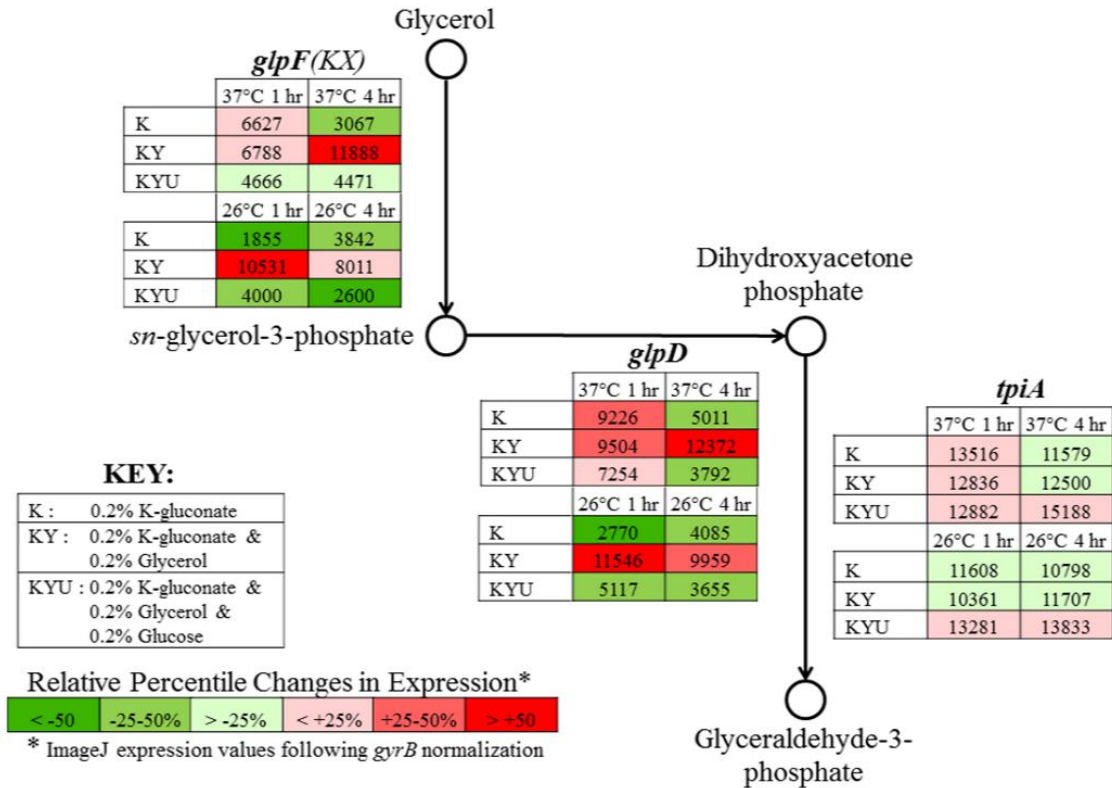


**Figure 36: Semi-quantitative RT-PCR of the Aerobic Glycerol Metabolic Pathway during Incubation at either 26°C or 37°C.**

Semi-quantitative RT-PCR of the aerobic glycerol metabolic pathway at 1 hour and 4 hours post-inoculation of BCS medium supplemented with either 0.2% K-gluconate (K); both 0.2% K-gluconate and 0.2% glycerol (KY); or 0.2% K-gluconate, 0.2% glycerol, and 0.2% glucose (KYU) at either 26°C or 37°C. RT-PCR conditions consisted of 25 ng total RNA for 25 cycles of amplification. Expression values were derived from ImageJ software analyses and normalized to *gyrB*. Color scale reflects relative percentile changes in gene expression from the mean. Reproduced with permission [111]

*Y. pestis* KIM5 was assessed during growth at both 26°C and following temperature shift to 37°C in chemically defined BCS medium containing 4 mM CaCl<sub>2</sub> supplemented with either 0.2% K-gluconate (BCS-K), both 0.2% K-gluconate and 0.2% glycerol (BCS-KY), or 0.2% K-gluconate, 0.2% glycerol and 0.2% glucose (BCS-KYU). The transition from 26°C to 37°C in BCS-K induced the expression of the aerobic

glycerol metabolic pathway *glpFKX* and *glpD* genes at 1 hour time point followed by a reduction in transcription to a degree comparable to the 26°C expression profile upon 4 hours post-inoculation. The expression of the *tpiA* gene encoding the triose phosphate isomerase which facilitates the glycolytic metabolism of glycerol remained constant despite growth temperature or media composition. The presence of glycerol in BCS-KY resulted in a steady expression of the aerobic glycerol pathway at both temperatures and both time points, demonstrating glycerol metabolism positive feedback. However, the presence of glucose in BCS-KYU resulted in carbon catabolite repression of *glpFKX* and *glpD* expression at both growth temperatures.

### **Glycerol Metabolism does not influence *Y. pestis* survival in macrophages**

*Y. pestis* viability following murine macrophage-like cell challenge was assessed for both the KIM6+ and CO92L *glpD* allelic exchange mutants. (Table 13).

**Table 13: *Y. pestis* Glycerol Mutant Log<sub>10</sub> CFU/mL Intracellular Viability upon RAW 264.7 Murine Macrophage-like Cell Challenge**

<i>Y. pestis</i> strain	0 hrs Post-Challenge	18 hrs Post-Challenge
CO92L	5.33 ± 0.09	4.58 ± 0.29
KIM 6+	5.64 ± 0.14	4.67 ± 0.24
KIM 6+ <i>glpD</i> '	5.55 ± 0.19	4.82 ± 0.06
KIM 6+ Δ <i>glpABC</i>	5.55 ± 0.2	4.74 ± 0.11
KIM 6+ <i>glpD</i> 'Δ <i>glpABC</i>	5.67 ± 0.25	5.03 ± 0.34
CO92L <i>glpD</i> +	5.31 ± 0.14	4.82 ± 0.12

Survival of the *glpD* allelic exchange mutants was not influenced by either inactivation or restoration of *glpD* in the respective KIM6+ and CO92L backgrounds. Furthermore, to circumvent unintentional shunting and enhanced induction of the anaerobic glycerol metabolic pathway, the *glpABC* system was deleted in both parental KIM6+ and the *glpD*-deficient strain. In either case, deletion of the *glpABC* operon had

no impact upon *Y. pestis* recovery after macrophage challenge. Therefore, *Y. pestis* aerobic glycerol metabolism does not contribute to intraphagosomal survival.

### Glycerol Metabolism does not alter *Y. pestis* virulence during *in vivo* infection

Swiss Webster mice were challenged with the KIM6+ aerobic glycerol metabolism mutants by the i.n. route with either 2,000 CFU (**Fig. 37A**) or 4,000 CFU (**Fig. 37B**).

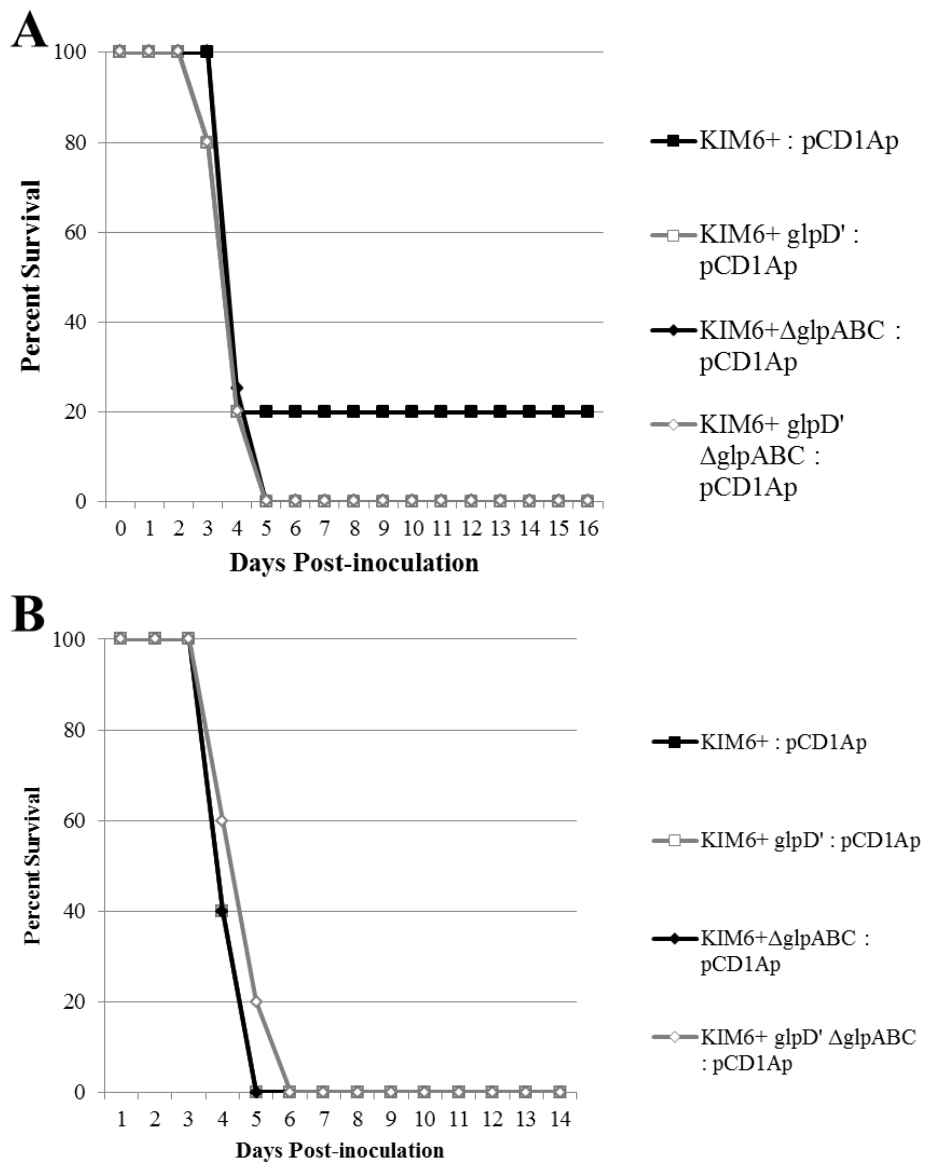


**Figure 37: *Y. pestis* Intranasal Virulence is not altered by Glycerol Metabolism**

Survival curves of intranasal murine challenge with KIM6+ and mutants deficient in *glpD* and/or the *glpABC* operon.

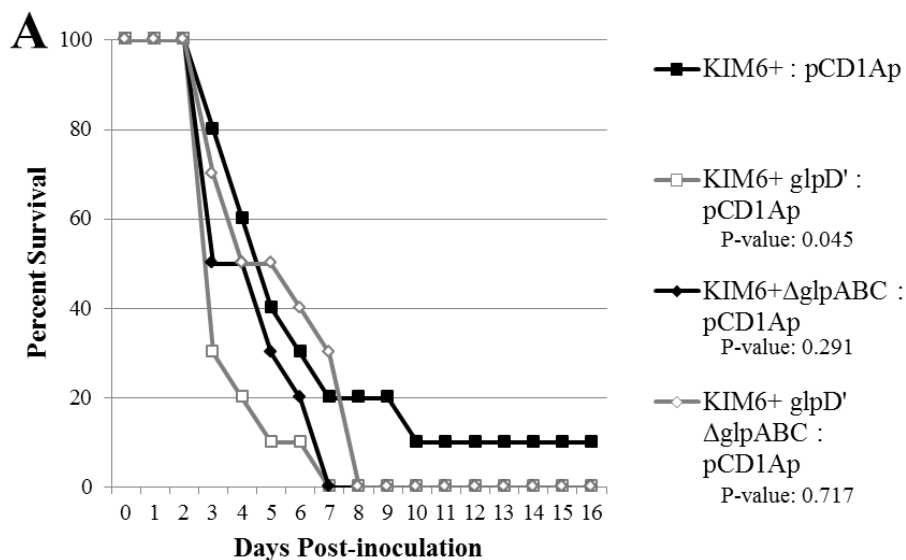
**A.** Intranasal inoculation with 2,000 CFU (~6 LD<sub>50</sub> KIM6+ : pCD1Ap), n = 5 mice per group.

**B.** Intranasal inoculation with 4,000 CFU (~10 LD<sub>50</sub> KIM6+ : pCD1Ap), n = 5 mice per group.

Verification of proper inoculum was determined by CFU enumeration. Statistical significance was determined by log-rank test. Reproduced with permission [111].

No change was observed in the time of death between mice challenged with the *glpD*-deficient mutant and parental KIM6+ upon i.n. inoculation with either dose. Moreover, deletion of the *glgCAP* operon in either the KIM6+ or the KIM6+ *glpD*' background did not impact virulence upon i.n. challenge. Therefore, pneumonic plague in the murine system is not affected by *Y. pestis* aerobic glycerol metabolism.

To determine the potential impact of *Y. pestis* aerobic glycerol metabolism upon a bubonic/septicemic model of plague, mice were challenged by the s.c. route of inoculation with either 200 CFU (**Fig. 38A**) or 500 CFU (**Fig. 38B**).



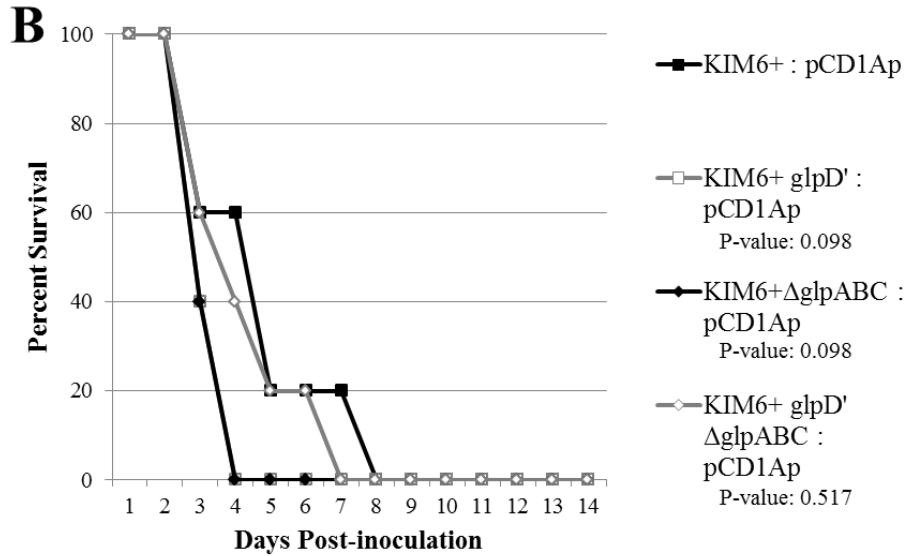


**Figure 38: *Y. pestis* Subcutaneous Virulence is Unaffected by Glycerol Metabolism**

Survival curves of murine subcutaneous challenge with KIM6+ and mutants deficient in *glpD* and/or the *glpABC* operon.

**A.** Subcutaneous inoculation 200 CFU (~20 LD<sub>50</sub> KIM6+ : pCD1Ap) n = 10 mice per group.

**B.** Subcutaneous inoculation 500 CFU (~50 LD<sub>50</sub> KIM6+ : pCD1Ap) n = 5 mice per group.

Verification of proper inoculum was determined by CFU enumeration. Statistical significance was determined by log-rank test. Reproduced with permission [111].

A mild, yet statistically insignificant, decrease in the mean time of death was observed for mice challenged with 500 CFU of the *glpD*-deficient mutant by the s.c. route in respect to those challenged with the KIM6+ control. A similar trend was observed upon challenge with 200 CFU. However, the potential reduction in virulence was very subtle and did not surpass the established threshold for statistical significance (P-value <0.025). Therefore, these findings can not conclude a contribution of *Y. pestis* glycerol metabolism toward virulence via s.c. route of inoculation. Taken together, the *in vivo* challenge data demonstrates that *Y. pestis* aerobic glycerol metabolism does not contribute to virulence in a mammalian system.

### 37°C Toxicity of the *csrA*-deficient *Y. pestis* Mutants

The 37°C growth kinetics of the *csrA*-deficient mutants were assessed in HIB and BCS medium supplemented with either 0.2% glucose or 0.2% K-gluconate (**Fig. 39**).

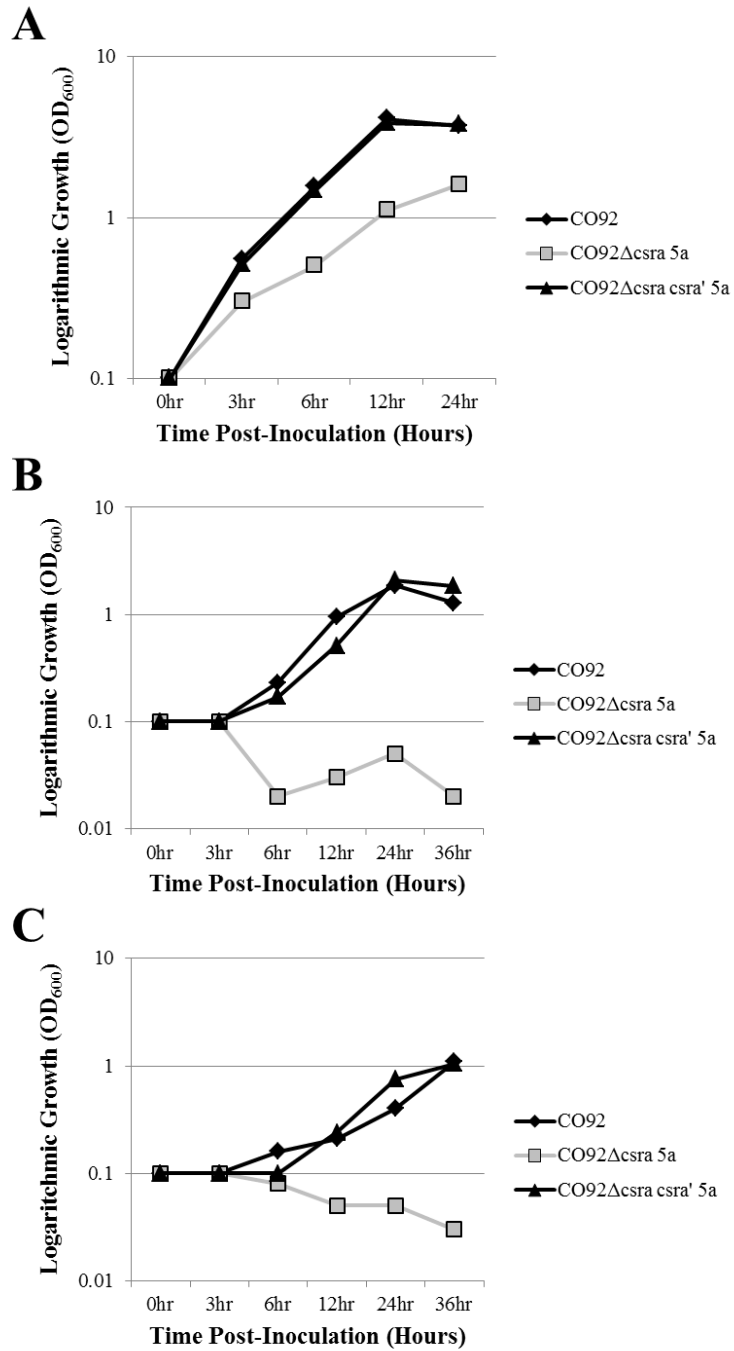


**Figure 39: CsrA Promotes *Y. pestis* CO92 Proliferation at 37°C**

Semi-logarithmic growth curves of CO92, the *csrA*-deficient mutant, and the *csrA* chromosomal restoration strain during incubation at 37°C.

A. Growth in peptide-rich HIB.

B. Cultured in BCS supplemented with 0.2% K-gluconate.

C. Cultured in BCS supplemented with 0.2% glucose.

Initial inoculum of OD<sub>600</sub> = 0.1 prepared in K-phosphate buffer suspension following experimental pre-growth in HIB.

Deletion of *csrA* was found to significantly impair growth of *Y. pestis* when cultured in HIB (**Fig. 39A**). Upon 12 hours post inoculation of HIB medium whilst incubating at 37°C, both wild-type CO92 and the *csrA* chromosomal restoration mutant achieved maximal growth density (OD<sub>600</sub> = 4.1 and 3.9, respectively); whereas, the *csrA*-deficient mutant demonstrated an approximate 3.5-fold reduction in growth (OD<sub>600</sub> = 1.1). Furthermore, after 24 hours post-inoculation, the CO92Δ*csrA* mutant reached an OD<sub>600</sub> = 1.6 which was reduced 2.3-fold relative to the control strains.

The 37°C growth defect of the *csrA*-deficient mutant was more pronounced upon inoculation of BCS medium regardless of alternate (**Fig. 39B**) or primary (**Fig. 39C**) carbon source supplementation. No growth was detected for CO92Δ*csrA* inoculated in BCS medium when incubated at 37°C. To the contrary, purely based upon absorbance readings, it appears that the *csrA*-deficient mutant demonstrates a reduction in growth density relative to the initial inoculum. Therefore, loss of *csrA* may confer a toxic effect during growth in BCS medium at 37°C. In order to determine whether the *csrA* mutants undergo a bacteriostatic or bactericidal state, subsequent experiments were supported by CFU statistics. Moreover, following 24 hours of experimental growth at 37°C, the entire *csrA* mutant cultures were transferred to 26°C to determine whether proliferation of any remaining viable cells could be restored.

It is important to note that the lag phase of all strains is severely prolonged during the growth in BCS medium at 37°C. No growth was detected up until 6 hours post-

inoculation of the BCS medium. The combined insults including the stark transition from peptide-rich HIB medium to restrictive BCS medium, wash and suspension in K-phosphate buffer, and the resulting temperature shift from 26°C to 37°C all likely contribute to the hindered viability. Therefore, the subsequent experimental setup was amended to allow initial experimental pre-growth in BCS medium supplemented with 0.2% K-gluconate, thereby circumventing the need for K-phosphate wash and preventing adaptation to a unique medium composition (**Fig. 40**).

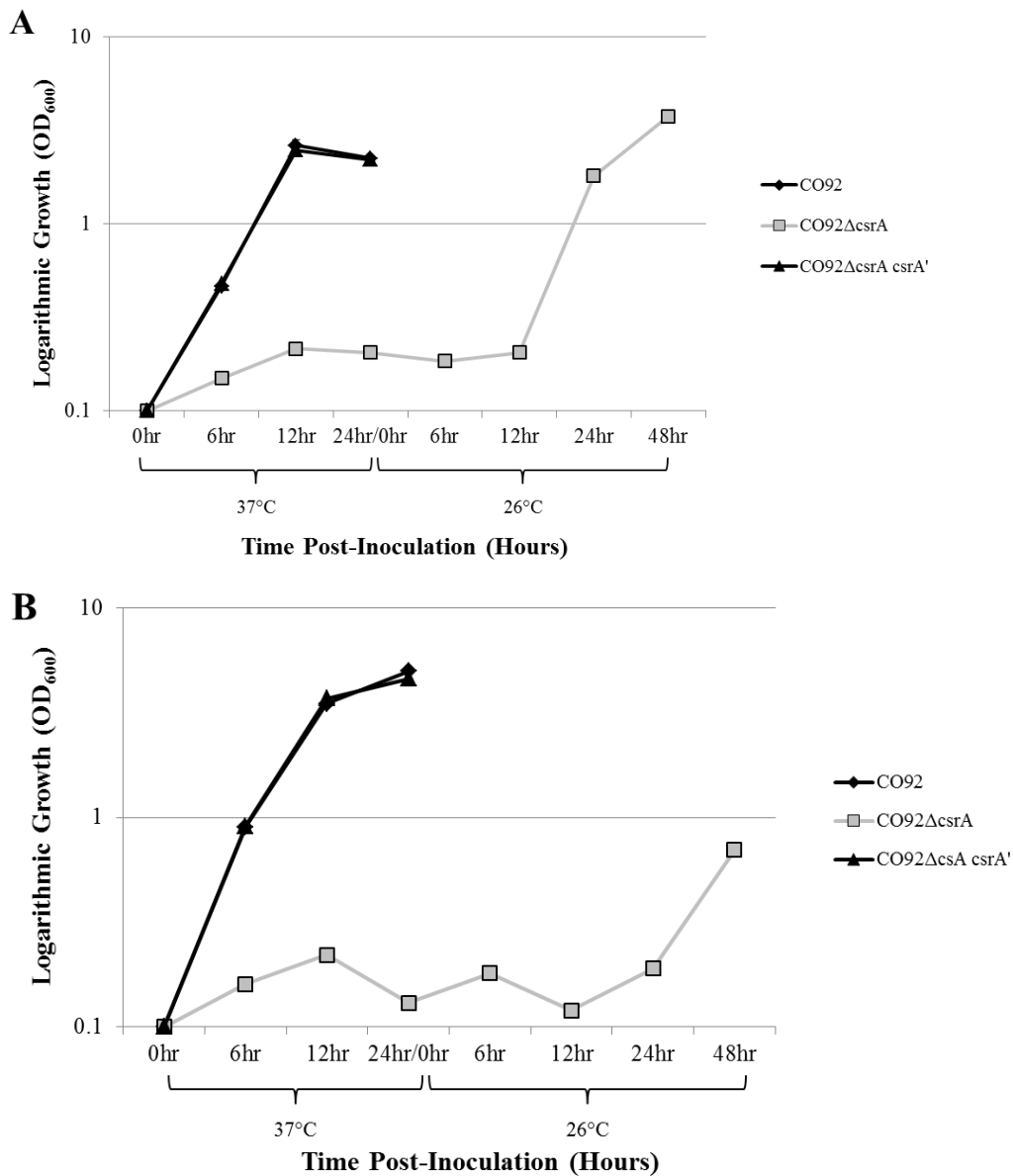


**Figure 40: Cessation of CO92 $\Delta$ *csrA* Growth at 37°C**

Semi-logarithmic growth of CO92, CO92 $\Delta$ *csrA*, and the CO92 $\Delta$ *csrA* *csrA*' 5a restoration control following direct inoculation from growth in BCS medium supplemented with 0.2% K-gluconate incubated at 26°C. The initial 24 hour post-inoculation time points were during incubation at 37°C; thereafter, the *csrA*-deficient cultures were transferred to 26°C for an additional 48 hours. Initial inoculum of OD<sub>600</sub> = 0.1.

**A.** Growth in BCS medium supplemented with 0.2% K-gluconate.

**B.** Growth in BCS medium supplemented with both 0.2% K-gluconate and 0.2% glucose.

Upon direct inoculation following 26°C pre-growth in BCS medium supplemented with 0.2% K-gluconate, growth of the CO92 $\Delta$ *csrA* mutant at 37°C was drastically impaired relative to the parent strain and chromosomal restoration mutant when inoculated in BCS medium supplemented with 0.2% K-gluconate (**Fig. 40A**) as well as BCS medium supplemented with a combination of both 0.2% K-gluconate and 0.2% glucose (**Fig. 40B**).

Irrespective of BCS medium carbon source supplementation, optical density readings indicated the *csrA*-deficient mutants multiplied by approximately one generation period, reaching an OD<sub>600</sub> of 0.2 upon 6 hours post-inoculation at 37°C. Thereafter, for the remainder of the 37°C incubation period, no alteration in growth density was observed. After 24 hours of incubation at 37°C, the growth temperature was shifted to 26°C. Following approximately 24 hours of incubation at 26°C, the *csrA*-deficient mutants demonstrated a restoration of growth which was most pronounced in the medium solely supplemented with 0.2% K-gluconate. At all time points, aliquots were extracted for CFU determination. Dilution series were prepared in K-phosphate buffer, plated upon HIA, and incubated at 26°C. CFU/mL statistics of the initial inoculum of wild-type CO92 and the *csrA* restoration control were calculated to be 4.6x10<sup>7</sup> and 4.9x10<sup>7</sup>, respectively. However, no colonies were detected for the *csrA*-deficient mutant at any time point, including the initial inoculum. To minimize potential stress, subsequent experiments were

further amended to prepare dilutions in HIB medium rather than K-phosphate buffer. Moreover, dilution series were plated upon Congo red agar supplemented with 0.2% K-gluconate.

Additionally, to determine whether the impaired growth at 37°C in the absence of *csrA* is a pCD1-dependent phenomenon, growth kinetics of the KIM6+ *csrA*-deficient mutant was assessed (Fig. 41).

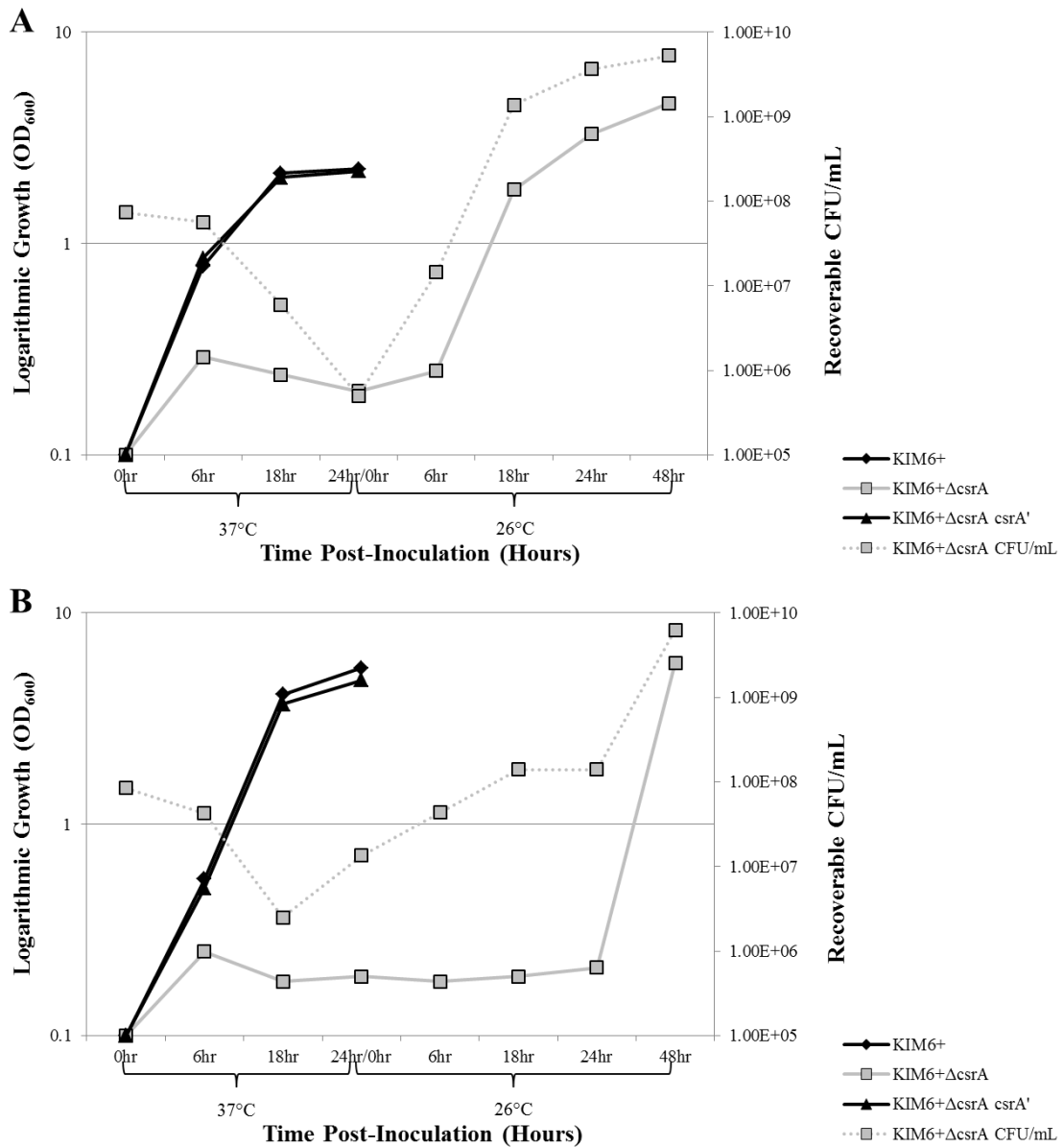


**Figure 41: 37°C Toxicity of the KIM6+ *csrA*-deficient Mutant.**

Semi-logarithmic growth of KIM6+, KIM6+ $\Delta$ *csrA* 2:14, and KIM6+ $\Delta$ *csrA* *csrA'* 2:6 restoration control following direct inoculation from growth in BCS medium supplemented with 0.2% K-gluconate incubated at 26°C. The initial 24 hour post-inoculation time points were during incubation at 37°C; thereafter, the *csrA*-deficient cultures were transferred to 26°C for an additional 48 hours. Initial inoculum for each strain was OD<sub>600</sub> = 0.1 as supported by CFU statistics. The dotted line reflects Log<sub>10</sub> CFU/mL statistics of the *csrA*-deficient mutant.

**A.** Growth in BCS medium supplemented with 0.2% K-gluconate.

**B.** Growth in BCS medium supplemented with both 0.2% K-gluconate and 0.2% glucose.

Comparable to CO92 $\Delta$ *csrA*, the KIM6+ *csrA*-deficient mutant demonstrated significantly impaired growth at during incubation at 37°C when cultured in BCS medium solely supplemented with 0.2% K-gluconate (**Fig. 41A**) or a combination of both 0.2% K-gluconate and 0.2% glucose (**Fig. 41B**). Similar to the CO92 $\Delta$ *csrA* growth kinetics, deletion of *csrA* from the KIM6+ background prevented growth following approximately 1 generational expansion, yielding an average OD<sub>600</sub> = ~0.2 throughout the experimental incubation at 37°C. Furthermore, CFU statistics indicated a reduction in viable cells during incubation at 37°C, reflective of a toxic effect. It is crucial to note that the initial inoculums for each strain regardless of media composition were relatively equivalent. In fact, the average initial inoculum of KIM6+ $\Delta$ *csrA* mutant (~7.9x10<sup>7</sup> CFU/mL) was superior to the KIM6+ parent strain (~3.5x10<sup>7</sup> CFU/mL).

Upon temperature transition from 37°C to 26°C, growth of the *csrA*-deficient mutant, as demonstrated by both optical density readings and supported by CFU statistics, was restored when cultured in both BCS solely supplemented with 0.2% K-gluconate as well as BCS supplemented with both 0.2% K-gluconate and 0.2% glucose. Comparable to what has been described for the CO92 $\Delta$ *csrA* mutant, the KIM6+ $\Delta$ *csrA* more readily recovered at 26°C in the sole presence of K-gluconate. During growth in BCS solely supplemented with 0.2% K-gluconate, the optical density readings and CFU statistics both surpassed the initial inoculum of the *csrA*-deficient mutant after 18 hours

post transfer to 26°C. However, growth surpassing the initial inoculum of the KIM6+ $\Delta csrA$  when cultured in BCS supplemented with both 0.2% K-gluconate and 0.2% glucose was only detected upon 48 hours after temperature shift to 26°C.

To provide insight regarding the mechanism by which CsrA provides *Y. pestis* resilience against 37°C toxicity, I assessed the potential involvement of characterized CsrA-repressed factors in *E. coli*, *glgCAP* and *nhaR*. To do so, both genes were independently excised from the *csrA*-deficient CO92 mutant. Cultures were pre-grown at 26°C in BCS supplemented with 0.2% K-gluconate, and subsequently transitioned to 37°C incubation for the experimental phase (Fig. 42).

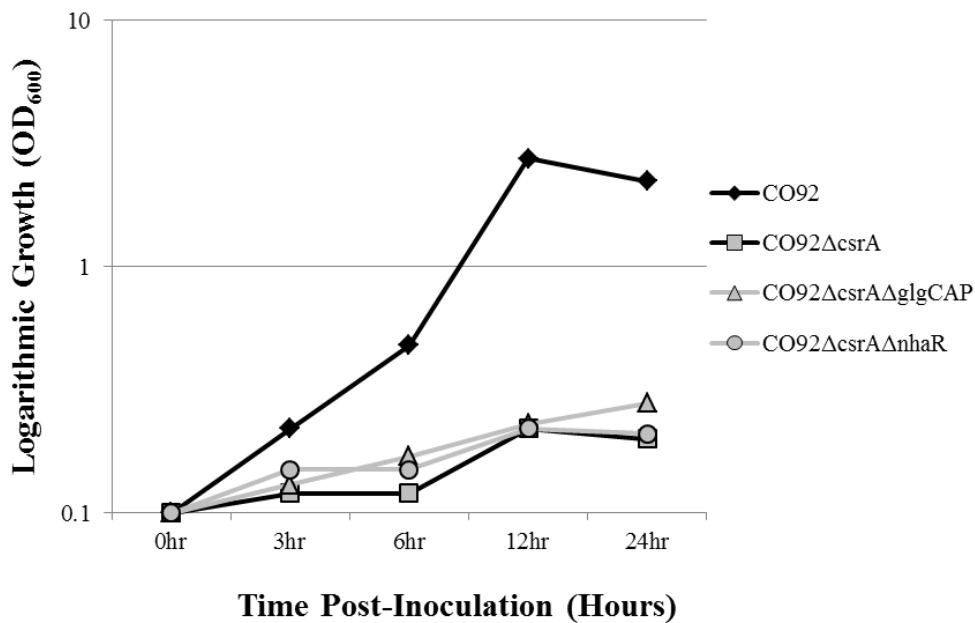


**Figure 42: 37°C Growth of  $\Delta csrA$  is not Restored by loss of *glgCAP* or *nhaR***

Semi-logarithmic growth of CO92, CO92 $\Delta csrA$  cl 5a, CO92 $\Delta csrA \Delta glgCAP$ , and CO92 $\Delta csrA \Delta nhaR$  during incubation at 37°C in BCS medium supplemented with 0.2% K-gluconate.

## CsrA Promotes *Y. pestis* survival in Macrophages

Since deletion of *csrA* was shown to impair *Y. pestis* growth at 37°C, I sought to assess the viability of *csrA*-deficient mutants upon macrophage challenge (Table 14).

**Table 14: Log<sub>10</sub> CFU/mL Intracellular Viability of *Y. pestis* CsrA Mutants after RAW Murine Macrophage-like Cell Challenge**

<i>Y. pestis</i> strain	0 hrs Post-Challenge	18 hrs Post-Challenge
CO92	5.36 ± 0.103	4.35 ± 0.083
CO92Δ <i>csrA</i> 5a	4.82 ± 0.053	3.39 ± 0.124
CO92Δ <i>csrA csrA</i> ' 5a	5.41 ± 0.133	4.65 ± 0.345
CO92Δ <i>csrA</i> 3b	5.26 ± 0.070	3.45 ± 0.304
CO92Δ <i>csrA csrA</i> ' 3b	5.41 ± 0.107	5.24 ± 0.311
CO92Δ <i>phoQP</i>	5.10 ± 0.066	2.86 ± 0.312

My results demonstrate a significantly impaired recovery of CO92Δ*csrA* following RAW murine-like macrophage cell challenge in respect to the wild-type parent as well as the chromosomally restored controls. Furthermore, the intracellular viability of the *csrA* deletion mutants was not as profound as the characterized CO92Δ*phoQP* mutant, indicating a moderate deficiency to survive macrophage clearing.

## DISCUSSION

My findings confirm prior studies demonstrating enhanced expression of the aerobic glycerol metabolic pathway during early phase temperature shift from 26°C to 37°C via semi-quantitative RT-PCR [145]. Upon incubation at 37°C, *Y. pestis* undergoes a short-lived up-regulation of the aerobic glycerol metabolic pathway. Thereafter, the expression normalizes to values consistent with growth at 26°C. The temporal enhancement in aerobic glycerol metabolism transcription is predominately induced in the sole presence of alternate carbon sources, potentially reflective of a mild carbon

repression effect. Expression of the *tpiA* gene remained constant throughout both time points regardless of incubation temperature. Therefore, the short-term up-regulation of glycerol metabolism upon temperature transition from 26°C to 37°C likely confers no impact upon energy metabolism. This notion is supported by 37°C growth kinetics which are comparable amongst the *glpD* dysfunctional mutant and the KIM6+ control. I conclude that the transient early phase enhanced expression of the glycerol metabolic pathway may be a consequence of temperature sensitive enzyme kinetics resulting in a temporary relaxation of carbon catabolite repression.

As described in Chapter 2, I demonstrate that functional GlpK in the presence of inactive GlpD represses intracellular accumulation of G3P in *Y. pestis*. In *E. coli*, G3P has been shown to mediate catabolite repression through inhibition of adenylate cyclase, thereby indirectly preventing activation of CRP [105]. Studies in *Y. pestis* have shown that loss of CRP results in significantly attenuated virulence. Therefore, I sought to assess whether the sole inactivation of *glpD*, as a consequence of reduced G3P-mediated inhibition of CRP, alters *Y. pestis* virulence. However, my findings demonstrate that sole dysfunction of *glpD* in the presence of functional *glpK* had no significant impact upon *Y. pestis* virulence in a murine system, regardless of macrophage-like cell challenge, murine s.c. inoculation, or murine i.n. inoculation. Therefore, the microevolution of *Y. pestis* glycerol fermentation does not affect virulence in a mammalian system.

To account for unintentional shunting of the anaerobic glycerol metabolic pathway, the *glpABC* operon was deleted from both parental KIM6+ as well as the *glpD* dysfunctional mutant. The *glpB* gene has been shown to be up-regulated in the rat bubo relative to *in vitro* growth at both 21°C and 37°C [151]. Moreover, virulence screening suggests that *glpABC* anaerobic respiration contributes to plague [152]. However, in my hands, deletion of the *glpABC* operon did not result in a significant alteration in virulence, despite route of inoculation. This discrepancy may result from two confounding variables. Foremost, the *glpABC*-deficient mutants utilized in this study

were constructed in a biovar *Medievalis* background; whereas, biovar *Orientalis* strains were evaluated in the aforementioned virulence screening assessments. As a consequence of reductionist gene loss or inactivation, isolates of Biovar *Orientalis* may have lost compensatory mechanisms that are maintained in progenitor isolates, including biovar *Medievalis* strains. Alternately, unique mammalian host physiology may exist amongst the murine model as used on my virulence studies in comparison to the rat model system as utilized by other investigators.

Contrary to 26°C growth kinetics described in Chapter 3, proliferation of the *csrA*-deficient mutants is severely repressed during growth at 37°C. When cultured in peptide rich HIB incubated, the *csrA*-deficient mutant demonstrates a greater than 2-fold reduction in growth density after 24 hours post-incubation at 37°C. Furthermore, the *csrA* deletion mutants demonstrate a complete cessation of growth when cultured in BCS chemically defined medium, regardless of primary or alternate carbon source supplementation. As demonstrated for the KIM6+ $\Delta$ *csrA* mutant, 37°C incubation in BCS medium is associated with a decrease in recoverable cells, indicative of a toxic effect.

Since the growth defect of the *csrA*-deficient mutants is consistent amongst the KIM6+ strain, which lacks the pCD1 plasmid, and the fully virulent CO92 genetic background, thus excluding an Lcr phenomenon [74]. It is important to note that a classical 37°C glucose toxicity response is not observed for *Y. pestis* when cultured in BCS medium supplemented with 0.2% glucose [77,78]. Rather, a moderate reduction in the rate of growth for both the fully virulent pCD1-positive CO92 as well as the attenuated pCD1-deficient KIM6+.

The intracellular viability of the *csrA* deficient mutants was impaired following RAW murine macrophage-like cell challenge. Deletion of *phoQP* has been characterized to confer a similar defect in *Y. pestis* macrophage survival. My findings demonstrate a comparable degree of recoverable *csrA*-deficient and *phoQP*-deficient mutants following macrophage challenge. It is important to note that the PhoP has been shown to directly

impair *rovA* transcription, thereby bridging the two regulons in *Y. pestis* [153]. Similarly, CsrA also represses RovA by enhancing the gene expression of the RovM negative regulator [154]. In conclusion, both CsrA and PhoP may converge to repress the RovA regulon, thereby promoting *Y. pestis* intraphagosomal survival.

## Chapter 6. Concluding Remarks and Future Directions

The overall objective of this study was to provide insight regarding carbon catabolite regulation of *Y. pestis* pathogenesis amid different aspects of the *Y. pestis* infectious cycle. Primarily, I sought to assess the role of carbon regulation upon *Y. pestis* biofilm production, a key natural transmission factor. My findings demonstrate that *Y. pestis* biofilm production is subject to carbon catabolite regulation (**Fig. 43**). The metabolism of primary carbon sources impairs biofilm production; whereas, the utilization of alternate carbon sources promotes robust biofilm formation. This observation was found to be facilitated by CRP principally through stimulation of alternate carbon source metabolism. Moreover, as demonstrated by exogenous addition of cAMP, CRP confers a positive regulatory impact upon *Y. pestis* biofilm production independent of growth kinetics. This observation corresponds with aspects of *Y. pestis* infection of the midgut in which primary carbon source metabolism is repressed, and alternate carbon source metabolic pathways are induced. Further studies are necessary to elucidate the precise mechanism by which CRP-mediated alternate carbon source metabolism promotes *Y. pestis* biofilm production.

*Y. pestis* biovar Orientalis stains have lost the capacity to ferment glycerol. I provide formal proof that the inability to ferment glycerol in these strains results from a conserved 93 bp in-frame deletion within the *glpD* gene. However, the inability to ferment glycerol is almost invariably ensured by a variety of disruptions within the

*glpFKX* operon, all of which notably impair *glpK*. In *E. coli*, the G3P enzymatic product of GlpK has been shown to inhibit CRP activation. Therefore, I sought to assess whether G3P may be differentially expressed in strains of *Y. pestis* that are capable of glycerol fermentation, have a sole deletion in *glpD*, or a combined defect in both *glpD* as well as the *glpFKX* operon. My findings reveal that upon sole deletion of *glpD*, intracellular accumulation of G3P is repressed. Additionally, I demonstrate that *glpD* promotes *Y. pestis* biofilm formation. Considering CRP-inhibitory G3P is repressed in *glpD*-deficient mutants, the mechanism by which *glpD* enhances *Y. pestis* biofilm production likely transpires through a mechanism independent of CRP regulation.

To further elucidate the role of carbon metabolism and storage upon *Y. pestis* biofilm regulation, I sought to characterize the impact of the carbon storage regulator protein, CsrA. Contrary to what has been described for *E. coli*, loss of *csrA* significantly impaired *Y. pestis* biofilm production and Congo red assimilation. The mechanism by which CsrA promotes *Y. pestis* biofilm production was found to be independent of glycogen synthesis regulation. In fact, our findings indicate that the *glgCAP* glycogen synthesis operon is entirely expendable for *Y. pestis* biofilm formation. I postulate that, due to a lack of discernable binding sites in the putative 5' UTR of the *hmsHFRS* operon, CsrA does not readily repress *Y. pestis* PNAG biofilm synthesis factors. However, this observation does not address how CsrA enhances *Y. pestis* biofilm production. I hypothesize that CsrA represses an uncharacterized inhibitor of *Y. pestis* biofilm production. There are two known negative regulators of *Y. pestis* biofilm formation, Fur and HmsP, which function through a conserved mechanism of cyclic diguanylate modulation. Interestingly, the predicted 5' UTR of *hmsP* contains an abundance of putative CsrA-binding motifs. Upon deletion of *hmsP* in the *csrA*-deficient mutant, I found that biofilm formation and Congo red assimilation is restored. Therefore, CsrA likely promotes *Y. pestis* biofilm production either through stimulation of cyclic

diguanylate synthesis or prevention of cyclic diguanylate degradation. Additional studies are necessary to discern the role of CsrA upon cyclic diguanylate regulation.

CsrA has been shown to regulate the Hfq chaperone molecule for sRNA:mRNA interactions. Studies by two independent investigative groups have shown that *Y. pestis* biofilm production is differentially regulated by Hfq. I demonstrate that the differential modulation of *Y. pestis* biofilm production is independent of the pCD1 plasmid. Both loss of pCD1 in *Y. pestis* strain CO92 as well as transformation of pCD1Ap in *Y. pestis* strain KIM6+ had no influence upon biofilm production when cultured in either HIB or BCS medium. Rather, Hfq differentially regulates *Y. pestis* biofilm formation in response to available carbon sources: Hfq enhances biofilm formation upon utilization of alternate carbon sources, yet represses biofilm production in the presence of primary carbon sources. Thus, Hfq likely contributes to carbon catabolite regulation of *Y. pestis* biofilm formation. However, the specific sRNA species and associated mRNA targets defining this observation have not been characterized.

Contrary to the more ancestral *Y. pestis* strains KIM6+ and CO92, the atypical biovar Microtus strain Pestoides F is not subject to carbon catabolite regulation of biofilm production. Pestoides F poorly produces biofilms irrespective of media composition and available carbon source. I sought to assess whether unique sRNA species sR084 and Ysr172, which are not present in Pestoides F, contribute to *Y. pestis* biofilm formation. However, my findings indicate that both sRNA species are dispensable for *Y. pestis* biofilm production. Therefore, the meager biofilm production observed by Pestoides F is likely a result of missense mutations within biofilm synthesis and regulation proteins.

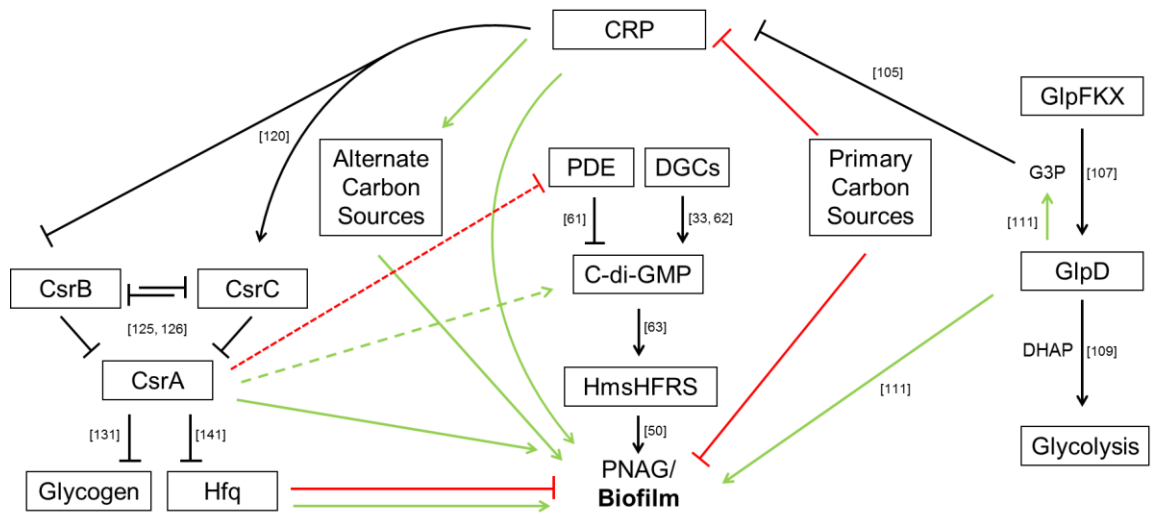


**Figure 43: Proposed *Y. pestis* Biofilm Regulation Network**

Comprehensive overview of the *Y. pestis* biofilm regulatory network incorporating the novel mechanisms of interplay as revealed in Chapters 2-4. Lines colored in black reflect previously-characterized associations alongside appropriate references. Solid green arrows indicate mechanisms revealed in this study to promote biofilm production; whereas, solid red lines demonstrate modes of inhibition discovered in this body of work. Dashed lines reflect putative areas of interplay.

As described in Chapter 5, I also sought to assess the impact of carbon catabolite regulation amid aspects reflective of *Y. pestis* infection of the mammalian host. Foremost, my findings demonstrate that *Y. pestis* aerobic glycerol metabolism does not affect 37°C growth kinetics, survival in macrophages, or virulence in a murine system. However, deletion of *CsrA* confers a significant defect during growth in both HIB medium as well as BCS medium, regardless of available carbon source. The impaired growth in BCS medium was supported by a reduction in recoverable CFU statistics, indicating a toxic effect. Furthermore, loss of *csrA* resulted in a significant reduction in survival during murine macrophage-like cell challenge. These observations provide a stable foundation for future *in vivo* challenge studies. I suspect that *CsrA* may serve a crucial virulence regulator during mammalian infection. Moreover, my future scopes aim to characterize the mechanism of 37°C toxicity induced by *csrA*-deficiency. Through omics-based

approaches, understanding the mechanism of 37°C toxicity may provide a framework for translational research focusing treatment and therapeutics development against plague.

## Appendix A. Chapter 2

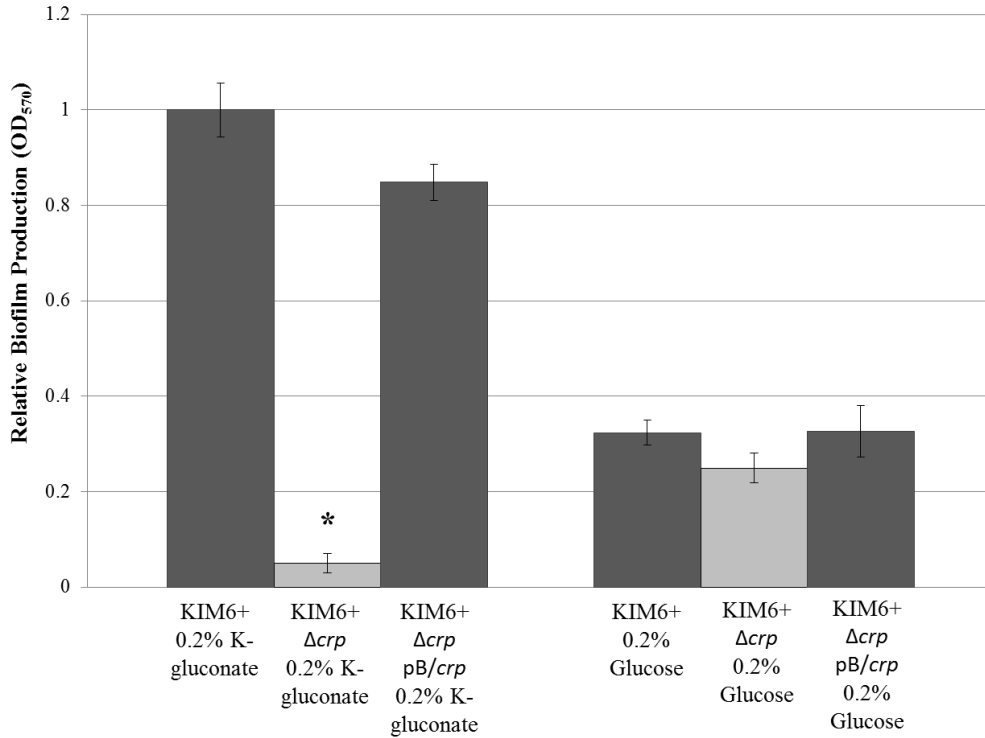
APPENDIX A TABLE 1: LIST OF OLIGONUCLEOTIDES.

Designation	Purpose	Sequence
SacB_F_Ngo	Forward primer for <i>sacB</i> amplification to incorporate in pKD4	CAGCCGGCATCGGCA TTTTCTTTTGCCTTT
SacB_R_Ngo	Reverse primer for <i>sacB</i> amplification to incorporate in pKD4	CAGCCGGCCAACTTTA TGCCCATGCAACAG
SacB_Det_F	Forward primer for detection of <i>sacB</i> incorporation	CACAAGAATGGTCAG GTTTCAGC
SacB_Det_R	Reverse primer for detection of <i>sacB</i> incorporation	TGACGGAAGAATGAT GTGCTTT
GlpD_F_HindIII	Forward primer for <i>glpD</i> amplification for pBluescript incorporation	CAAAGCTTAGATTCAG GGTTTCGTTCCAGA
GlpD_R_BamHI	Reverse primer for <i>glpD</i> amplification for pBluescript incorporation	CAGGATCCTGAGGTG CTTGAACAACGCTAT
GlpD_long_F	Forward primer for KmR-SucS cassette amplification containing <i>glpD</i> overhang	AATCTTGGCTTATTTG TTGGTTTTTGATTACA ATCGTGAGCGAAAAC GAACATTAAGCGCT GTTTCGAACATTCAGA GGAAGGTGTGTAGGC TGGAGCTGCTTCG
GlpD_long_R	Reverse primer for KmR-SucS cassette amplification containing <i>glpD</i> overhang	GGCCAGTGGCATTAC TAAGCCTTTAGCCCGC CAGGTGAAGGTTTTGC CGGTATTGACATCAAG GGCTTCAACCATCCAT AGGCCCATATGAATAT CCTCCTTAGT
GlpD_Rec_F	Forward primer for upstream amplification of <i>glpD</i> for allelic exchange	AGATTAATTCTGGCGA TCAGAGC
GlpD_Rec_R	Reverse primer for downstream amplification of <i>glpD</i> for allelic exchange	CACACCAGAGTAGGT CCAGACG

glpD-1R.seq	Sequencing of <i>glpD</i>	GTAGATGAGGCTGGT GGGGTAG
glpD-2R.seq	Sequencing of <i>glpD</i>	TTCCTGATCGTCAATT TTCACC
glpD-3F.seq	Sequencing of <i>glpD</i>	TGAATTCCGCTTGGTA AGTGAA
glpD-4F.seq	Sequencing of <i>glpD</i>	CGTACCGTAAATTGGC AGAACA
GlpFKX_F_XbaI	Forward primer for <i>glpFKX</i> operon amplification for pBBR1Tp incorporation	CATCTAGACTTGGGCG CAGTCATCATTA
GlpFKX_R_XhoI	Reverse primer for <i>glpFKX</i> operon amplification for pBBR1Tp incorporation	CACTCGAGGCGCCGT GCAGAATAAAAAT
glpFKX_1R.seq	Sequencing of <i>glpFKX</i>	GCCCCAAATGATACTG ATTTC
glpFKX_2R.seq	Sequencing of <i>glpFKX</i>	ATGCGACTCCAATGAC TTGTGT
glpFKX_3R.seq	Sequencing of <i>glpFKX</i>	ACCGATATTGGTTTTG CCGTAG
glpFKX_4R.seq	Sequencing of <i>glpFKX</i>	GCGTTCAATGCTTGCT TACTC
glpFKX_5R.seq	Sequencing of <i>glpFKX</i>	GCGATATTGCACAGGT TCTGTT
glpFKX_6F.seq	Sequencing of <i>glpFKX</i>	AAAATTACGCGAAAA CGCTCAT
glpFKX_7F.seq	Sequencing of <i>glpFKX</i>	TCTGATCGCAGTTATT GGTGCT
glpFKX_8F.seq	Sequencing of <i>glpFKX</i>	ACTCTGATGAAATCGC GGGTAT
glpFKX_9F.seq	Sequencing of <i>glpFKX</i>	TGGAAGGGGCTGTATT TATTTGG
glpFKX_10F.seq	Sequencing of <i>glpFKX</i>	CCAGTTTTAGCCAGTC CGTTTT
glpFKX_11F.seq	Sequencing of <i>glpFKX</i>	CACATTCTTACATGCC CCTGAT
crp_long_F	Forward primer for KmR- SucS cassette amplification containing <i>crp</i> overhang	CCGACTCTCGAATGGT TCCTGTCTCATTGCCA TATCCATAAGTACCCA TCCAAAAGTACGCTG ATCACCAGGGTGAA AAAGCCGGTGTAGGC TGGAGCTGCTTCG

crp_long_R	Reverse primer for KmR-SucS cassette amplification containing <i>crp</i> overhang	GGAGATCAAGTTTTGA TCTTCCAGCATTTTTA GTATCCGCCCCACAGT TTCGCGGGAGCAGCC AACTATTTGACCAATT TCCTGGCATATGAATA TCCTCCTTAGT
crp_gBlock	gBlock containing <i>crp</i> upstream and downstream flanking regions for scarless deletion	GTGAAGGGTTTCTATT CGGTACGAACCTTGGC TATACCTTTTCGGCAGT TGAGCAAGTTAATATG CTAAAAAGAAAGTGT ATTCTATAAGCACGCC GTACAGGGAACTCTG AGCCCTGTTAAGTTAG GCAGCGATAACAACA GAGGATAACAGCGAA TGGTTCTCGGTAAGCC ACAAACAGACCCGAC TCTCGAATGGTTCCTG TCTCATTGCCATATCC ATAGCGGATACTAAA AATGCTGGAAGATCA AACTTGATCTCCGCA CACGGTAAAACGATC GTCGTTTACGGCACCC GTTAATTCCCTCTAAA AACCGGCGTTAAAGC TGAAGCTATTAGCGCC GGTTTTTCCCGTTTTCT GTGAGTAATAAATTTT TGGGGCCTATATGAA GTGGCAACGGCTTATT TATCATCCTGAAGTTA ACTACGCACTACGTCA AACATTGGTCCTTTGC CTA
crp_g_F	Forward amplification primer for <i>crp</i> gBlock	GTGAAGGGTTTCTATT CGGTACG
crp_g_R	Reverse amplification primer for <i>crp</i> gBlock	TAGGCAAAGGACCAA TGTTTGA
crp_det_F	Forward primer for upstream detection of <i>crp</i> scarless deletion	TTCTCGGTAAGCCACA AACAGA

crp_det_R	Reverse primer for downstream detection of <i>crp</i> scarless deletion	AACGACGATCGTTTTA CCGTGT
gyrB_qPCR_F	Forward qPCR primer for <i>gyrB</i>	TGTGGTATTGGCCGGG ATGAATAT
gyrB_qPCR_R	Reverse qPCR primer for <i>gyrB</i>	GAGGCTGAGCGATAA ACACATGAC
hmsP_qPCR_F	Forward qPCR primer for <i>hmsP</i>	TCAGGATGATGAACT GGGTGTGTT
hmsP_qPCR_R	Reverse qPCR primer for <i>hmsP</i>	GAGGCAATTTCTTTCT CCAGCAGG
hmsT_qPCR_F	Forward qPCR primer for <i>hmsT</i>	TCTCAGTCGCCGGGAA ATCATTAT
hmsT_qPCR_R	Reverse qPCR primer for <i>hmsT</i>	CACCACGATATCTCTT GAACGCAC
hmsC/N_qPCR_F	Forward qPCR primer for <i>hmsC/N</i>	CGTTGGTGGGGCGTTT ATCTATTC
hmsC/N_qPCR_R	Reverse qPCR primer for <i>hmsC/N</i>	CGGCCAGCGTGAATA ACTGATAAT
hmsD_qPCR_F	Forward qPCR primer for <i>hmsD</i>	ATTTGTCTGTCGCCAT TGTGTCTG
hmsD_qPCR_R	Reverse qPCR primer for <i>hmsD</i>	AACTCGTTAGCCTCCA CGTTATCA
hmsH_qPCR_F	Forward qPCR primer for <i>hmsH</i>	CCCCTCTCAAGAATTA GATCGCCA
hmsH_qPCR_R	Reverse qPCR primer for <i>hmsH</i>	CTGTAAAGGAGAGTTT CGACCCCA
hmsF_qPCR_F	Forward qPCR primer for <i>hmsF</i>	GTTTACTTCCCGAACC GTTGGATC
hmsF_qPCR_R	Reverse qPCR primer for <i>hmsF</i>	GTCCATATCAAACGCC AATACCGG
hmsR_qPCR_F	Forward qPCR primer for <i>hmsR</i>	GTGGCTGCTGTTTCTG GAGTATTC
hmsR_qPCR_R	Reverse qPCR primer for <i>hmsR</i>	GCGGGAAGACACTTT GAACATGAA
hmsS_qPCR_F	Forward qPCR primer for <i>hmsS</i>	TACAATCAGGTCCGTT TCCAGGTT
hmsS_qPCR_R	Reverse qPCR primer for <i>hmsS</i>	GAGACACGAGCCACT TTTGAGTTG
pla_qPCR_F	Forward qPCR primer for <i>pla</i>	AACTATTCTGTCCGGG AGTGCTAA
pla_qPCR_R	Reverse qPCR primer for <i>pla</i>	TCTTCCTGTTTCTGCG TCATAAAGC

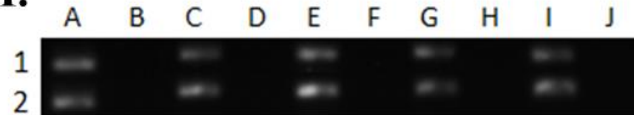


**APPENDIX A FIGURE 1. CRP PROMOTES KIM6+ BIOFILM PRODUCTION.**

Biofilm production 24 hours post-inoculation of KIM6+, KIM6+ $\Delta crp$ , and the KIM6+ *crp*-deficient mutant plasmid complemented with *crp* in BCS medium supplemented with either 0.2% K-gluconate or 0.2% glucose. Loss of *crp* results in a significant decrease in biofilm production when grown in the presence of K-gluconate, but has no significant impact upon biofilm formation when media is supplemented with glucose. Error bars reflect standard deviation from the mean derived from two independent experiments, each consisting of 6 technical replicates. \* P-value <0.05 determined by two-tailed Student's T test.

**A.**

**I.**

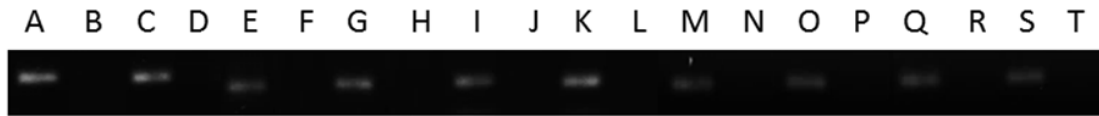


**II.**



## B.

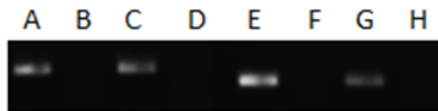
### I.



### II.



### III.



#### APPENDIX A FIGURE 2. BIOFILM QRT-PCR AGAROSE GELS.

Semi-quantitative RT-PCR of *Y. pestis* Hms system biofilm regulation genes visualized by EtBR.

A. Comparison of CO92 grown in BCS medium supplemented with either 0.2% K-gluconate or 0.2% glucose:

#### I.

Row: 1 = 0.2% glucose; 2 = 0.2% K-gluconate

Columns: A = *gyrB*; C = *hmsH*; E = *hmsF*; G = *hmsR*; I = *hmsS*  
(Directly flanked to the right by RT negative controls)

#### II.

0.2% glucose: A = *gyrB*; E = *hmsP*; I = *hmsT*; M = *hmsN*; Q = *hmsD*

0.2% K-gluconate: C = *gyrB*; G = *hmsP*; K = *hmsT*; O = *hmsN*; S = *hmsD*  
(Directly flanked to the right by RT negative controls)

B. Comparison of CO92 and CO92 $\Delta$ *crp* when grown in HIB medium:

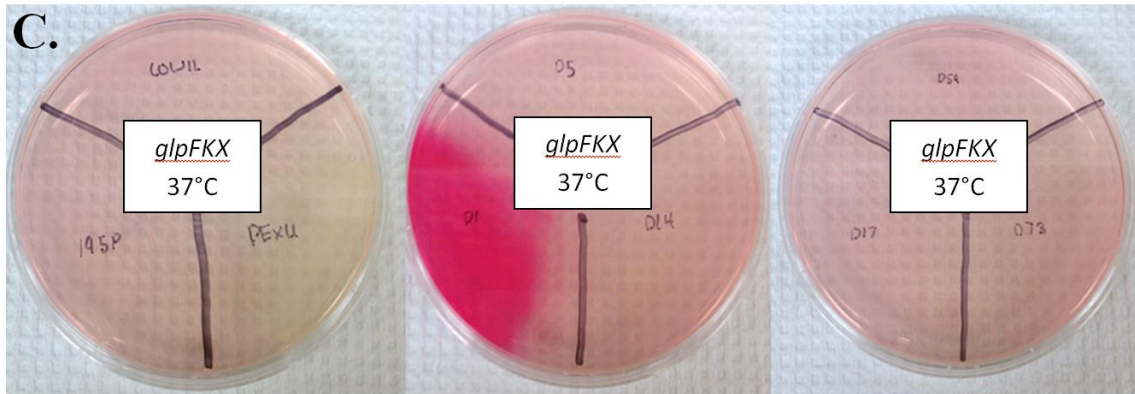
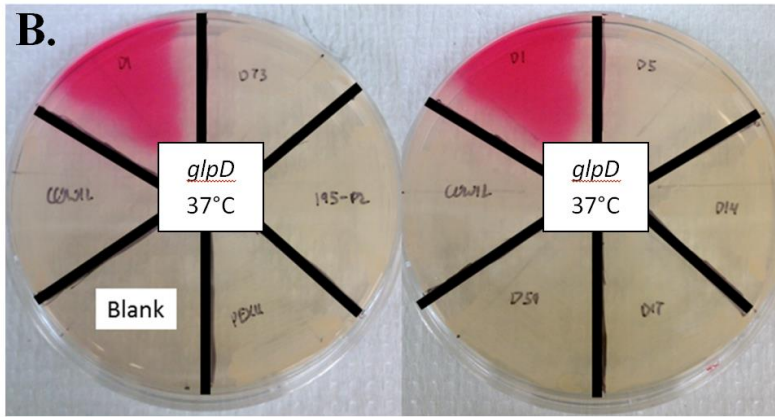
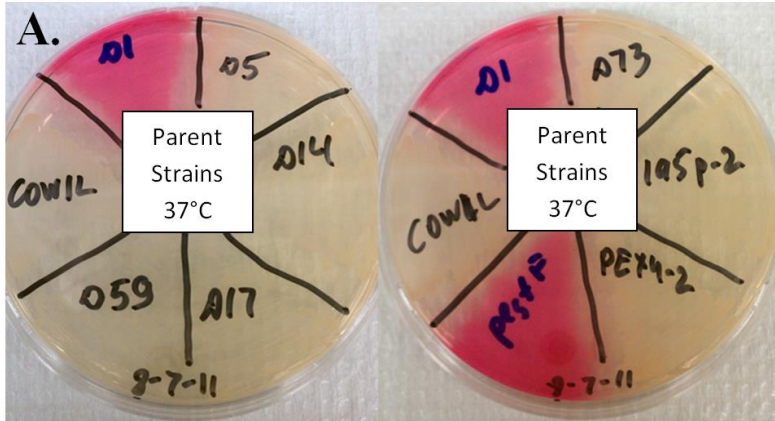
I. A, E, I, M, Q = CO92 *gyrB*, *hmsH*, *hmsF*, *hmsR*, *hmsS*;

C, G, K, O, S = CO92 $\Delta$ *crp* *gyrB*, *hmsH*, *hmsF*, *hmsR*, *hmsS*  
(Directly flanked to the right by RT negative controls)

II. A, E, I, M, Q = CO92 *gyrB*, *hmsP*, *hmsT*, *hmsN*, *hmsD*;

C, G, K, O, S = CO92 $\Delta$ *crp* *gyrB*, *hmsP*, *hmsT*, *hmsN*, *hmsD*  
(Directly flanked to the right by RT negative controls)

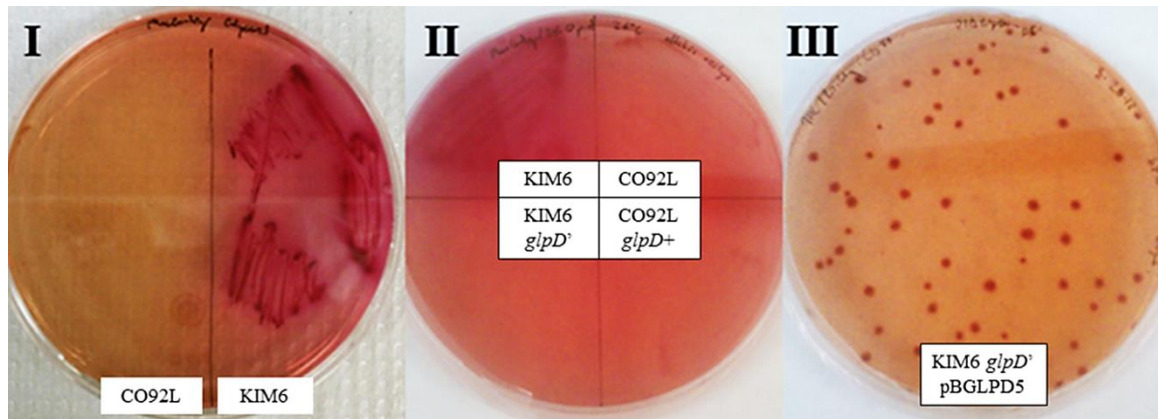
III. A, E = CO92 *gyrB*, *pla*; C, G = CO92 $\Delta$ *crp* *gyrB*, *pla*  
(Directly flanked to the right by RT negative controls)



**APPENDIX A FIGURE 3. PHENOTYPIC *Y. PESTIS* GLYCEROL FERMENTATION**

Determination of *Y. pestis* glycerol metabolism upon fuchsin acid plates supplemented with 0.2% glycerol following 24-48 hours incubation at 37°C.

- A.** Parent *Y. pestis* strains: COW1L = CO92L; D1 = KIM6+; D5 = TS; D14 = Salazar; D17 = Kimberley; D59 = EV76H; D73 = M23; 195-P2; PEXU-2; Pest F = Pestoides F.
- B.** *Y. pestis* strains expressing pBGLPD5: COW1L = CO92L; D1 = KIM6+; D73 = M23; 195-P2; PEXU= PEXU-2; D5 = TS; D14 = Salazar; D17 = Kimberley; D59 = EV76H.
- C.** *Y. pestis* strains expressing pTpGLPFKX6: COW1L = CO92L; 195 = 195-P2; PEXU= PEXU-2; D5 = TS; D14 = Salazar; D1 = KIM6+; D59 = EV76H; D73 = M23; D17 = Kimberley.
- D.** *Y. pestis* strains co-expressing both pBGLPD5 and pTpGLPFKX6: COW1L = CO92L; 195P = 195-P2; PEXU= PEXU-2; D5 = TS; D14 = Salazar; D1 = KIM6+; D59 = EV76H; D73 = M23; D17 = Kimberley.



**APPENDIX A FIGURE 4. GLPD ALLELIC EXCHANGE GLYCEROL FERMENTATION**

Phenotypic analyses of glycerol fermentation using MacConkey agar supplemented with 0.2% glycerol.

- I.** Parent strains CO92L and KIM6+;
- II.** Allelic exchange mutant assessment: KIM6+, CO92L, KIM6+ *glpD*<sup>-</sup>, CO92L *glpD*<sup>+</sup>;
- III.** Plasmid complementation restores glycerol fermentation of *glpD*-impaired KIM6+ mutant: Colonies of KIM6+ *glpD*<sup>-</sup> : pBGLPD5.

**Appendix B. Chapter 3**

**APPENDIX B TABLE 1: LIST OF OLIGONUCLEOTIDES.**

<b>Designation</b>	<b>Purpose</b>	<b>Sequence</b>
csrA_long_F	Forward primer for KmR-SucS cassette amplification containing <i>csrA</i> overhang	AATGGCTTACGTTTTTCACG GTGTATGATGGATAATGGC GGGAAACAGAGAGACCC GACTCTTTTAATTTTTCAA GGAGCAAAGAGTGTAGGC TGGAGCTGCTTCG
csrA_long_R	Reverse primer for KmR-SacB cassette amplification containing <i>csrA</i> overhang	AAAGGAGAATTAGGGGAA ACAAAACAGAGAGTAGAG ACAATAAAAAGCAGTAGC GCCTCGTGTTACACGAGAC GCTGCTTCAAAACATATGA ATATCCTCCTTAGT
csrA_gBlock	gBlock containing <i>csrA</i> upstream and downstream flanking regions for scarless deletion	GTAATCATCTATTAAATCA ACACGCCATATCTCGGTAC TAGGTATGGCGTTTTTTAA TTTTCCTGTCATAGTTCAA TCACAAAGTTAAACGCAA AGTTGTTTGCTTCAGCTAA ACTTGTATTAGTTAGGGAC TCGACCAAGCTACTTACAT TTTATATGAATGTAATGGC TTACGTTTTACGGTGTAT GATGGATAATGGCGGGGA AACAGAGAGACCCGACTC TTTTAATTTTTCAAGGAGC AAAGATTTTGAAGCAGCG TCTCGTGTAACACGAGGCG CTACTGCTTTTTATTGTCTC TACTCTCTGTTTTGTTTCCC CTAATTCTCCTTTCTTTTCG CTATTTCTCTCTACTTCGTC TGCCCAGTCACTACCGCTC AGATAAATTCAACTTCTCC TGTATTTGGTTATATCCCA ATAATAGCTATCTTGCCCTG TTGATAAAACACTCTTTTT GGTTTCAAACCTGGCCATGT TGTGTGTGAAGTGTGCAAA TAAACG
csrA_g_F	Forward amplification primer for <i>csrA</i> gBlock	GTAATCATCTATTAAATCA ACACGCC
csrA_g_R	Reverse amplification primer for <i>csrA</i> gBlock	CGTTTATTTGCACACTTCA CACAC

csrA_det_F	Forward primer for upstream detection of <i>csrA</i> scarless deletion	ATTAATCGCGGACATTGCTCAG
csrA_det_R	Reverse primer for downstream detection of <i>csrA</i> scarless deletion	ATAGTAAATGGCGGTGAGGGAG
glgCAP_long_F	Forward primer for KmR-SucS cassette amplification containing <i>glgCAP</i> overhang	GTCAGACCATGCGGAGCG ATTAACCACATGGCGCGG GTCCGCGCATACCATTGT GTGCTCATAAAGAGAGAT TAAGGAGCTTTTGTGTAGG CTGGAGCTGCTTCG
glgCAP_long_R	Reverse primer for KmR-SucS cassette amplification containing <i>glgCAP</i> overhang	AAATTTAAAAACCCTCTTC AATCGGATAACCGCGAAG AGGGTTTTTACGGTGGCA CTGGCGGTTGAATATGTCA TTACCGCACACATATGAAT ATCCTCCTTAGT
glgCAP_gBlock	gBlock containing <i>glgCAP</i> upstream and downstream flanking regions for scarless deletion	TAGTCAGGGACAGGCGCT GAGTGATGCTGCTTGGGA GCAAGGCTGCCAGCAGCA ACTACAGATTTTGTATCT CAGCGCTGGTTGGTGCTCA TCAATGCCACTGATCACGA GTGTGAAATGCACTTACCT GAAGGGGAATGGGAGGGG ATCCTCCCTTTGGGGTGT CAGACCATGCGGAGCGAT TAACCACATGGCGCGGGT CCGCGCATACCATTGTGT GCTCATAAAGAGAGATTA AGGAGCTTTTGTGCGGTA ATGACATATTCAACCGCCA GTGCCACCGTAAAAAACC CTCTTCGCGGTTATCCGAT TGAAGAGGGTTTTTAAATT TCTTGAGGTGCTTGAACAA CGCTATGCAGCCCAGAAA GGCAAAAATTGACGAAAG TTAAACAATGTTAACTTT GCTATTAAGAAACCAGCG GCAGCGCCTGTTGTTTTTC AGTGTGCGCATCAGCCAG CCACTGGGCTACCCGCTGT TTCTTTCATCGC

glgCAP_g_F	Forward amplification primer for <i>glgCAP</i> gBlock	TAGTCAGGGACAGGCGCT GAGTGATG
glgCAP_g_R	Reverse amplification primer for <i>glgCAP</i> gBlock	GCGATGAAGAGAAACAGC GGGTAGCC
glgCAP_det_F	Forward primer for upstream detection of <i>glgCAP</i> scarless deletion	GCAAATCCCAGCCCTGACT CAG
glgCAP_det_R	Reverse primer for downstream detection of <i>glgCAP</i> scarless deletion	GCTATTTGGTTGAGAACGA GTGGG
hsmP_long_F	Forward primer for KmR-SucS cassette amplification containing <i>hmsP</i> overhang	CTTACTCGATGGGGACTAA AAAGGGGCGTCTAAACAC CAAGCACTTGAACACCAA ACGTCTGAACACCAAAAA CAGTACTGCGAAGTGTAG GCTGGAGCTGCTTCG
hsmP_long_R	Reverse primer for KmR-SucS cassette amplification containing <i>hmsP</i> overhang	GTCAGAATTGACGGTGGG TAGGCGGTCATTCCTGCA GATTCTCGGCGTGTTAAGT ACTGCTGGTGGACACCGCC ATACAAAGAGCATATGAA TATCCTCCTTAGT

hsmP_gBlock	gBlock containing <i>hmsP</i> upstream and downstream flanking regions for scarless deletion	GATTATTACAGTGCTATTC TGACCCTGTTTGGTCAGGG GTGGTTACAGCATCGTTAT CATTTTACCCATCAGGGAG AGCTACAGCCCTCATGGCA CCGTCAACGTTAAGATTTC AGGATAGCGGATCTGGCC TAATGATAGGGAAATGCG CTTAAGGGATCACAACCTTA CTCGATGGGGACTAAAAA GGGGCGTCTAAACACCAA GCACTTGAACACCAAACG TCTGAACACCAAAAACAG TACTGCGAACTCTTTGTAT GGCGGTGTCCACCAGCAG TACTTAACACGCCGAGAAT CTGCAGTGAATGACCGCCT ACCCACCGTCAATTCTGAC GACAGCCGATGACGCTGT GAAGTCCCTACATATTAGA AAACACTTGTCAGCAAGA AGGGCGGCATATTATCTCT TCTATCTGGAATTAATTTT ATTATGTTGTGTGAATTC ACTCTTAATAGGATTATCG GTTAC
hsmP_g_F	Forward amplification primer for <i>hmsP</i> gBlock	GATTATTACAGTGCTATTC TGACC
hsmP_g_R	Reverse amplification primer for <i>hmsP</i> gBlock	GTAACCGATAATCCTATTA AGAGTG
hsmP_det_F	Forward primer for upstream detection of <i>hmsP</i> scarless deletion	AGCAAACACTGAATCTCC AACAGC
hsmP_det_R	Reverse primer for downstream detection of <i>hmsP</i> scarless deletion	GGAGCAATTAAACCCATA CGCGAT

## Appendix C. Chapter 4

**APPENDIX C TABLE 1: LIST OF OLIGONUCLEOTIDES.**

<b>Designation</b>	<b>Purpose</b>	<b>Sequence</b>
hfq_long_F	Forward primer for KmR-SacB cassette amplification containing <i>hfq</i> overhang	ATGGCTAAGGGGCAAT CTTTGCAAGATCCGTT CTGAACGCATTGCGTC GTGAGTGTAGGCTGGA GCTGCTTCG
hfq_long_R	Reverse primer for KmR-SacB cassette amplification containing <i>hfq</i> overhang	TTATTCAGCGTCATCAC TGTCCTGCTGCGGCTGT TGCGGCGCAGACGGAT TACTACCATCATATGA ATATCCTCCTTAGT
hfq_gBlock	gBlock containing <i>hfq</i> upstream and downstream flanking regions for scarless deletion	ACAGTGATAAGCCGGG AGAGGCTTTAGACTCC GTAATACAGTTGTTA GTGCATAGGTTGAATG ATTGTGTACAATTGATT AGTACTCAACGCACAG ATTTTTTTACGCAGTTT ATTTTCGAGCCGATAG GTTCTTAGTTAAAAAC ACAAGCAAATAAGGA AAATATAGAAACGGAT TCAAGCTTATGTTCTCC GCACTAGCGGCTTTGA TCCGTTTGAGAGGTTG CACGTTTGTTGACCGC TATGAAGCTGGTGAGC AGGCCGTA CTGGTTCA TATTTATTTCTCGCAA ACAAAGACACAGAGGA TCTGCGCGAGTTTGAA GCGCTGGTATCTTCTGC GGGTGTA
hfq_g_F	Forward amplification primer for <i>hfq</i> gBlock	ACAGTGATAAGCCGGG AGAGGC
hfq_g_R	Reverse amplification primer for <i>hfq</i> gBlock	TACACCCGCAGAAGAT ACCAGC
hfq_det_F	Forward primer for upstream detection of <i>hfq</i> scarless deletion	TGGAGTTCAGTTCAAT GGCTCG
hfq_det_R	Reverse primer for downstream detection of <i>hfq</i> scarless deletion	GGATGTGGTGCTTTGC GACTAC

ysr172_long_F	Forward primer for KmR-SacB cassette amplification containing Ysr172 overhang	GATTTTTTGATCCGCAG GTCAACGACCTTAAAT TGAGCATGATTTAACC TGTATTGGTTCCCAAGT AAGCTACACATAAATC AGGGTGTAGGCTGGAG CTGCTTCG
ysr172_long_R	Reverse primer for KmR-SacB cassette amplification containing Ysr172 overhang	ATGGAGTATGCCGATC CAGAACTGGCGGTTAG CGATGAGCCGTTTTATT ATCGAGTTCGGTGACC GCCTGAGCGATCACCT TTAACATATGAATATC CTCCTTAGT
ysr172_gBlock	gBlock containing Ysr172 upstream and downstream flanking regions for scarless deletion	GTCGAATTATTCAACA CTCGTGGACGTGATGG ATACGCCAAAGCAATG GCATCGGTTCTCCCAT TTAAGCCGCCGAGCT AAGGAATTCGGTTGAT AACCCAATCTCTTGGC CGCATCGATAATCCGC TCACGTGTTTCGGCCGC AACATCATCATAGCCA TTAACGCGCGGCTTA CCGTTGTGGAGGACAG CCCAAGCTCATTGCA ATTTTCTTCAATGACAT TTAAAGGTGATCGCTC AGGCGGTCACCGAACT CGATAATAAACGGCT CATCGCTAACCGCCAG TTCTGGATCGGCATACT CCATTTTTTTGATGCAT CCTTGATCGCCAAATA ACAACCTTCCGCACT GAGTCGTCTGTCGGGA ACACTTTCGCTTTTTA ATGGCTGCACGGATCA CGCTGTTACCGATTTCG ATGGCATTCTGTGGTGT AGATAGCCTTGCGGAT ATCG
ysr172_g_F	Forward amplification primer for Ysr172 gBlock	GTCGAATTATTCAACA CTCGTGGAC

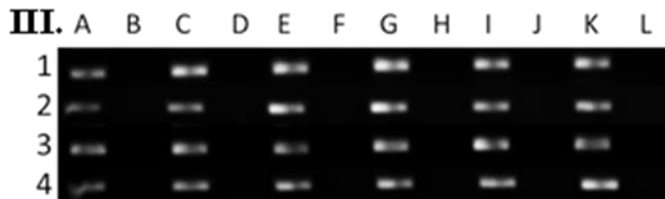
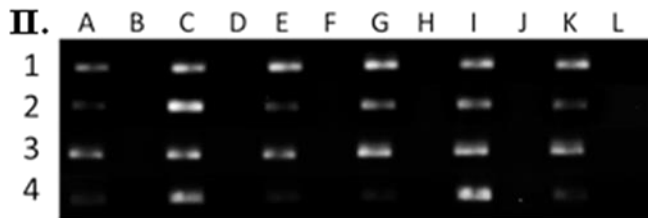
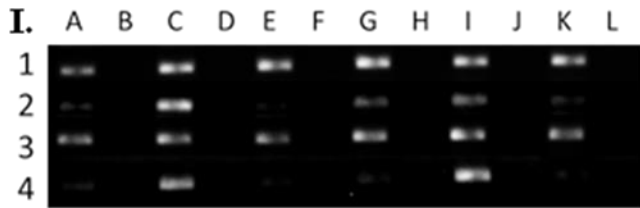
ysr172_g_R	Reverse amplification primer for Ysr172 gBlock	CGATATCCGCAAGGCT ATCTACAC
ysr172_det_F	Forward primer for upstream detection of Ysr172 scarless deletion	CAGTCGGTGATAATGG CAGTAGGA
ysr172_det_R	Reverse primer for downstream detection of Ysr172 scarless deletion	TGTTTATCCGCAGACTC ACATCCA

## Appendix D. Chapter 5

**APPENDIX D TABLE 1: LIST OF OLIGONUCLEOTIDES.**

Designation	Purpose	Sequence
glpABC_long_F	Forward primer for KmR deletion cassette amplification with <i>glpABC</i> overhang	CATGACATCGCTACTG GGGCCACGGGGCGTAA TCATGGTCTCCTGCACA GTGGCGCTCGCTATGC GGTAACCGACGGTGAG TCAGGTGTAGGCTGGA GCTGCTTCG
glpABC_long_R	Reverse primer for KmR deletion cassette amplification with <i>glpABC</i> overhang	TTTCTTACTGGTCGACA TTTCGATCTGCCATTTG CAGGTTTCGCAATCGG TAATCACCAAATCAAC CCCGCTATCCTCAATTT GCCATATGAATATCCT CCTTAGT
glpABC_Det_F	Forward primer for upstream detection of <i>glpABC</i> deletion	CCGTGGTTTTGGCTTGTA CTTTA
glpABC_Det_R	Reverse primer for downstream detection of <i>glpABC</i> deletion	GCCAGTAAAGTAATCG GGTGCT
gyrB_qPCR_F	Forward qPCR primer for <i>gyrB</i>	TGTGGTATTGGCCGGG ATGAATAT
gyrB_qPCR_R	Reverse qPCR primer for <i>gyrB</i>	GAGGCTGAGCGATAAA CACATGAC
glpD_qPCR_F	Forward qPCR primer for <i>glpD</i>	CCGGCTTGTTCTTGTAT GACCATT

glpD_qPCR_R	Reverse qPCR primer for <i>glpD</i>	ACAGTCAGAATATTCG AAACCGCG
glpF_qPCR_F	Forward qPCR primer for <i>glpF</i>	TACTGATTGAAGTC CTGGCCAA
glpF_qPCR_R	Reverse qPCR primer for <i>glpF</i>	CAATGGCGTTATACAC CGGCTTAC
tpiA_qPCR_F	Forward qPCR primer for <i>tpiA</i>	CCCACGGGCGATCTAT CTAAATCA
tpiA_qPCR_R	Reverse qPCR primer for <i>tpiA</i>	TATTGCGCACCGATAT CTTTCAGC
katY_qPCR_F	Forward qPCR primer for <i>katY</i>	GATGTCAGTTCTTTCGC GGTACTG
katY_qPCR_R	Reverse qPCR primer for <i>katY</i>	CAGTTCCAGTTTATTCG CCCGATC



**APPENDIX D FIGURE 1. GLYCEROL METABOLISM QRT-PCR AGAROSE GELS**

**I.** *glpD*; **II.** *glpF*; **III.** *tpiA*

**Rows:**

**1** = 1hr *gyrB*; **2** = 1hr gene of interest; **3** = 4hr *gyrB*; **4** = 4hr gene of interest

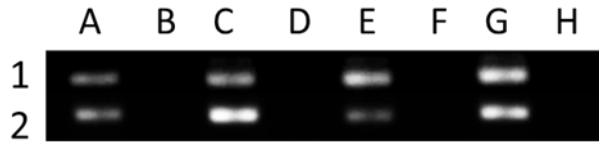
**Columns:**

**A** = 26°C 0.2% K-gluconate; **C** = 26°C 0.2% K-gluconate & 0.2% glycerol;

**E** = 26°C 0.2% K-gluconate & 0.2% glycerol & 0.2% glucose

**G** = 37°C 0.2% K-gluconate; **I** = 37°C 0.2% K-gluconate & 0.2% glycerol;

**K** = 37°C 0.2% K-gluconate & 0.2% glycerol & 0.2% glucose  
All samples are directly flanked by respective reverse transcriptase negative controls.



**APPENDIX D FIGURE 2. QRT-PCR TEMPERATURE SENSITIVE CONTROL**

**Rows:**

**1** = *gyrB*; **2** = *katY*

**Columns:**

**A** = 1 hr 26°C 0.2% K-gluconate; **C** = 1 hr 37°C 0.2% K-gluconate;

**E** = 4 hr 26°C 0.2% K-gluconate; **G** = 4 hr 37°C 0.2% K-gluconate;

All samples are directly flanked by respective reverse transcriptase negative controls

## Bibliography/References

1. Perry RD & Fetherston JD (1997) *Yersinia pestis*--etiologic agent of plague. *Clin Microbiol Rev* 10(1):35-66.
2. Russell JC (1968) That earlier plague. *Demography* 5:174-184.
3. Gottfried RS (1983) *The black death. Natural and human disaster in medieval europe*. (The Free Press, New York, NY).
4. Butler T (1983) *Plague and other Yersinia infections*. (Plenum Press, New York, NY).
5. Duplax N (1988) Fleas—the lethal leapers. *Natl. Geogr.* 173(5):672–694.
6. Silkroad Foundation (2009) The Bridge between Eastern and Western Cultures. Retrieved from: <http://www.silkroadfoundation.org/toc/index.html>
7. Morelli G, *et al.* (2010) *Yersinia pestis* genome sequencing identifies patterns of global phylogenetic diversity. *Nat Genet* 42(12):1140-1143.
8. Butler T (2014) Plague history: Yersin's discovery of the causative bacterium in 1894 enabled, in the subsequent century, scientific progress in understanding the disease and the development of treatments and vaccines. *Clin Microbiol Infect* 20(3):202-209.
9. WHO (2009) Human plague: review of regional morbidity and mortality, 2004-2009. *Wkly Epidemiol Rec* 85(6):40-45.
10. WHO Global Alert and Response (2014) Plague-Madagascar. Retrieved from: <http://www.who.int/csr/don/21-november-2014-plague/en/>
11. CDC (2013) Plague in the United States. Retrieved from: <http://www.cdc.gov/plague/maps/index.html>
12. Riedel S (2005) Plague: from natural disease to bioterrorism. *Proc (Bayl Univ Med Cent)* 18(2):116-124.
13. Derbes VJ (1966) De Mussis and the great plague of 1348. A forgotten episode of bacteriological warfare. *JAMA* 196(1):59-62.
14. Inglesby TV, *et al.* (2000) Plague as a biological weapon: medical and public health management. Working Group on Civilian Biodefense. *JAMA* 283(17):2281-2290.
15. WHO Group of Consultants (1970) Health aspects of chemical and biological weapons. (World Health Organization, Geneva, Switzerland), pp 96-109.
16. Pearson GS (1998) The threat of deliberate disease in the 21st century. Biological weapons proliferation: reasons for concern, courses of action. Henry L. Stimson Centre.
17. CDC, HHS (2012) Possession, use, and transfer of select agents and toxins; biennial review. Final rule. *Fed Regist* 77(194):61083-61115.
18. Young GM, Smith MJ, Minnich SA, & Miller VL (1999) The *Yersinia enterocolitica* motility master regulatory operon, *flhDC*, is required for flagellin

- production, swimming motility, and swarming motility. *J Bacteriol* 181(9):2823-2833.
19. Chain PS, *et al.* (2004) Insights into the evolution of *Yersinia pestis* through whole-genome comparison with *Yersinia pseudotuberculosis*. *Proc Natl Acad Sci U S A* 101(38):13826-13831.
  20. Knirel YA, *et al.* (2005) Temperature-dependent variations and intraspecies diversity of the structure of the lipopolysaccharide of *Yersinia pestis*. *Biochemistry* 44(5):1731-1743.
  21. Prior JL, *et al.* (2001) The failure of different strains of *Yersinia pestis* to produce lipopolysaccharide O-antigen under different growth conditions is due to mutations in the O-antigen gene cluster. *FEMS Microbiol Lett* 197(2):229-233.
  22. Devignat, R (1951) Varieties of *Pasteurella pestis*; new hypothesis. *Bull World Health Organ* 4(2):247-263.
  23. Zhou D, *et al.* (2004) Genetics of metabolic variations between *Yersinia pestis* biovars and the proposal of a new biovar, microtus. *J Bacteriol* 186(15):5147-5152.
  24. Achtman M, *et al.* (1999) *Yersinia pestis*, the cause of plague, is a recently emerged clone of *Yersinia pseudotuberculosis*. *Proc Natl Acad Sci U S A* 96(24):14043-14048.
  25. Achtman M, *et al.* (2004) Microevolution and history of the plague bacillus, *Yersinia pestis*. *Proc Natl Acad Sci U S A* 101(51):17837-17842.
  26. Viboud GI & Bliska JB (2005) *Yersinia* outer proteins: role in modulation of host cell signaling responses and pathogenesis. *Annu Rev Microbiol* 59:69-89.
  27. Du Y, Rosqvist R, & Forsberg A (2002) Role of fraction 1 antigen of *Yersinia pestis* in inhibition of phagocytosis. *Infect Immun* 70(3):1453-1460.
  28. Sodeinde OA, *et al.* (1992) A surface protease and the invasive character of plague. *Science* 258(5084):1004-1007.
  29. Chouikha I & Hinnebusch BJ (2014) Silencing urease: A key evolutionary step that facilitated the adaptation of *Yersinia pestis* to the flea-borne transmission route. *Proc Natl Acad Sci U S A* 111(52):18709-18714.
  30. Sun YC, Hinnebusch BJ, & Darby C (2008) Experimental evidence for negative selection in the evolution of a *Yersinia pestis* pseudogene. *Proc Natl Acad Sci U S A* 105(23):8097-8101.
  31. Bleves S, Marenne MN, Detry G, & Cornelis GR (2002) Up-regulation of the *Yersinia enterocolitica* yop regulon by deletion of the flagellum master operon *flhDC*. *J Bacteriol* 184(12):3214-3223.
  32. Zheng Y, *et al.* (2013) The EAL domain containing protein STM2215 (*rtm*) is needed during *Salmonella* infection and has cyclic di-GMP phosphodiesterase activity. *Mol Microbiol* 89(3):403-419
  33. Sun YC, *et al.* (2011) Differential control of *Yersinia pestis* biofilm formation in

- vitro* and in the flea vector by two c-di-GMP diguanylate cyclases. *PLoS One* 6(4):e19267.
34. Gage KL & Kosoy MY (2005) Natural history of plague: perspectives from more than a century of research. *Annu Rev Entomol* 50:505-528.
  35. Pollitzer, R (1954) Plague. W. H. O. Monogr. Ser. 22:1-698.
  36. Hinnebusch BJ (2005) The evolution of flea-borne transmission in *Yersinia pestis*. *Curr Issues Mol Biol* 7(2):197-212.
  37. Eisen RJ & Gage KL (2009) Adaptive strategies of *Yersinia pestis* to persist during inter-epizootic and epizootic periods. *Vet Res* 40(2):1.
  38. Lorange EA, Race BL, Sebbane F, & Hinnebusch BJ (2005) Poor vector competence of fleas and the evolution of hypervirulence in *Yersinia pestis*. *J Infect Dis* 191(11):1907-1912.
  39. Bacot AW & Martin CJ (1914) LXVII. Observations on the mechanism of the transmission of plague by fleas. *J Hyg (Lond)* 13(Suppl):423-439.
  40. Chouikha I & Hinnebusch BJ (2012) *Yersinia*--flea interactions and the evolution of the arthropod-borne transmission route of plague. *Curr Opin Microbiol* 15(3):239-246.
  41. Hinnebusch J, *et al.* (2000) Murine toxin of *Yersinia pestis* shows phospholipase D activity but is not required for virulence in mice. *Int J Med Microbiol* 290(4-5):483-487.
  42. Hinnebusch BJ, *et al.* (2002) Role of *Yersinia* murine toxin in survival of *Yersinia pestis* in the midgut of the flea vector. *Science* 296(5568):733-735.
  43. Erickson DL, Jarrett CO, Wren BW, & Hinnebusch BJ (2006) Serotype differences and lack of biofilm formation characterize *Yersinia pseudotuberculosis* infection of the *Xenopsylla cheopis* flea vector of *Yersinia pestis*. *J Bacteriol* 188(3):1113-1119.
  44. Webb CT, Brooks CP, Gage KL, & Antolin MF (2006) Classic flea-borne transmission does not drive plague epizootics in prairie dogs. *Proc Natl Acad Sci U S A* 103(16):6236-6241.
  45. Bacot AW (1915) LXXXI. Further notes on the mechanism of the transmission of plague by fleas. *J Hyg (Lond)* 14(Suppl):774-776.773.
  46. Bibikova VA (1977) Contemporary views on the interrelationships between fleas and the pathogens of human and animal diseases. *Annu Rev Entomol* 22:23-32.
  47. Eisen RJ, *et al.* (2006) Early-phase transmission of *Yersinia pestis* by unblocked fleas as a mechanism explaining rapidly spreading plague epizootics. *Proc Natl Acad Sci U S A* 103(42):15380-15385.
  48. Vetter SM, *et al.* (2010) Biofilm formation is not required for early-phase transmission of *Yersinia pestis*. *Microbiology* 156(Pt 7):2216-2225.
  49. Burroughs AL (1947) Sylvatic plague studies: The vector efficiency of nine species of fleas compared with *Xenopsylla cheopis*. *J Hyg (Lond)* 45(3):371-396.

50. Perry RD, Pendrak ML, & Schuetze P (1990) Identification and cloning of a hemin storage locus involved in the pigmentation phenotype of *Yersinia pestis*. *J Bacteriol* 172(10):5929-5937.
51. Brubaker RR (1969) Mutation rate to nonpigmentation in *Pasteurella pestis*. *J Bacteriol* 98(3):1404-1406.
52. Buchrieser C, *et al.* (1999) The 102-kilobase pgm locus of *Yersinia pestis*: sequence analysis and comparison of selected regions among different *Yersinia pestis* and *Yersinia pseudotuberculosis* strains. *Infect Immun* 67(9):4851-4861.
53. Surgalla MJ & Beesley ED (1969) Congo red-agar plating medium for detecting pigmentation in *Pasteurella pestis*. *Appl Microbiol* 18(5):834-837.
54. Wang X, Preston JF, & Romeo T (2004) The *pgaABCD* locus of *Escherichia coli* promotes the synthesis of a polysaccharide adhesin required for biofilm formation. *J Bacteriol* 186(9):2724-2734.
55. Götz F (2002) Staphylococcus and biofilms. *Molecular Microbiology* 43(6):11.
56. Gerke C, Kraft A, Süssmuth R, Schweitzer O, & Götz F (1998) Characterization of the N-acetylglucosaminyltransferase activity involved in the biosynthesis of the *Staphylococcus epidermidis* polysaccharide intercellular adhesin. *J Biol Chem* 273(29):18586-18593.
57. Pendrak ML & Perry RD (1991) Characterization of a hemin-storage locus of *Yersinia pestis*. *Biol Met* 4(1):41-47.
58. Perry RD, *et al.* (2004) Temperature regulation of the hemin storage (Hms+) phenotype of *Yersinia pestis* is posttranscriptional. *J Bacteriol* 186(6):1638-1647.
59. Bobrov AG, Kirillina O, Forman S, Mack D, & Perry RD (2008) Insights into *Yersinia pestis* biofilm development: topology and co-interaction of Hms inner membrane proteins involved in exopolysaccharide production. *Environ Microbiol* 10(6):1419-1432.
60. Jones HA, Lillard JW, & Perry RD (1999) HmsT, a protein essential for expression of the haemin storage (Hms+) phenotype of *Yersinia pestis*. *Microbiology* 145 (Pt 8):2117-2128.
61. Bobrov AG, Kirillina O, & Perry RD (2005) The phosphodiesterase activity of the HmsP EAL domain is required for negative regulation of biofilm formation in *Yersinia pestis*. *FEMS Microbiol Lett* 247(2):123-130.
62. Kirillina O, Fetherston JD, Bobrov AG, Abney J, & Perry RD (2004) HmsP, a putative phosphodiesterase, and HmsT, a putative diguanylate cyclase, control Hms-dependent biofilm formation in *Yersinia pestis*. *Mol Microbiol* 54(1):75-88.
63. Bobrov AG, *et al.* (2011) Systematic analysis of cyclic di-GMP signalling enzymes and their role in biofilm formation and virulence in *Yersinia pestis*. *Mol Microbiol* 79(2):533-551.
64. Marceau M (2005) Transcriptional regulation in *Yersinia*: an update. *Curr Issues Mol Biol* 7(2):151-177.

65. Qu Y, *et al.* (2012) Identification by cDNA cloning of abundant sRNAs in a human-avirulent *Yersinia pestis* strain grown under five different growth conditions. *Future Microbiol* 7(4):535-547.
66. Beauregard A, *et al.* (2013) Identification and characterization of small RNAs in *Yersinia pestis*. *RNA Biol* 10(3):397-405.
67. Yan Y, *et al.* (2013) Determination of sRNA expressions by RNA-seq in *Yersinia pestis* grown *in vitro* and during infection. *PLoS One* 8(9):e74495.
68. Waters LS & Storz G (2009) Regulatory RNAs in bacteria. *Cell* 136(4):615-628.
69. Vogel J & Luisi BF (2011) Hfq and its constellation of RNA. *Nat Rev Microbiol* 9(8):578-589.
70. Brubaker RR & Surgalla MJ (1964) The effect of Ca<sup>++</sup> and Mg<sup>++</sup> on lysis, growth, and production of virulence antigens by *Pasteurella pestis*. *J Infect Dis* 114:13-25.
71. Goguen JD, Yother J, & Straley SC (1984) Genetic analysis of the low calcium response in *Yersinia pestis* mu d1(Ap lac) insertion mutants. *J Bacteriol* 160(3):842-848.
72. Straley SC, Plano GV, Skrzypek E, Haddix PL, & Fields KA (1993) Regulation by Ca<sup>2+</sup> in the *Yersinia* low-Ca<sup>2+</sup> response. *Mol Microbiol* 8(6):1005-1010.
73. Michiels T, Wattiau P, Brasseur R, Ruyschaert JM, & Cornelis G (1990) Secretion of Yop proteins by *Yersinia*. *Infect Immun* 58(9):2840-2849.
74. Price SB, Cowan C, Perry RD, & Straley SC (1991) The *Yersinia pestis* V antigen is a regulatory protein necessary for Ca<sup>2+</sup>(+)-dependent growth and maximal expression of low-Ca<sup>2+</sup> response virulence genes. *J Bacteriol* 173(8):2649-2657.
75. Zahorchak RJ, Charnetzky WT, Little RV, & Brubaker RR (1979) Consequences of Ca<sup>2+</sup> deficiency on macromolecular synthesis and adenylate energy charge in *Yersinia pestis*. *J Bacteriol* 139(3):792-799.
76. Fowler JM & Brubaker RR (1994) Physiological basis of the low calcium response in *Yersinia pestis*. *Infect Immun* 62(12):5234-5241.
77. Wessman GE, Miller DJ, & Surgalla MJ (1958) Toxic effect of glucose on virulent *Pasteurella pestis* in chemically defined media. *J Bacteriol* 76(4):368-375.
78. Brownlow WJ & Wessman GE (1960) Nutrition of *Pasteurella pestis* in chemically defined media at temperatures of 36 to 38 C. *J Bacteriol* 79:299-304.
79. Fukuto HS, Svetlanov A, Palmer LE, Karzai AW, & Bliska JB (2010) Global gene expression profiling of *Yersinia pestis* replicating inside macrophages reveals the roles of a putative stress-induced operon in regulating type III secretion and intracellular cell division. *Infect Immun* 78(9):3700-3715.
80. Campbell GL & Dennis DT (1998) *Plague and other Yersinia infections*. (McGraw-Hill, New York, NY).
81. Butler T (1995) *Yersinia species (including plague)*. (Churchill Livingstone, New

- York, NY).
82. Meyer K (1961) Pneumonic plague. *Bacteriol Rev* 25:249-261.
  83. Finegold MJ (1969) Pneumonic plague in monkeys. An electron microscopic study. *Am J Pathol* 54(2):167-185.
  84. (CDC) (1997) Fatal human plague--Arizona and Colorado, 1996. *MMWR Morb Mortal Wkly Rep* 46(27):617-620.
  85. Dennis D & Meier F (1997) *Plague*. (ASM Press, Washington, DC).
  86. Becker TM, *et al.* (1987) Plague meningitis--a retrospective analysis of cases reported in the United States, 1970-1979. *West J Med* 147(5):554-557.
  87. Isaäcson M, *et al.* (1973) Unusual cases of human plague in Southern Africa. *S Afr Med J* 47(44):2109-2113.
  88. Smiley ST (2008) Current challenges in the development of vaccines for pneumonic plague. *Expert Rev Vaccines* 7(2):209-221.
  89. FDA (2014) Complete list of vaccines licensed for immunization and distribution in the US.  
Retrieved from:  
<http://www.fda.gov/BiologicsBloodVaccines/Vaccines/ApprovedProducts/ucm093833.htm>
  90. Girard G & Robic J (1942) Current status of the plague in Madagascar and vaccinal prophylaxis with the aid of the EV virus-vaccine. *Bull. Soc. Path. Exot.* 35:43-49.
  91. Podladchikova ON, Rykova VA, Ivanova VS, Eremenko NS, & Lebedeva SA (2002) Study of PGM mutation mechanism in *Yersinia pestis* (plague pathogen) vaccine strain EV76. *Mol Gen Mikrobiol Virusol* (2):14-19.
  92. Cui Y, *et al.* (2014) Genetic variations of live attenuated plague vaccine strains (*Yersinia pestis* EV76 lineage) during laboratory passages in different countries. *Infect Genet Evol* 26:172-179.
  93. Titball RW & Williamson ED (2004) *Yersinia pestis* (plague) vaccines. *Expert Opin Biol Ther* 4(6):965-973.
  94. Bashaw J, *et al.* (2007) Development of in vitro correlate assays of immunity to infection with *Yersinia pestis*. *Clin Vaccine Immunol* 14(5):605-616.
  95. Rosenzweig JA, *et al.* (2011) Progress on plague vaccine development. *Appl Microbiol Biotechnol* 91(2):265-286.
  96. Sun W & Curtiss R (2013) Rational considerations about development of live attenuated *Yersinia pestis* vaccines. *Curr Pharm Biotechnol* 14(10):878-886.
  97. FDA (2012) FDA approves new antibacterial treatment for plague.  
Retrieved from:  
<http://www.fda.gov/NewsEvents/Newsroom/PressAnnouncements/ucm302220.htm>
  98. Galimand M, *et al.* (1997) Multidrug resistance in *Yersinia pestis* mediated by a transferable plasmid. *N Engl J Med* 337(10):677-680.

99. Guiyoule A, *et al.* (2001) Transferable plasmid-mediated resistance to streptomycin in a clinical isolate of *Yersinia pestis*. *Emerg Infect Dis* 7(1):43-48.
100. Ryzhko IV, Trishina AV, & Verkina LM (2010) Lack of levofloxacin and moxyfloxacin efficacy in experimental plague of albino mice infected with nalidixic acid resistant pathogen (Nal(r)). *Antibiot Khimioter* 55(11-12):22-24.
101. Vadyvaloo V, Jarrett C, Sturdevant DE, Sebbane F, & Hinnebusch BJ (2010) Transit through the flea vector induces a pretransmission innate immunity resistance phenotype in *Yersinia pestis*. *PLoS Pathog* 6(2):e1000783.
102. Busby S & Ebricht RH (1999) Transcription activation by catabolite activator protein (CAP). *J Mol Biol* 293(2):199-213.
103. Zhan L, *et al.* (2008) The cyclic AMP receptor protein, CRP, is required for both virulence and expression of the minimal CRP regulon in *Yersinia pestis* biovar microtus. *Infect Immun* 76(11):5028-5037.
104. Jackson DW, Simecka JW, & Romeo T (2002) Catabolite repression of *Escherichia coli* biofilm formation. *J Bacteriol* 184(12):3406-3410.
105. Eppler T, Postma P, Schütz A, Völker U, & Boos W (2002) Glycerol-3-phosphate-induced catabolite repression in *Escherichia coli*. *J Bacteriol* 184(11):3044-3052.
106. Charusanti P, *et al.* (2011) An experimentally-supported genome-scale metabolic network reconstruction for *Yersinia pestis* CO92. *BMC Syst Biol* 5:163.
107. Edgar JR & Bell RM (1978) Biosynthesis in *Escherichia coli* of sn-glycerol 3-phosphate, a precursor of phospholipid. Kinetic characterization of wild type and feedback-resistant forms of the biosynthetic sn-glycerol-3-phosphate dehydrogenase. *J Biol Chem* 253(18):6354-6363.
108. Lin EC (1976) Glycerol dissimilation and its regulation in bacteria. *Annu Rev Microbiol* 30:535-578.
109. Anderson A & Cooper RA (1969) Gluconeogenesis in *Escherichia coli* The role of triose phosphate isomerase. *FEBS Lett* 4(1):19-20.
110. Motin VL, *et al.* (2002) Genetic variability of *Yersinia pestis* isolates as predicted by PCR-based IS100 genotyping and analysis of structural genes encoding glycerol-3-phosphate dehydrogenase (*glpD*). *J Bacteriol* 184(4):1019-1027.
111. Willias SP, Chauhan S, & Motin VL (2014) Functional characterization of *Yersinia pestis* aerobic glycerol metabolism. *Microb Pathog* 76:33-43.
112. Doll JM, *et al.* (1994) Cat-transmitted fatal pneumonic plague in a person who traveled from Colorado to Arizona. *Am J Trop Med Hyg* 51(1):109-114.
113. Datsenko KA & Wanner BL (2000) One-step inactivation of chromosomal genes in *Escherichia coli* K-12 using PCR products. *Proc Natl Acad Sci U S A* 97(12):6640-6645.
114. Donnenberg MS & Kaper JB (1991) Construction of an *eae* deletion mutant of enteropathogenic *Escherichia coli* by using a positive-selection suicide vector.

- Infect Immun* 59(12):4310-4317.
115. Girish V & Vijayalakshmi A (2004) Affordable image analysis using NIH Image/ImageJ. *Indian J Cancer* 41(1):47.
  116. Cathelyn JS, Crosby SD, Lathem WW, Goldman WE, & Miller VL (2006) RovA, a global regulator of *Yersinia pestis*, specifically required for bubonic plague. *Proc Natl Acad Sci U S A* 103(36):13514-13519.
  117. Robinson JB, *et al.* (2009) Evaluation of a *Yersinia pestis* mutant impaired in a thermoregulated type VI-like secretion system in flea, macrophage and murine models. *Microb Pathog* 47(5):243-251.
  118. Holman WL (1914) The Use of Decolorized Acid Fuchsin as an Acid Indicator in Carbohydrate Fermentation Tests with Some Remarks on Acid Production by Bacteria. *The Journal of Infectious Diseases* 15(1):7.
  119. Gouy M, Guindon S, & Gascuel O (2010) SeaView version 4: A multiplatform graphical user interface for sequence alignment and phylogenetic tree building. *Mol Biol Evol* 27(2):221-224.
  120. Heroven AK, *et al.* (2012) Crp induces switching of the CsrB and CsrC RNAs in *Yersinia pseudotuberculosis* and links nutritional status to virulence. *Front Cell Infect Microbiol* 2:158.
  121. Austin D & Larson TJ (1991) Nucleotide sequence of the *glpD* gene encoding aerobic *sn*-glycerol 3-phosphate dehydrogenase of *Escherichia coli* K-12. *J Bacteriol* 173(1):101-107.
  122. Cui Y, *et al.* (2013) Historical variations in mutation rate in an epidemic pathogen, *Yersinia pestis*. *Proc Natl Acad Sci U S A* 110(2):577-582.
  123. Feodorova V & Motin V (2011) Vaccines against bacterial biothreat pathogens. (Research Signpost, Kerala, India) p 57.
  124. Korobkova EI & Pavlova LP (1964) Influence of repeated passages at conditions of aeration on properties of vaccine strains 1, EV, 17 (Medicine, Moscow, Russia) p 10.
  125. Liu MY, *et al.* (1997) The RNA molecule CsrB binds to the global regulatory protein CsrA and antagonizes its activity in *Escherichia coli*. *J Biol Chem* 272(28):17502-17510.
  126. Weilbacher T, *et al.* (2003) A novel sRNA component of the carbon storage regulatory system of *Escherichia coli*. *Mol Microbiol* 48(3):657-670.
  127. Jackson DW, *et al.* (2002) Biofilm formation and dispersal under the influence of the global regulator CsrA of *Escherichia coli*. *J Bacteriol* 184(1):290-301.
  128. Jones MK, Warner EB, & Oliver JD (2008) *csrA* inhibits the formation of biofilms by *Vibrio vulnificus*. *Appl Environ Microbiol* 74(22):7064-7066.
  129. Wang X, *et al.* (2005) CsrA post-transcriptionally represses *pgaABCD*, responsible for synthesis of a biofilm polysaccharide adhesin of *Escherichia coli*. *Mol Microbiol* 56(6):1648-1663.

130. Jonas K, *et al.* (2008) The RNA binding protein CsrA controls cyclic di-GMP metabolism by directly regulating the expression of GGDEF proteins. *Mol Microbiol* 70(1):236-257.
131. Baker CS, Morozov I, Suzuki K, Romeo T, & Babitzke P (2002) CsrA regulates glycogen biosynthesis by preventing translation of *glgC* in *Escherichia coli*. *Mol Microbiol* 44(6):1599-1610.
132. Rahimpour M, *et al.* (2013) GlgS, described previously as a glycogen synthesis control protein, negatively regulates motility and biofilm formation in *Escherichia coli*. *Biochem J* 452(3):559-573.
133. Solovyev V & Salamov A (2011) Automatic Annotation of Microbial Genomes and Metagenomic Sequences. In *Metagenomics and its Applications in Agriculture, Biomedicine and Environmental Studies*. (Nova Science Publisher) p 17.
134. Sun YC, Guo XP, Hinnebusch BJ, & Darby C (2012) The *Yersinia pestis* Rcs phosphorelay inhibits biofilm formation by repressing transcription of the diguanylate cyclase gene *hmsT*. *J Bacteriol* 194(8):2020-2026.
135. Koo JT, Alleyne TM, Schiano CA, Jafari N, & Lathem WW (2011) Global discovery of small RNAs in *Yersinia pseudotuberculosis* identifies *Yersinia*-specific small, noncoding RNAs required for virulence. *Proc Natl Acad Sci U S A* 108(37):E709-717.
136. Garcia E, *et al.* (2007) Pestoides F, an atypical *Yersinia pestis* strain from the former Soviet Union. *Adv Exp Med Biol* 603:17-22.
137. Li Y, *et al.* (2009) Genotyping and phylogenetic analysis of *Yersinia pestis* by MLVA: insights into the worldwide expansion of Central Asia plague foci. *PLoS One* 4(6):e6000.
138. Fang N, *et al.* (2014) HmsB enhances biofilm formation in *Yersinia pestis*. *Front Microbiol* 5:685.
139. Bellows LE, Koestler BJ, Karaba SM, Waters CM, & Lathem WW (2012) Hfq-dependent, co-ordinate control of cyclic diguanylate synthesis and catabolism in the plague pathogen *Yersinia pestis*. *Mol Microbiol* 86(3):661-674.
140. Rempe KA, Hinz AK, & Vadyvaloo V (2012) Hfq regulates biofilm gut blockage that facilitates flea-borne transmission of *Yersinia pestis*. *J Bacteriol* 194(8):2036-2040.
141. Baker CS, *et al.* (2007) CsrA inhibits translation initiation of *Escherichia coli* *hfq* by binding to a single site overlapping the Shine-Dalgarno sequence. *J Bacteriol* 189(15):5472-5481.
142. Hinnebusch BJ, Fischer ER, & Schwan TG (1998) Evaluation of the role of the *Yersinia pestis* plasminogen activator and other plasmid-encoded factors in temperature-dependent blockage of the flea. *J Infect Dis* 178(5):1406-1415.
143. Kim TJ, *et al.* (2007) Direct transcriptional control of the plasminogen activator

- gene of *Yersinia pestis* by the cyclic AMP receptor protein. *J Bacteriol* 189(24):8890-8900.
144. Sun W, Roland KL, Kuang X, Branger CG, & Curtiss R (2010) *Yersinia pestis* with regulated delayed attenuation as a vaccine candidate to induce protective immunity against plague. *Infect Immun* 78(3):1304-1313.
  145. Motin VL, *et al.* (2004) Temporal global changes in gene expression during temperature transition in *Yersinia pestis*. *J Bacteriol* 186(18):6298-6305.
  146. Zhou D, *et al.* (2006) Genome-wide transcriptional response of *Yersinia pestis* to stressful conditions simulating phagolysosomal environments. *Microbes Infect* 8(12-13):2669-2678.
  147. Avican K, *et al.* (2015) Reprogramming of *Yersinia* from Virulent to Persistent Mode Revealed by Complex *In Vivo* RNA-seq Analysis. *PLoS Pathog* 11(1):e1004600.
  148. Revell PA & Miller VL (2000) A chromosomally encoded regulator is required for expression of the *Yersinia enterocolitica* *inv* gene and for virulence. *Mol Microbiol* 35(3):677-685.
  149. Nagel G, Lahrz A, & Dersch P (2001) Environmental control of invasins expression in *Yersinia pseudotuberculosis* is mediated by regulation of RovA, a transcriptional activator of the SlyA/Hor family. *Mol Microbiol* 41(6):1249-1269.
  150. Dube PH, Handley SA, Revell PA, & Miller VL (2003) The *rovA* mutant of *Yersinia enterocolitica* displays differential degrees of virulence depending on the route of infection. *Infect Immun* 71(6):3512-3520.
  151. Sebbane F, *et al.* (2006) Adaptive response of *Yersinia pestis* to extracellular effectors of innate immunity during bubonic plague. *Proc Natl Acad Sci U S A* 103(31):11766-11771.
  152. Pradel E, *et al.* (2014) New Insights into How *Yersinia pestis* Adapts to Its Mammalian Host during Bubonic Plague. *PLoS Pathog* 10(3):e1004029.
  153. Zhang Y, *et al.* (2011) Molecular characterization of transcriptional regulation of *rovA* by PhoP and RovA in *Yersinia pestis*. *PLoS One* 6(9):e25484.
  154. Heroven AK, Böhme K, Rohde M, & Dersch P (2008) A Csr-type regulatory system, including small non-coding RNAs, regulates the global virulence regulator RovA of *Yersinia pseudotuberculosis* through RovM. *Mol Microbiol* 68(5):1179-1195.

## Vita

Stephan P. Willias, the son of SCPO. Jeffrey W. Willias and Mary E. Willias, was born on July 20, 1988 in Jacksonville, Florida. He acquired a Bachelor's degree in Biology at Texas A&M University – Corpus Christi (TAMU-CC). During his studies at TAMU-CC, he researched environmental stress responses of local *Vibrio vulnificus* isolates under the direction of Dr. Gregory W. Buck as supported by an NSF-Undergraduate Mentoring in Environmental Biology award. Thereafter, he was admitted to the University of Texas Medical Branch (UTMB) Experimental Pathology graduate program in Galveston, Texas. During his research at UTMB in Dr. Vladimir L. Motin's lab, he was competitively awarded financial support through a McLaughlin fellowship and T32 Training Grant in Tropical and Emerging Infectious Diseases.

### Education:

B.S., Biology. May 2010, Texas A&M University – Corpus Christi. Corpus Christi, TX.

### Publications:

Willias, S., Chauhan, S., and Motin, V.L. (2014) Functional Characterization of *Yersinia pestis* Aerobic Glycerol Metabolism *Microbial Pathogenesis* 76: 33-43.

### Dissertation Summary:

In order to survive in the unique environments associated with different aspects of the infectious cycle, *Yersinia pestis* evokes adaptive responses to concertedly regulate

gene expression. The overall objective of this project was to ascertain the impact of carbon catabolite regulation upon *Y. pestis* pathogenesis. Specifically, this research encompassed two major aspects: 1) regulation of *Y. pestis* biofilm formation, a key transmission factor, and 2) characterization of carbon catabolite regulation amid conditions reflective of mammalian infection. Findings demonstrate that *Y. pestis* biofilm formation is subject to carbon catabolite regulation in which primary carbon sources inhibit biofilm production, and alternate carbon sources induce robust biofilm development. The differential modulation of *Y. pestis* biofilm production was found to be facilitated by the cAMP receptor protein, CRP. The microevolution of *Y. pestis* biovar Orientalis is characterized by loss of glycerol fermentation resulting from dysfunction of *glpD* and ensured by impairment of the *glpFKX* operon. Through a mode of action presumably independent of CRP regulation, *glpD* has been shown to promote *Y. pestis* biofilm production. Findings in this study also clarified conflicting observations made by independent investigative groups, indicating that the Hfq sRNA chaperone differentially modulates *Y. pestis* biofilm production in response to primary or alternate available carbon sources. The thermo-regulated sRNA species, Ysr172 and sR084, were shown to be dispensable for *Y. pestis* biofilm production. Contrary to what has been described for *E. coli*, the carbon storage regulator protein, CsrA, was found to be a positive regulator of *Y. pestis* biofilm formation. Loss of *hmsP*, encoding a cyclic diguanylate phosphodiesterase, restored biofilm production in a *csrA*-deficient mutant, providing insight regarding the mechanism of *Y. pestis* biofilm regulation. Deletion of *csrA* severely impaired *Y. pestis* growth in peptide-rich HIB at 37°C. Furthermore, loss of *csrA* resulted in a toxic effect at 37°C during growth in chemically defined BCS medium, regardless of available carbon source. Lethality was described for both pCD1 positive and negative *Y. pestis* strains, thereby refuting a low-calcium response (Lcr). Mutants deficient in *csrA* had reduced survival upon murine macrophage-like cell challenge, demonstrating CsrA may serve a crucial *Y. pestis* virulence regulator.

Permanent address: 104 Pompano Ave., Galveston, Texas 77550

This dissertation was typed by Stephan P. Willias.